(12) INTERNATIONAL APPLICATION PUBLISHED UNDER THE PATENT COOPERATION TREATY (PCT)

(19) World Intellectual Property Organization
International Bureau

(43) International Publication Date
13 March 2025 (13.03.2025)

WIPO | PCT

(10) International Publication Number
WO 2025/054580 A1

(51) International Patent Classification:
C12N 15/113 (2010.01) *A61P 9/04* (2006.01)
C12Q 1/68 (2018.01) *A61P 9/10* (2006.01)
G01N 33/53 (2006.01)

(21) International Application Number:
PCT/US2024/045782

(22) International Filing Date:
09 September 2024 (09.09.2024)

(25) Filing Language: English

(26) Publication Language: English

(30) Priority Data:
63/581,451 08 September 2023 (08.09.2023) US

(71) Applicant: **UNIVERSITY OF PITTSBURGH-OF THE COMMONWEALTH SYSTEM OF HIGHER EDUCATION** [US/US]; 1st Floor Gardner Steel Conference Center, 130 Thackeray Avenue, Pittsburgh, Pennsylvania 15260 (US).

(72) Inventor: **BECKER, Jason Robert**; 4923 Wallingford St., Pittsburgh, Pennsylvania 15213 (US).

(74) Agent: **PAVENTO, Lisa C.** et al.; Meunier Carlin & Curfman LLC, 999 Peachtree Street, NE, Suite 1300, Atlanta, Georgia 30309 (US).

(81) Designated States *(unless otherwise indicated, for every kind of national protection available)*: AE, AG, AL, AM, AO, AT, AU, AZ, BA, BB, BG, BH, BN, BR, BW, BY, BZ, CA, CH, CL, CN, CO, CR, CU, CV, CZ, DE, DJ, DK, DM, DO, DZ, EC, EE, EG, ES, FI, GB, GD, GE, GH, GM, GT, HN, HR, HU, ID, IL, IN, IQ, IR, IS, IT, JM, JO, JP, KE, KG, KH, KN, KP, KR, KW, KZ, LA, LC, LK, LR, LS, LU, LY, MA, MD, MG, MK, MN, MU, MW, MX, MY, MZ, NA, NG, NI, NO, NZ, OM, PA, PE, PG, PH, PL, PT, QA, RO, RS, RU, RW, SA, SC, SD, SE, SG, SK, SL, ST, SV, SY, TH, TJ, TM, TN, TR, TT, TZ, UA, UG, US, UZ, VC, VN, WS, ZA, ZM, ZW.

(84) Designated States *(unless otherwise indicated, for every kind of regional protection available)*: ARIPO (BW, CV, GH, GM, KE, LR, LS, MW, MZ, NA, RW, SC, SD, SL, ST, SZ, TZ, UG, ZM, ZW), Eurasian (AM, AZ, BY, KG, KZ, RU, TJ, TM), European (AL, AT, BE, BG, CH, CY, CZ, DE, DK, EE, ES, FI, FR, GB, GR, HR, HU, IE, IS, IT, LT, LU, LV, MC, ME, MK, MT, NL, NO, PL, PT, RO, RS, SE, SI, SK, SM, TR), OAPI (BF, BJ, CF, CG, CI, CM, GA, GN, GQ, GW, KM, ML, MR, NE, SN, TD, TG).

Published:
— *with international search report (Art. 21(3))*
— *with sequence listing part of description (Rule 5.2(a))*

(54) Title: COMPOSITIONS AND METHODS FOR INCREASING MYOCARDIAL CAPILLARY FORMATION, REDUCING LEFT VENTRICULAR HYPERTROPHY AND/OR REDUCING VENTRICULAR DYSFUNCTION

(57) Abstract: Provided herein are methods of treating a cardiomyopathy and/or myocardial microvascular dysfunction, increasing myocardial capillary growth, reducing left ventricular hypertrophy, and/or reducing left ventricular dysfunction in a subject comprising administering an MDM2 inhibitor to the subject.

WO 2025/054580 A1

COMPOSITIONS AND METHODS FOR INCREASING MYOCARDIAL CAPILLARY FORMATION, REDUCING LEFT VENTRICULAR HYPERTROPHY AND/OR REDUCING VENTRICULAR DYSFUNCTION

CROSS-REFERENCE TO RELATED APPLICATIONS

[0001] This application claims the benefit of U.S. Provisional Application No. 63/581,451, filed September 8, 2023, which is expressly incorporated herein by reference in its entirety.

REFERNCE TO SEQUENCE LISTING

[0002] The sequence listing submitted on September 9, 2024, as an .XML entitled "10504-098WO1_ST26.xml" created on September 9, 2024, and having a file size of 12,412 bytes is hereby incorporated by reference pursuant to 37 C.F.R. § 1.52(e)(5).

STATEMENT OF GOVERNMENT INTEREST

[0003] This invention was made with government support under HL160890 awarded by the National Institutes of Health (NIH). The government has certain rights in the invention.

BACKGROUND OF THE INVENTION

[0004] Hypertrophic cardiomyopathy (HCM) is a disease characterized by pathologic thickening of the left ventricular (LV) myocardium which can lead to heart failure and sudden death in humans. The prevalence of HCM in humans is approximately 1:500 and mutations in sarcomere protein genes have been shown to cause this disease. The most commonly mutated genes in HCM are MYBPC3 (myosin binding protein C3) and MYH7 (myosin heavy chain 7) and mutations in these 2 genes account for approximately 80% of mutation-positive HCM cases. The cause of myocardial hypertrophy in HCM is increased cardiomyocyte growth that occurs during childhood or in adult life in humans. However, pathologic ventricular remodeling in HCM is also associated with changes in the noncardiomyocyte myocardial cell populations. It remains incompletely understood how sarcomere protein mutations that are expressed primarily in the cardiomyocyte cell population lead to changes in the other cell types of the myocardium.

[0005] Microvascular dysfunction or disease (MVD), occurs secondary to abnormalities of the capillary beds of multiple different organs such as the brain, kidney, retina, skin, lung, and heart. MVD has been consistently identified in many different forms of human cardiomyopathy secondary to both ischemic and nonischemic etiologies. Mechanistically, MVD often involves an imbalance of proangiogenic and antiangiogenic factors which are critical for capillary formation and maintenance. For example, reduced expression of the proangiogenic factors such as VegfA (vascular endothelial growth factor A) and angiopoietin 1 and 2 and increased production of the antiangiogenic factors angiopoietin 4 and thrombospondin 1, induce capillary rarefaction secondary to pressure overload. However, the molecular mechanisms regulating the development of MVD in HCM remain poorly defined.

[0006] What is need in the art are methods of increasing myocardial capillary formation, reducing left ventricular hypertrophy, reducing left ventricular dysfunction, treating MVD and/or treating cardiomyopathy.

SUMMARY OF THE INVENTION

[0007] Provided herein is a method of treating a cardiomyopathy in a subject in need thereof comprising administering an E3 ubiquitin-protein ligase MDM2 polypeptide (MDM2) inhibitor to a heart cell in the subject.

[0008] In some embodiments, the cardiomyopathy is a myocardial hypertrophy or a dilated cardiomyopathy. In some embodiments, the cardiomyopathy is a myocardial hypertrophy. In some embodiments, the myocardial hypertrophy is selected from the group consisting of hypertrophic cardiomyopathy, hypertensive heart disease and aortic stenosis. In some embodiments, the myocardial hypertrophy is a hypertrophic cardiomyopathy. In certain aspects, the administration occurs during a pre or early left ventricular hypertrophy period of the hypertrophic cardiomyopathy. In some embodiments the dilated cardiomyopathy comprises reduced LV systolic function and increased left ventricular dilation.

[0009] In some embodiments, the administration reduces myocardial microvascular dysfunction in the subject. In some embodiments, the administration reduces myocardial hypertrophy in the subject. In some embodiments, the administration increases left ventricular function in the subject. In some embodiments, the administration decreases chronic angina. In some embodiments, the administration decreases adverse ventricular remodeling.

[0010] Also included herein is a method of treating a myocardial microvascular dysfunction in a subject in need thereof comprising administering an E3 ubiquitin-protein ligase MDM2 polypeptide (MDM2) inhibitor to a heart cell in the subject. Further includes is a method of increasing myocardial capillary growth in a subject comprising administering an E3 ubiquitin-protein ligase MDM2 polypeptide (MDM2) inhibitor to a heart cell in the subject.

[0011] In some embodiments, the heart cell is a cardiomyocyte. In some embodiments, the subject is a human.

[0012] In certain aspects, the MDM2 inhibitor reduces expression of MDM2. In some embodiments, MDM2 expression is reduced by between about 10% and about 90% as compared to an untreated heart cell. In some embodiments, MDM2 expression is reduced by between about 30% and about 70% as compared to an untreated heart cell. In some embodiments, MDM2 expression is reduced by about 50% as compared to an untreated heart cell.

[0013] In certain aspects the MDM2 inhibitor reduces MDM2-mediated hypoxia-inducible factor (HIF) signaling.

[0014] In some embodiments, the inhibition of MDM2 is transient.

BRIEF DESCRIPTION OF FIGURES

[0015] Figure 1(A-K) shows reduced postnatal capillary formation in the Mybpc3-/- myocardium is associated with microvascular dysfunction and tissue hypoxia. (A) Representative immunohistochemistry images for the endothelial cell markers CD31 (left) or TIE2 (right) costained with WGA (top) in left ventricular tissue cross-sections from postnatal day 7 (P7) WT and Mybpc3–/– mice. Scale bars=25 μm. (B) Capillary-to-cardiomyocyte ratios from WT and Mybpc3–/– (n=6–8/group) left ventricular tissue at postnatal day 2 (P2), P7, postnatal day 25 (P25), or postnatal day 180 (P180). Capillaries were identified with CD31 (top) or TIE2 (bottom). Minimum 120 cardiomyocytes per sample. (C) Representative immunohistochemistry images for the pericyte marker NG2 (neural/glial antigen 2) costained with WGA in left ventricular tissue from P7 WT and Mybpc3–/– mice. Scale bars=25 μm. (D) Pericyte-to cardiomyocyte ratios from WT (n=6) and Mybpc3–/– (n=6) left ventricular tissue at P7. Minimum 200 cardiomyocytes per sample. (E) Representative fluorescence images for the intravascularly injected endothelial cell stain, tomato lectin (T-lectin) in left ventricular tissue from P7 WT and Mybpc3–/– mice. Scale bars=80 μm. (F) Capillaries per mm2 in WT (n=6) and Mybpc3–/– (n=6) left ventricular tissue at P7. Three cross-

sectional images per sample were analyzed. (G) Representative myocardial blood flow velocity tracings using pulsed wave Doppler echocardiography in postnatal day 60 WT and Mybpc3–/– mice. Myocardial blood flow at baseline and after retro-orbital injection with adenosine (postadenosine) to induce maximal hyperemia. H, Myocardial blood flow in postnatal day 60 WT after adenosine (right bars) were normalized to heart weight. (I) Coronary flow reserve in postnatal day 60 WT (n=6) and Mybpc3–/– (n=5) mice. Coronary flow reserve is the ratio of myocardial blood flow after adenosine to myocardial blood flow at baseline. (J) Representative H&E–stained heart cross-sections from P2 or P7 WT and Mybpc3–/– mice (top) and representative immunohistochemistry images of heart cross-sections from P2 or P7 WT and Mybpc3–/– mice injected with pimonidazole ([Hypoxyprobe] bottom). Scale bars=0.5 mm. K, Comparison of left ventricular tissue hypoxia in WT and Mybpc3–/– mice at P2 or P7 (n=6–8/group). Green fluorescent intensity for each sample was obtained and then normalized to P2 WT samples. All results are shown as mean±SEM. Student or Welch t tests were used for (D), (F), (H), (I), and (K); 2-way ANOVA with Tukey multiple comparison test used for (B). CD31 indicates cluster of differentiation 31; DAPI, 4′,6-diamidino-2-phenylindole; H&E, hematoxylin–eosin; IHC, immunohistochemistry; Mybpc3-/-, cardiac myosin binding protein 3 homozygous deletion; Post-Ado, post adenosine; TIE2, TEK receptor kinase; WGA, wheat germ agglutinin; and WT, wild-type.

[0016] Figure 2(A-G) shows dynamic changes in HIF1α and HIF2α occur during the early postnatal period in the Mybpc3-/- myocardium. Immunoblots for HIF1α (A) and HIF2α (B) in left ventricular tissue lysates from WT and Mybpc3–/– mice at postnatal day 2 (P2), postnatal day 7 (P7), or postnatal day 25 (P25). (C) HIF1α protein quantification from WT (n=6) and Mybpc3–/– (n=6) left ventricular tissue lysates from P2, P7, or P25 mice normalized to β-actin protein expression and relative to postnatal day 2 WT mice. (D) HIF2α protein quantification from WT (n=7–9) and Mybpc3–/– (n=7–8) left ventricular tissue from postnatal days 2, 7, or 25 mice normalized to β-actin and relative to postnatal day 2 WT mice. (E) Representative immunohistochemistry images for HIF1α (top) and HIF2α (bottom) costained with sarcomeric α-actinin, in left ventricular tissue from postnatal day 7 WT and Mybpc3–/– mice. Scale bars=5 um (HIF1) or 10 μm (HIF2). (F) HIF1α-positive CM nuclei (% of total nuclei) in left ventricular tissue from postnatal day 7 WT (n=6) and Mybpc3–/– (n=6) mice. Minimum 100 nuclei per sample. (G) HIF2α-positive CM nuclei (% of total nuclei) in left ventricular tissue from postnatal day 7 WT (n=6) and Mybpc3–/– (n=6) mice. Minimum 100 nuclei per sample. All results are shown as mean±SEM; Student or Welch t test were

used for (C), (D), (F), and (G). CM indicates cardiomyocyte; DAPI, 4′,6-diamidino-2-phenylindole; HIF1α, hypoxia-inducible factor 1 alpha; HIF2α, hypoxia-inducible factor 2 alpha; Mybpc3-/-, cardiac myosin binding protein 3 homozygous deletion; and WT, wild-type.

[0017] Figure 3(A-R) shows the noncanonical degradation of HIF1α in the Mybpc3-/- myocardium is regulated by cardiomyocyte MDM2. (A) Hif1α gene expression in left ventricular tissue RNA from postnatal day 7 (P7) WT (n=6) and Mybpc3–/– (n=6) mice. Hif1α gene expression was normalized to Rpl32 and fold change relative to WT. (B) and (C), Immunoblots and protein quantification for HIF1α in left ventricular tissue lysates from P7 WT (n=6), Mybpc3–/– (n=6), and BTZ-injected Mybpc3–/– (n=6) mice normalized to β-actin and relative to WT. (D) and (E), Representative in situ proximity ligation assay images and quantification for Ub-modified HIF1α in left ventricular tissue from BTZ injected P7 WT (n=4) and Mybpc3–/– (n=4) mice. Three nonoverlapping left ventricular images per sample; scale bars=25 μm. (F) and (G), Immunoblot and quantification for VHL in left ventricular tissue lysate from P7 WT (n=7) and Mybpc3–/– (n=7) mice normalized to beta-actin and relative to WT. (H) and (I), Representative in situ proximity ligation assay images and quantification for HIF1α and VHL protein complexes in left ventricular tissue from P7 WT (n=4) and Mybpc3–/– (n=4) mice; 3 nonoverlapping left ventricular images per sample; scale bars=25 μm. (J) and (K), Immunoblot and quantification for MDM2 in left ventricular tissue from P7 WT (n=9) and Mybpc3–/– (n=8) mice normalized to β-actin and relative to WT. (L) Schematic of cardiomyocyte selective reduction of MDM2 in Mybpc3-/- mice generated by crossing Mdm2fl/fl, Mybpc3-/-, and Myh6:Cre mouse lines to create Mybpc3–/–Mdm2fl/+/Myh6:Cre. M, Immunoblot for MDM2, HIF1α, HIF2α, MYPBC3, and β-actin in left ventricular tissue from P7 WT, Mybpc3–/–, Mybpc3-/-/Myh6:Cre, and Mybpc3–/–Mdm2fl/+/Myh6:Cre mice. N and O, Representative in situ proximity ligation assay images and quantification for MDM2 and HIF1α protein complexes in left ventricular tissue from P7 WT (n=4), Mybpc3–/– (n=4), and Mybpc3–/–Mdm2fl/+/Myh6:Cre (n=4) mice. Three nonoverlapping left ventricular images per sample; scale bars=25 μm. (P) and (Q), Representative in situ proximity ligation assay images and quantification for Ub-modified HIF1α in left ventricular tissue from BTZ-injected P7 WT (n=4), Mybpc3–/– (n=4), and Mybpc3–/–Mdm2fl/+/Myh6:Cre (n=4) mice. Three nonoverlapping left ventricular images per sample; scale bars=25 μm. (R) Immunoprecipitation (IP) for HIF1α was performed on left ventricular tissue lysates from BTZ-injected P7 WT, Mybpc3–/– and

Mybpc3–/–Mdm2fl/+/Myh6:Cre mice and then immunoblots were performed for K48-linked Ub and HIF1α. The input left ventricular tissue lysates also underwent immunoblotting for HIF1α and β-actin. All results are shown as mean±SEM. Student t test was used for A, E, G, I, and K; 1-way ANOVA with Tukey or Dunnett T3 multiple comparison test were used for C, O, and Q. BTZ indicates bortezomib; DAPI, 4′,6-diamidino-2-phenylindole; HC, heavy chain; HIF1α, hypoxia-inducible factor 1 alpha; HIF2α, hypoxia-inducible factor 2 alpha; IB, immunoblot; LC, light chain; MDM2, murine double minute 2; Mdm2fl/+, Mdm2 heterozygous floxed; Mybpc3-/-, cardiac myosin binding protein 3 homozygous deletion; Myh6:Cre, myosin heavy chain 6:Cre recombinase; Poly-Ub, K48-linked ubiquitin; Rpl32; ribosomal protein L32; Ub, Ubiquitin; VHL, Von Hippel-Lindau; and WT, wild-type.

[0018] Figure 4(A-O) shows increased HIF2α in the Mybpc3-/- myocardium occurs secondary to MDM2 facilitated degradation of VHL. (A) Vhlgene expression in left ventricular tissue RNA from postnatal day 7 (P7) WT (n=14) and Mybpc3–/– (n=14) mice. Vhl gene expression was normalized to Rpl32 expression and fold-change is relative to WT. (B) and (C) Immunoblots and protein quantification for VHL in left ventricular tissue from P7 WT (n=6), Mybpc3–/– (n=6) and BTZ-injected Mybpc3–/– (n=6) mice normalized to β-actin and relative to WT. (D) Coimmunoprecipitation for MDM2 was performed in left ventricular tissue lysates from P7 WT and Mybpc3–/– mice and then immunoblots were performed for VHL and MDM2. The third WT sample (WT(-)Ab) and the third Mybpc3–/– sample (Mybpc3–/– (-) Ab) also underwent bead only precipitation without the MDM2 antibody as a negative control experiment (WT (-) Ab and Mybpc3-/- (-) Ab). The input left ventricular tissue lysates also underwent immunoblotting for MDM2, VHL, and β-actin. (E) and (F) Representative in situ proximity ligation assay images and quantification for MDM2 and VHL protein complexes in left ventricular tissue from P7 WT (n=4), Mybpc3–/– (n=4), and Mybpc3–/–Mdm2fl/+/Myh6:Cre (n=4) mice. Three nonoverlapping left ventricular images per sample; scale bars=25 μm. (G) and (H) Representative in situ proximity ligation assay images and quantification for Ub-modified VHL in left ventricular tissue from BTZ-treated P7 WT (n=4), Mybpc3–/– (n=4), and Mybpc3–/–Mdm2fl/+/Myh6:Cre (n=4) mice. Three nonoverlapping left ventricular images per sample; scale bars=25 μm. (I) Immunoprecipitation (IP) for VHL was performed on left ventricular tissue lysates from BTZ-injected P7 WT, Mybpc3–/–, and Mybpc3–/–Mdm2fl/+/Myh6:Cre mice and then immunoblots were performed Poly-Ub and VHL. The input left ventricular tissue lysates also underwent immunoblotting for

VHL and β-actin. J, Hif2α gene expression in left ventricular tissue RNA from P7 WT (n=6) and Mybpc3–/– (n=6) mice. Hif2α gene expression was normalized to Rpl32 and fold change is relative to WT. (K) and (L) Representative in situ proximity ligation assay images for VHL and HIF2α protein complexes in left ventricular tissue from P7 WT (n=4), Mybpc3–/– (n=4), and Mybpc3–/–Mdm2fl/+/Myh6:Cre (n=4) mice. Three nonoverlapping left ventricular images per sample; scale bars=25 μm. (M) and (N) Representative in situ proximity ligation assay images and quantification for Ub-modified HIF2α in left ventricular tissue from BTZ-injected P7 WT (n=4), Mybpc3–/– (n=4), and Mybpc3–/–Mdm2fl/+/Myh6:Cre (n=4) mice. Three nonoverlapping left ventricular images per sample; scale bars=25 μm. (O) IP for HIF2α was performed on left ventricular tissue lysates from BTZ-injected P7 WT, Mybpc3–/–, and Mybpc3–/–Mdm2fl/+/Myh6:Cre mice, and then immunoblots for Poly–Ub and HIF2α. The input left ventricular tissue lysates also underwent immunoblotting for HIF2α and β-actin. All results are shown as mean±SEM. Student t test was used for (A) and (J); 1-way ANOVA with Tukey or Dunnett T3 multiple comparison test were used for (C), (F), (H), (L), and (N). BTZ indicates bortezomib; DAPI, 4′,6-diamidino-2-phenylindole; HC, heavy chain; HIF1α, hypoxia-inducible factor 1 alpha; HIF2α, hypoxia-inducible factor 2 alpha; IB, immunoblot; LC, light chain; MDM2, murine double minute 2; Mdm2fl/+, Mdm2 heterozygous floxed; Mybpc3-/-, cardiac myosin binding protein 3 homozygous deletion; Myh6:Cre, myosin heavy chain 6:Cre recombinase; Poly-Ub, K48-linked ubiquitin; Ub, Ubiquitin; VHL, Von Hippel-Lindau; and WT, wild-type.

[0019] Figure 5(A-I) shows reduction of cardiomyocyte MDM2 in Mybpc3-/- mice increases myocardial capillary formation and proangiogenic gene expression. (A) Representative immunohistochemistry images for CD31 costained with WGA in left ventricular tissue from postnatal day 7 (P7) WT, Mdm2fl/+/Myh6:Cre, Mybpc3–/–, and Mybpc3–/–Mdm2fl/+/Myh6:Cre mice. Nuclei are blue (DAPI); scale bars=30 μm. (B) Capillary to cardiomyocyte ratios in left ventricular tissue from P7 WT (n=6), Mdm2fl/+/Myh6:Cre (n=5), Mybpc3–/– (n=6), and Mybpc3–/– Mdm2fl/+/Myh6:Cre (n=4) mice. Minimum 100 cardiomyocytes per sample. (C) Proangiogenic gene expression (e.g., Vegfa, Vegfb, Vegfc [vascular endothelial growth factor a/b/c], Angpt1, Angpt2 [angiopoietin 1/2], Pgf [placental growth factor], Pdgfb [platelet-derived growth factor subunit b]) in left ventricular tissue RNA from P7 WT (n=6), Mybpc3–/– (n=6), and Mybpc3–/– Mdm2fl/+/Myh6:Cre (n=5) mice. The genes of interest were normalized to Rpl32 (ribosomal protein L32) and fold changes are relative to WT. (D) Representative immunohistochemistry images for CD3 costained with WGA in left

ventricular tissue from P7 Myh6:MerCreMer (MCM) and Hif1αfl/flMCM mice injected with tamoxifen at postnatal days 1 (P1) and 4 (P4). Nuclei are blue (DAPI); scale bars=50 μm. (E) Capillary-to-cardiomyocyte ratios in left ventricular tissue from P7 MCM (n=9) and Hif1αfl/flMCM (n=10) injected with tamoxifen at P1 and P4. Minimum 200 cardiomyocytes per sample. F, Heart weight (mg)–to–body weight (g) ratios (HW/BW) from P7 MCM (n=9) and Hif1αfl/fl MCM (n=10) mice injected with tamoxifen at P1 and P4. (G) Representative immunohistochemistry images for CD31 (green) costained with WGA (red) in left ventricular tissue from P7 Mybpc3–/– and Mybpc3–/–Hif2αfl/fl/Myh6:Cre mice. Scale bars=50 μm. H, Capillary-to-cardiomyocyte ratios in left ventricular tissue from P7 WT (n=6), Hif2αfl/fl/Myh6:Cre (n=6), Mybpc3–/– (n=6), and Mybpc3–/–Hif2αfl/fl/Myh6:Cre (n=5) mice. Minimum 200 cardiomyocytes per sample. I, HW/BW from P7 WT (n=6), Hif2αfl/fl/Myh6:Cre (n=6), Mybpc3–/– (n=6), and Mybpc3–/–Hif2αfl/fl/Myh6:Cre (n=6) mice. All results are shown as mean±SEM. Student t test used for (E) and (F); 1-way ANOVA with Tukey or Dunnett T3 multiple comparison test used for (C); 2-way ANOVA with Tukey multiple comparison test used for (B), (H), and (I). CD31 indicates cluster of differentiation 31; DAPI, 4′,6-diamidino-2-phenylindole; HIF1α, hypoxia-inducible factor 1 alpha; HIF2α, hypoxia-inducible factor 2 alpha; Hif2αfl/fl, Hif2α homozygous floxed; IB, immunoblot; MDM2, murine double minute 2; Mdm2fl/+, Mdm2 heterozygous floxed; MerCreMer, tamoxifen inducible Cre recombinase; Mybpc3-/-, cardiac myosin binding protein 3 homozygous deletion; WGA, wheat germ agglutinin; and WT, wild-type.

[0020] Figure 6(A-O) shows MDM2 regulates capillary formation in Myh6R404Q/WT mice before the development of ventricular hypertrophy. (A) Representative hematoxylin-eosin–stained heart cross-sections of postnatal days 25 (P25) and 60 (P60) WT and Myh6R404Q/WT mice. Scale bars=1 mm. Echocardiography assessment of (B) interventricular septal thickness at end diastole (IVSd) and (C) left ventricular posterior wall thickness at end diastole (LVPWd) in WT (n=10–11) and Myh6R404Q/WT (n=19–24) mice at P25, P60, or postnatal day 180 (P180). (D) Representative images of WGA–stained left ventricular tissue from WT and Myh6R404Q/WT mice at P25 or P60. Scale bar=75 μm. (E) Cardiomyocyte cross-sectional areas from WGA-stained left ventricular tissue from WT (n=5–6) and Myh6R404Q/WT (n=5–6) mice at postnatal day 7 (P7), P25, or P60. Minimum 50 cardiomyocytes per sample. (F) Representative immunohistochemistry images for CD31 (green) costained with WGA in left ventricular tissue from P7 WT and Myh6R404Q/WT mice. Scale bars=50 μm. G, Capillary-to-cardiomyocyte ratios in left ventricular tissue from WT (n=5–6) and Myh6R404Q/WT

(n=5–6) mice at postnatal day 2, P7, or P25. Minimum 200 cardiomyocytes per sample. (H) Representative fluorescence images for the intravascularly injected endothelial cell stain T-lectin in left ventricular tissue from P7 WT and Myh6R404Q/WT mice. Scale bars=80 μm. I, Capillaries per mm2 in left ventricular tissue from P7 WT (n=6) and Myh6R404Q/WT (n=6) mice; 3 cross-sectional images per sample were analyzed. (J) through (M) Immunoblots and quantification for MDM2, HIF1α, and HIF2α in left ventricular tissue lysates from P7 WT (n=6–9) and Myh6R404Q/WT (n=6–9) mice normalized to β-actin and relative to WT. (N) Capillary to cardiomyocyte ratios were calculated from left ventricular tissue in P7 WT (n=6), Mdm2fl/+/Myh6:Cre (n=6), Myh6R404Q/WT (n=6), and Myh6R404Q/WTMdm2fl/+/Myh6:Cre (n=6) mice. Minimum 200 cardiomyocytes per sample. (O) Coronary flow reserve in P25 WT (n=5), Mdm2fl/+/Myh6:Cre (n=5), Myh6R404Q/WT (n=6), and Myh6R404Q/WTMdm2fl/+/Myh6:Cre (n=5) mice. All results are shown as mean±SEM. Student or Welch t test used for (I), (K), (L), and (M); 2-way ANOVA with Tukey multiple comparison test used for (B), (C), (E), (G), (N), and (O). CD31 indicates cluster of differentiation 31; DAPI, 4′,6-diamidino-2-phenylindole; HIF1α, hypoxia-inducible factor 1 alpha; HIF2α, hypoxia-inducible factor 2 alpha; MDM2, murine double minute 2; Mdm2fl/+Cre, Mdm2 heterozygous floxed and Myh6:Cre; Mybpc3-/-, cardiac myosin binding protein 3 homozygous deletion; Myh6:Cre, myosin heavy chain 6:Cre recombinase; Myh6R404Q/WT, myosin heavy chain 6 arginine to glutamine substitution at amino acid 404 heterozygous; T-lectin, tomato lectin; WGA, wheat germ agglutinin; and WT, wild-type.

[0021] Figure 7(A-I) shows chemical inhibition of MDM2 prevents microvascular dysfunction in 2 distinct HCM models. (A) Schematic of injections of vehicle or MDM2 PROTAC (MD-224) from postnatal days 1 (P1) to 6 (P6). (B) Immunoblots for MDM2, HIF1α, and HIF2α in left ventricular tissue from postnatal day 7 (P7) WT or Mybpc3–/– injected with vehicle or MD-224. (C) Immunoblots for MDM2, HIF1α, and HIF2α in left ventricular tissue from P7 WT and Myh6R404Q/WT injected with vehicle or MD-224. (D) Representative immunohistochemistry images for CD31 costained with WGA in left ventricular tissue from P7 Mybpc3–/– and Myh6R404Q/WT injected with vehicle or MD-224 from P1 to P6. Nuclei are blue (DAPI); scale bars=50 μm. E, Capillary-to-cardiomyocyte ratios in left ventricular tissue from P7 WT vehicle (n=6), WT MD-224 (n=6), Mybpc3–/– vehicle (n=6), Mybpc3–/– MD-224 (n=5), Myh6R404Q/WT vehicle (n=7), and Myh6R404Q/WT MD-224 (n=6) mice. All groups injected from P1 to P6 with either vehicle or MD-224. Minimum 200 cardiomyocytes per sample. F, Schematic

of WT or Myh6R404Q/WT mice injected with vehicle or MDM2 PROTAC (MD-224) from P1 to postnatal day 24 (P24), and then analyzed at postnatal day 60 (P60). (G) Representative immunohistochemistry images for CD3 costained with WGA in left ventricular tissue from P60 Myh6R404Q/WT mice injected with vehicle or MD-224 from P1 to P24. Scale bars=15 μm. (H) Capillary-to-cardiomyocyte ratios in left ventricular tissue from P60 WT vehicle (n=6), WT MD-224 (n=6), Myh6R404Q/WT vehicle (n=6), and Myh6R404Q/WT MD-224 (n=6) mice. All groups injected from P1 to P24 with vehicle or MD-224. Minimum 140 cardiomyocytes per sample. (I) Coronary flow reserve was calculated in P60 WT vehicle (n=6), WT MD-224 (n=6), Myh6R404Q/WT vehicle (n=5), and Myh6R404Q/WT MD-224 (n=6) mice. All results are shown as mean±SEM. Student or Welch t test used for (E), (H), and (I). CD31 indicates cluster of differentiation 31; DAPI, 4′,6-diamidino-2-phenylindole; HIF1α, hypoxia inducible factor 1 alpha; HIF2α, hypoxia-inducible factor 2 alpha; MDM2, murine double minute 2; Mybpc3-/-, cardiac myosin binding protein 3 homozygous deletion; Myh6R404Q/WT, myosin heavy chain 6 arginine to glutamine substitution at amino acid 404 heterozygous; PROTAC, proteolysis targeting chimera; WGA, wheat germ agglutinin; and WT, wild-type.

[0022] Figure 8(A-F) shows reduced postnatal capillary formation in the Mybpc3-/- myocardium. (A) Representative immunohistochemistry images for endothelial cell marker CD31 co-stained with WGA in LV tissue from WT and Mybpc3–/– mice at post-natal day 2 (P2), P7, P25 or P180. Cardiomyocytes were counted from WGA images and capillaries were counted from CD31 images. Scale bars=40 μm. (B) Total fluorescence of immunohistochemistry images for CD31 in LV tissue from WT (n=6) and Mybpc3–/– (n=7) mice at P2, P7, P25 or P180. Average fluorescence of 3 non-overlapping LV images/sample. (C) Capillary to cardiomyocyte ratios in LV tissue from WT (male n=3-4, female n=3-4) and Mybpc3–/– (male n=3-4, female n=3-4) at P7 or P25. Minimum 120 cardiomyocytes/sample. (D) Total fluorescence of immunohistochemistry images for TIE2 in LV tissue from WT (n=6) and Mybpc3–/– (n=6-7) mice at P2, P7, P25 or P180. Average fluorescence of 3 non-overlapping LV images/sample. (E) Representative immunohistochemistry images for CD31 and TIE2 in LV tissue from P7 WT and Mybpc3–/– mice. Scale bars=30 μm. (F) CD31-TIE2 colocalization in LV tissue from WT (n=4) and Mybpc3–/– (n=4) mice. Minimum 100 endothelial cells/samples. All results are shown as mean±SEM. Student's t-test was utilized for C and F. Two-way ANOVA with Tukey multiple comparison test was utilized for B and D.

[0023] Figure 9(A-L) shows reduced pericytes and coronary diameter in Mybpc3-/- mice . (A) Representative immunohistochemistry images for NG2 and CD31 in LV tissue from P7 WT and Mybpc3–/– mice. Scale bars=40 μm. (B) Representative fluorescence images for the intravascularly injected endothelial cell stain tomato lectin (TLectin) in LV tissue cross-sections or longitudinal-sections from P60 WT and Mybpc3–/– mice. Scale bars=80 μm. (C) Capillaries per mm2 in LV tissue from P7 WT (n=6) and Mybpc3–/– (n=6) mice. Three cross-sectional images per sample were analyzed. (D) Representative fluorescence images for the intravascularly injected endothelial cell stain tomato lectin (T-Lectin) followed by immunohistochemistry for CD31 in LV tissue from P7 WT mice. Scale bars=10 μm (E) Representative fluorescence images for the intravascularly injected endothelial cell stain tomato lectin (T-Lectin) followed by immunohistochemistry for NG2 in LV tissue from P7 WT mice. Scale bars=10 μm. (F) Representative H&E–stained LV tissue cross-sections showing coronary artery and vein from P7 WT mice. Scale bars=30 μm. (G) Representative immunohistochemistry images for CD31 (green) and CX40 (red) of left coronary artery (LCA) in LV tissue from P7 WT and Mybpc3-/- mice. Scale bars=30 μm. (H) [Top] Representative H&E–stained mid-ventricular LV tissue cross-sections with LCA magnified in WT and Mybpc3–/– mice at P2 or P7. (H) [Bottom] Representative immunohistochemistry images for CD31 (green) with arrow indicating the LCA in LV tissue from WT and Mybpc3–/– mice at P2 or P7. Scale bars=100 μm. (I) LCA cross-sectional area from LV tissue in WT (n=6) and Mybpc3–/– (n=6) mice at P2 or P7. Three independent mid-ventricular images/sample. (J) Representative B-mode echocardiographic images of the proximal LCA from P60 Mybpc3-/- mice with pulsed wave Doppler imaging (left) and without pulsed wave Doppler (right). Aorta (AO) outlined and LCA (arrow) outlined. LCA internal diameter noted by blue line. (K) Representative myocardial blood flow velocity tracing in LCA using pulsed wave Doppler. (L) Representative myocardial blood flow velocity tracing with diastolic specific velocity time integral (VTI) outlined. All results are shown as mean±SEM. Student's t-test was utilized for C and I.

[0024] Figure 10(A-O) shows alterations in MDM2 gene expression and MDM2 protein levels in Mybpc3-/- mice. (A) Representative in situ proximity ligation assay (PLA) images for secondary antibody PLA probes only (+/-), HIF1α antibody and probes, and Ub antibody and probes in LV tissue from P7 WT mice. Scale bars=25 μm. (B) Representative in situ PLA images for secondary antibody PLA probes only (+/-), HIF1α antibody and probes, and Von Hippel Lindau (VHL) antibody and probes in LV tissue from P7 WT mice. Scale bars=25 μm. (C-E) Gene expression for Prolyl domain

hydroxylase 1 (Phd1) (C), Phd2 (D) and Phd3 (E) in LV tissue RNA from P7 WT (n=4) and Mybpc3–/– (n=4) mice. The genes of interest were normalized to Rpl32 and fold changes are relative to WT. (F) Immunoblots for HIF1α and β-actin in LV tissue from P7 Mybpc3–/– vehicle and Mybpc3–/– injected with PHD inhibitor (Molidustat, 10 mg/kg) from P1 to P6. (G) Mdm2 gene expression in LV tissue RNA from WT (n=6-10) and Mybpc3–/– (n=6-10) mice at P2, P7 and P25. Mdm2 gene expression was normalized to Rpl32 and fold change relative to WT. (H) Mdm2 gene expression in LV tissue RNA from P7 WT (n=6), Mybpc3–/– (n=6) and Mybpc3–/–MDM2fl/+/Myh6:Cre (n=6) mice. Mdm2 gene expression was normalized to Rpl32 and fold change relative to WT. (I) Immunoblot for murine double minute 2 (MDM2) LV tissue from WT (n=4-6) and Mybpc3–/– (n=4-6) mice at P2 and P25. (J) Immunoprecipitation (IP) for MDM2 was performed on LV tissue lysates from BTZ injected P7 WT, Mybpc3–/– and Mybpc3–/–MDM2fl/+/Myh6:Cre mice and then immunoblots were performed for K48-linked ubiquitin (Poly-Ub). The input LV tissue lysates also underwent immunoblotting for MDM2 and β-actin. (K) Left Blot: Bead only precipitation without antibody was performed on LV tissue lysates from BTZ injected P7 WT, Mybpc3–/– and Mybpc3–/–MDM2fl/+/Myh6:Cre mice and then immunoblots were performed for K48-linked ubiquitin (Poly-Ub). Right Blot: Immunoprecipitation (IP) for IgG was performed on LV tissue lysates from BTZ injected P7 WT and Mybpc3–/– mice and then immunoblots were performed for K48-linked ubiquitin (Poly-Ub). (L) Representative in situ PLA images and quantification for MDM2 and MDM4 complexes in LV tissue from P7 WT (n=4) and Mybpc3–/– (n=4) mice. Three non-overlapping LV images/sample. Scale bars=25 μm. (M) Immunoblots for murine double minute (MDM2) using three different MDM2 antibodies (clone SMP14, clone Ab-3, clone 4B2C1.11), HIF1α, HIF2α and β-actin in LV tissue from P7 WT, MDM2fl/+/Myh6:Cre, Mybpc3–/– and Mybpc3–/–MDM2fl/+/Myh6:Cre mice. (N) Representative in situ PLA images for secondary antibody PLA probes only (+/-), MDM2 antibody and probes, and HIF1α antibody and probes in LV tissue from P7 WT mice. Non-specific complexes are red and nuclei are blue (DAPI). Scale bars=25 μm. (O) Immunoblot for p53 and β-actin in LV tissue from P7 WT, Mybpc3–/– and Mybpc3–/–MDM2fl/+/Myh6:Cre mice. All results are shown as mean±SEM. Student's or Welch's t-test were utilized for C, D, E, G, and L. One-way ANOVA with Tukey multiple comparison test was utilized for H.

[0025] Figure 11(A-H) shows that VHL NEDD8 post-translational modifications are not altered in Mybpc3-/- mice. Representative in situ proximity ligation assay (PLA) images for secondary antibody PLA probes only (+/-), MDM2 antibody and probes, and VHL

antibody and probes in LV tissue from P7 WT mice. Scale bars=25 μm. (B) Representative in situ PLA images for secondary antibody PLA probes only (+/-), VHL antibody and probes, and Ub antibody and probes in LV tissue from P7 WT mice. Scale bars=25 μm. (C+D) Representative in situ PLA images and quantification for NEDD8 modified VHL in LV tissue from P7 WT (n=4), Mybpc3–/– (n=4) and Mybpc3–/–MDM2fl/+/Myh6:Cre (n=4) mice. VHL-NEDD8 complexes are red, and nuclei are blue (DAPI). Scale bars=25 μm. Three non-overlapping LV images/sample. (E) Representative in situ PLA images for secondary antibody PLA probes only (+/-), VHL antibody and probes, and HIF2α antibody and probes in LV tissue from P7 WT mice. Non-specific complexes are red, and nuclei are blue (DAPI). Scale bars=25 μm. (F+G) Representative in situ PLA images and quantification for MDM2 and HIF2α protein complexes in LV tissue from P7 WT (n=4), Mybpc3–/– (n=4) and Mybpc3–/–MDM2fl/+/Myh6:Cre (n=4) mice. Scale bars=25 μm. Three non-overlapping LV images/sample. (H) Representative in situ PLA images for secondary antibody PLA probes only (+/-), HIF2α antibody and probes, and Ub antibody and probes in LV tissue from P7 WT mice. Scale bars=25 μm. All results are shown as mean±SEM. One-way ANOVA with Tukey multiple comparison test was utilized for D and G.

[0026] Figure 12(A-M) shows genetic reduction of MDM2 protein levels in cardiomyocytes prevents the development of left ventricular hypertrophy and systolic dysfunction in Mybpc3-/- mice. (A) Representative immunohistochemistry images for pericyte marker NG2 and counterstained for WGA in LV tissue from P7 WT, Mybpc3–/– and Mybpc3–/–MDM2fl/+/Myh6:Cre mice. Scale bars=25 μm. (B) Pericyte to cardiomyocyte ratios in LV tissue from P7 WT (n=6), Mybpc3–/– (n=6) and Mybpc3–/–MDM2fl/+/Myh6:Cre (n=6) mice. Minimum 200 cardiomyocytes/sample. (C) Immunoblots for HIF1α and β-actin in LV tissue from WT and HIF1αfl/fl/Myh6:MerCreMer mice injected with tamoxifen at P1 and P4. Left panel - NB100-479 HIF1α antibody, Right panel – NB100-105 HIF1α antibody. (D) Immunoblots for HIF2α and β-actin in LV tissue from P7 WT, HIF2αfl/fl/Myh6:Cre, Mybpc3–/–, and Mybpc3–/–HIF2αfl/fl/Myh6:Cre mice. (E-G) Echocardiography assessment of (E) LV posterior wall thickness at end diastole (LVPWd), (F) LV internal diameter at end diastole (LVIDd) and (G) LV fractional shortening (FS) in P7 WT (n=6), Mdm2fl/+/Myh6:Cre (n=6), Mybpc3–/– (n=7), and Mybpc3–/–MDM2fl/+/Myh6:Cre (n=6) mice. (H-J) Echocardiography assessment of (H) LVPWd, (I) LVIDd and (J) FS in P7 MCM (n=6) and HIF1αfl/fl/Myh6:MerCreMer (n=6) mice injected with tamoxifen at P1 and P4. (K-M) Echocardiography assessment of (K) LVPWd, (L) LVIDd and (M) FS

in P7 WT (n=5), HIF2αfl/fl/Myh6:Cre (n=6), Mybpc3–/– (n=6), and Mybpc3–/–HIF2αfl/fl/Myh6:Cre (n=5) mice. All results are shown as mean±SEM. One-way ANOVA with Tukey multiple comparison test was utilized for B. Student's t-test was utilized for H-J. Two-way ANOVA with Tukey multiple comparison test was utilized for E-G and K-M.

[0027] Figure 13(A-P) shows Myh6R404Q/WT mice have reduced left ventricular capillaries and VHL protein levels. (A) Amino acid comparison between human MYH7 WT and R403Q mutation and the mouse MYH6 WT and R404Q mutation. (B) Chromatogram of DNA sequencing from WT and Myh6R404Q/WT mice. The mutated base pairs create the R404Q amino acid change and the remaining base pair mutations are silent DNA changes which facilitate genotyping and prevent CRISPR/Cas9 mediated cutting of the donor DNA. (C) Fractional shortening (FS) in P60 WT (n=10) and Myh6R404Q/WT (n=9) mice. (D-G) Echocardiography assessment of (D) interventricular septal thickness at end diastole (IVSd), (E) left ventricular [LV] posterior wall thickness at end diastole (LVPWd), (F) LV internal diameter at end diastole (LVIDd), and (G) FS in male (n=8-11) and female (n=8-11) Myh6R404Q/WT mice at P25, P60 or P180. (H) Capillary to cardiomyocyte ratios in LV tissue from WT (male n=4, female n=3-4) and Myh6R404Q/WT (male n=4-5, female n=4) mice at P7 or P25. Minimum 100 cardiomyocytes/sample. (I) Representative H&E–stained heart cross-sections of P7 WT and Myh6R404Q/WT mice showing left coronary artery (LCA) [top]. Representative immunohistochemistry images for CD31with LCA (arrow) in LV tissue from P7 WT and Myh6R404Q/WT mice [bottom]. Scale bars=100 μm. (J) LCA cross-sectional area in LV tissue from P7 WT and Myh6R404Q/WT mice (n=6/group). Three independent mid-ventricular images/sample. (K) Representative immunohistochemistry images for the DNA damage marker γH2AX and cardiomyocyte (CM) nuclei marker pericentriolar material 1 (PCM1) in LV tissue from P7 WT and Myh6R404Q/WT mice. Scale bars=25 μm. (L) CM nuclear γH2AX fluorescence in LV tissue from P7 WT (n=4) and Myh6R404Q/WT (n=4) mice. Minimum 100 CM nuclei/sample. (M) Representative immunohistochemistry images for γH2AX and endothelial cell (EC) marker CD31 in LV tissue from P7 WT and Mybpc3–/– mice. Scale bars=10 μm. (N) EC nuclear γH2AX fluorescence in LV tissue from P7 WT (n=4) and Mybpc3–/– (n=4) mice. Minimum 50 EC nuclei/sample. (O+P) Immunoblots and quantification for VHL in LV tissue lysates from P7 WT (n=6) and Myh6R404Q/WT (n=6) mice normalized to βactin and relative to WT. Student's t-test was utilized for C, H, J, L, N and P. Two-way ANOVA with Tukey multiple comparison test was utilized for D, E, F, and G.

[0028] Figure 14(A-D) shows genetic reduction of cardiomyocyte MDM2 protein levels improves myocardial capillary density and myocardial coronary flow reserved in Myh6R404Q/WT mice. (A) Representative immunohistochemistry images for CD31 co-stained with WGA in LV tissue from P7 WT, Mdm2fl/+Cre, Myh6R404Q/WT and Myh6R404Q/WTMdm2fl/+Cre mice. Scale bars=40 μm. (B) Representative myocardial blood flow velocity tracings from pulsed wave Doppler echocardiography of P25 WT, Mdm2fl/+Cre, Myh6R404Q/WT and Myh6R404Q/WTMdm2fl/+Cre mice. Myocardial blood flow before (baseline) and after injection with adenosine (post-ado) to induce maximal hyperemia. (C) Myocardial blood flow in P25 WT (n=5), Mdm2fl/+Cre (n=5), Myh6R404Q/WT (n=6) and Myh6R404Q/WTMdm2fl/+Cre (n=5) mice. Myocardial blood flow before adenosine (left bars) and postadenosine (right bars) was calculated and normalized to heart weight. All results are shown as mean±SEM. (D) Representative immunohistochemistry images of heart cross sections from P7 WT, Mybpc3–/– and Myh6R404Q/WT mice injected with pimonidazole (hypoxyprobe). Scale bars=0.5 mm. Student's or Welch's t-test were utilized for C.

[0029] Figure 15(A-M) shows MD-224 reduces left ventricular cardiomyocyte size and myocardial hypertrophy with improvement in left ventricular systolic function in Mybpc3-/- and Myh6R404Q/WT mice. (A) Cardiomyocyte cross-sectional areas from WGA stained LV tissue from P7 and P25 Mybpc3–/– (n=6) mice injected with vehicle or MD-224 (MD). Minimum 50 cardiomyocytes/sample. (B) Heart weight to body weight ratio (HW/BW) from P7 and P25 Mybpc3–/– (n=6-12) mice injected with vehicle or MD-224. Echocardiography assessment of (C) fractional shortening (FS), (D) interventricular septal thickness at end diastole (IVSd), (E) left ventricular [LV] posterior wall thickness at end diastole (LVPWd), and (F) LV internal diameter at end diastole (LVIDd) in P7 and P25 Mybpc3–/– (n=6-13) injected with vehicle or MD-224. (G) Representative myocardial blood flow velocity tracings from pulsed wave Doppler echocardiography of P60 Myh6R404Q/WT mice injected with vehicle or MDM2 PROTAC (MD-224) from P1 to P24. Myocardial blood flow before (baseline) and after retro-orbital injection with adenosine (post-ado) to induce maximal hyperemia. (H) Cardiomyocyte cross-sectional areas from WGA stained LV tissue from P60 WT and Myh6R404Q/WT (n=6) mice injected with vehicle or MD-224. Minimum 50 cardiomyocytes/sample. (I) Heart weight to tibial length ratio (HW/TL) from P60 WT (n=6) and Myh6R404Q/WT (n=6-7) mice injected with vehicle or MD-224. Echocardiography assessment of (J) fractional shortening (FS), (K) interventricular septal thickness at end diastole (IVSd), (L) left ventricular [LV] posterior wall thickness

at end diastole (LVPWd), and (M) LV internal diameter at end diastole (LVIDd) in P60 WT (n=6) and Myh6R404Q/WT (n=6-7) injected with vehicle or MD-224. Student's or Welch's t-test were utilized for A-F and H-M.

[0030] Figure 16(A-C) shows genetic reduction of cardiomyocyte MDM2 prevents the development of cardiomyopathy in pressure overload mice. (**A+B**) Echocardiograms were performed before thoracic aortic constriction (Pre-TAC) and 6 weeks after TAC in Myh6:Cre only and $MDM2^{fl/+}$/Myh6:Cre mice for (**A**) left ventricular posterior wall thickness at end diastole (LVPWd) and **(B)** LV fractional shortening (FS) were measured. **(C)** Heart weight and tibia lengths ratios were calculated in mice 6 weeks after sham or TAC surgery.

[0031] Figure 17 shows Table I.

DETAILED DESCRIPTION

[0001] Provided herein are methods of increasing myocardial capillary growth in a subject and treating a myocardial microvascular dysfunction and/or a cardiomyopathy in a subject comprising administering an MDM2 inhibitor to the subject. One surprising finding described herein is that reducing an MDM2 level or functioning reduces or prevents the development of microvascular dysfunction in hypertrophic cardiomyopathy (HCM) models. These and other embodiments are described below.

[0002] Terminology

[0003] Terms used throughout this application are to be construed with ordinary and typical meaning to those of ordinary skill in the art. However, Applicants desire that the following terms be given the particular definition as defined below.

[0004] As used in the specification and claims, the singular form "a," "an," and "the" include plural references unless the context clearly dictates otherwise. For example, the term "a cell" includes a plurality of cells, including mixtures thereof.

[0005] The terms "about" and "approximately" are defined as being "close to" as understood by one of ordinary skill in the art. In one non-limiting embodiment the terms are defined to be within 10%. In another non-limiting embodiment, the terms are defined to be within 5%. In still another non-limiting embodiment, the terms are defined to be within 1%.

[0006] The term "administering" refers to an administration that is oral, topical, intravenous, subcutaneous, transcutaneous, transdermal, intramuscular, intra-joint, parenteral, intra-arteriole, intradermal, intraventricular, intracranial, intraperitoneal, intralesional, intranasal, rectal, vaginal, by inhalation or via an implanted reservoir. The

term “parenteral” includes subcutaneous, intravenous, intramuscular, intra-articular, intra-synovial, intrasternal, intrathecal, intrahepatic, intralesional, and intracranial injections or infusion techniques.

[0007] A "composition" is intended to include a combination of active agent and another compound or composition, inert (for example, a detectable agent or label) or active, such as an adjuvant.

[0008] A "control" is an alternative subject or sample used in an experiment for comparison purpose. A control can be "positive" or "negative." In some embodiments, a control is a subject, a sample from a subject, or a heart cell from a subject prior to treatment. In other embodiments, a control is a study population having a cardiomyopathy such as a hypertrophic cardiomyopathy.

[0009] As used herein, the term “expression” refers to either or both “gene expression” and “protein expression.” “Gene expression” refers to the process by which polynucleotides are transcribed into mRNA and “protein expression” refers to the process by which mRNA is translated into peptides, polypeptides, or proteins.

[0010] The term "identity" shall be construed to mean the percentage of nucleotide bases or amino acid residues in the candidate sequence that are identical with the bases or residues of a corresponding sequence to which it is compared, after aligning the sequences and introducing gaps, if necessary to achieve the maximum percent identity for the entire sequence, and not considering any conservative substitutions as part of the sequence identity. Neither N- nor C-terminal extensions nor insertions shall be construed as reducing identity or homology. A polynucleotide or polynucleotide region (or a polypeptide or polypeptide region) that has a certain percentage (for example, 80%, 85%, 90%, or 95%) of "sequence identity" to another sequence means that, when aligned over their full lengths, that percentage of bases (or amino acids) are the same in comparing the two sequences. This alignment and the percent homology or sequence identity can be determined using software programs known in the art. In one embodiment, default parameters are used for alignment. In one embodiment a BLAST program is used with default parameters. In one embodiment, BLAST programs BLASTN and BLASTP are used with the following default parameters: Genetic code=standard; filter=none; strand=both; cutoff=60; expect=10; Matrix=BLOSUM62; Descriptions=50 sequences; sort by=HIGH SCORE; Databases=non-redundant, GenBank+EMBL+DDBJ+PDB+GenBank CDS translations+SwissProtein+SPupdate+PIR.

[0011] As used herein, the terms “increase,” “increased” and “increasing” mean to increase by a statistically significant amount. In some embodiments, the increase is about

10%, about 20%, about 30%, about 40%, about 50%, about 60%, about 70, about 80%, about 90%, or about 95%.

[0012] "Mammal" for purposes of treatment refers to any animal classified as a mammal, including human, domestic and farm animals, nonhuman primates, and zoo, sports, or pet animals, such as dogs, horses, cats, cows, etc.

[0013] A "pharmaceutical composition" is intended to include the combination of an active agent with a pharmaceutically acceptable carrier, inert or active, making the composition suitable for diagnostic or therapeutic use in vivo or ex vivo.

[0014] The term "pharmaceutically acceptable carrier" means a carrier or excipient that is useful in preparing a pharmaceutical composition that is generally safe and non-toxic, and includes a carrier that is acceptable for veterinary and/or human pharmaceutical use. As used herein, the term "pharmaceutically acceptable carrier" encompasses any of the standard pharmaceutical carriers, such as a phosphate buffered saline solution, water, and emulsions, such as an oil/water or water/oil emulsion, and various types of wetting agents. As used herein, the term "carrier" encompasses any excipient, diluent, filler, salt, buffer, stabilizer, solubilizer, lipid, stabilizer, or other material well known in the art for use in pharmaceutical formulations and as described further below. The pharmaceutical compositions also can include preservatives. A "pharmaceutically acceptable carrier" as used in the specification and claims includes both one and more than one such carrier.

[0015] The terms "pharmaceutically effective amount", "therapeutically effective amount" or "therapeutically effective dose" refer to the amount of a compound such as an MDM2 inhibitor that will elicit the biological or medical response of a tissue, system, animal, or human that is being sought by the researcher, veterinarian, medical doctor or other clinician. In some embodiments, a desired response is reduction, prevention or treatment of hypertrophic cardiomyopathy or microvascular dysfunction. In some instances, a desired biological or medical response is achieved following administration of multiple dosages of the composition to the subject over a period of days, weeks, or years. The terms "pharmaceutically effective amount", "therapeutically effective amount" or "therapeutically effective dose" include that amount of a compound such as an MDM2 inhibitor that, when administered, is sufficient to prevent development of, or alleviate to some extent, one or more of the symptoms of the condition or disorder being treated. The therapeutically effective amount will vary depending on the compound such as an MDM2 inhibitor, the disorder or conditions and its severity, the route of administration, time of administration, rate of excretion, drug combination, judgment of the treating physician, dosage form, and the age, weight, general health, sex and/or diet of the subject to be

treated. In the context of the present method, a pharmaceutically or therapeutically effective amount or dose of an MDM2 inhibitor includes an amount that is sufficient to prevent, reduce or treat hypertrophic cardiomyopathy or microvascular dysfunction. In some instances, a desired biological or medical response is achieved following administration of multiple dosages of the MDM2 inhibitor composition to the subject over a period of days, weeks, or years.

[0016] As used herein, the terms "reduce," "reduced" and "reducing" mean to decrease by a statistically significant amount. In some embodiments, the reduction is about 10%, about 20%, about 30%, about 40%, about 50%, about 60%, about 70, about 80%, about 90%, or about 95%.

[0017] As used herein, "RNAi" or RNA interference" refers to a process where a small RNA molecule, including but not limited to tinyRNA, cityRNA, siRNA, miRNA, and shRNA, reduces gene expression by binding and blocking the mRNA, protein translation enzymes, or a combination thereof, from performing intended functions.

[0018] The term "subject" is defined herein to include animals such as mammals, including, but not limited to, primates (e.g., humans), cows, sheep, goats, horses, dogs, cats, rabbits, rats, mice and the like. In some embodiments, the subject is a human.

[0019] The terms "treat," "treating," "treatment," and grammatical variations thereof as used herein, include partially or completely delaying, alleviating, mitigating or reducing the intensity of one or more attendant symptoms of a disorder or condition and/or alleviating, mitigating or impeding one or more causes of a disorder or condition. Treatments according to the invention may be applied preventively, prophylactically, pallatively or remedially. Treatments are administered to a subject prior to onset (*e.g.*, before obvious signs of myocardial microvascular dysfunction and/or a cardiomyopathy), during early onset (*e.g.*, upon initial signs and symptoms of myocardial microvascular dysfunction and/or a cardiomyopathy), or after an established development of myocardial microvascular dysfunction and/or a cardiomyopathy. Prophylactic administration can occur for several days to years prior to the manifestation of symptoms of myocardial microvascular dysfunction and/or a cardiomyopathy.

[0020] In some instances, the terms "treat", "treating", "treatment" and grammatical variations thereof, include partially or completely reducing myocardial microvascular dysfunction, reducing left ventricular hypertrophy, reducing left ventricular dysfunction, reducing chronic angina, reducing adverse ventricular remodeling and/or reducing a cardiomyopathy as compared with prior to treatment of the subject or as compared with the incidence of such symptom in a general or study population. In some embodiments,

the method provided herein reduces a hypertrophic cardiomyopathy as compared with prior to treatment of the subject or as compared with the incidence of such symptom in a general or study population. In some embodiments, the method provided herein reduces a left ventricular hypertrophy as compared with prior to treatment of the subject or as compared with the incidence of such symptom in a general or study population. In some embodiments, the method provided herein reduces a left ventricular dysfunction as compared with prior to treatment of the subject or as compared with the incidence of such symptom in a general or study population. The terms "treat", "treating", "treatment" and grammatical variations thereof, can also include preventing myocardial microvascular dysfunction, left ventricular hypertrophy, left ventricular dysfunction, chronic angina, adverse ventricular remodeling and/or cardiomyopathy as compared with the incidence of such symptom in a general or study population.

[0021] **Detailed Description**

[0022] Provided herein are methods of increasing myocardial capillary growth in a subject and treating a myocardial microvascular dysfunction and/or a cardiomyopathy in a subject comprising administering an MDM2 inhibitor to the subject. Described herein is a surprising finding that reducing MDM2 level or functioning reduces or prevents the development of microvascular dysfunction in hypertrophic cardiomyopathy (HCM) models. Accordingly, in some embodiments, a method of treating a myocardial microvascular dysfunction in a subject is provided comprising administering an E3 ubiquitin-protein ligase MDM2 polypeptide (MDM2) inhibitor to a heart cell in the subject. In other embodiments, a method of treating a cardiomyopathy in a subject is provided comprising administering an E3 ubiquitin-protein ligase MDM2 polypeptide (MDM2) inhibitor to a heart cell in the subject. In certain aspects, the heart cell is a cardiomyocyte.

[0023] As used herein, "MDM2" refers herein to a polypeptide that, in humans, is encoded by the MDM2 gene. MDM2 is also referred to as the E3 Ubiquitin-Protein Ligase since the gene encodes an E3 ubiquitin ligase. In some embodiments, the MDM2 polypeptide or polynucleotide is that identified in one or more publicly available databases as follows: HGNC: 6973, NCBI: 4193, Ensembl: ENSG00000135679, OMIM: 164785, UniProtKB: Q00987. In some embodiments, the MDM2 polypeptide comprises the sequence of SEQ ID NO: 1, or a polypeptide sequence having at or greater than about 70%, about 75%, about 80%, about 85%, about 90%, about 95%, or about 98% identity with SEQ ID NO: 1, or a polypeptide comprising a portion of SEQ ID NO: 1. The MDM2 polypeptide of SEQ ID NO:1 may represent an immature or pre-processed form

of mature MDM2, and accordingly, included herein are mature or processed portions of the MDM2 polypeptide in SEQ ID NO: 1. In some embodiments, the MDM2 polynucleotide encodes an MDM2 polypeptide comprising the sequence of SEQ ID NO: 1, or a polypeptide sequence having at or greater than about 70%, about 75%, about 80%, about 85%, about 90%, about 95%, or about 98% identity with SEQ ID NO: 1, or a polypeptide comprising a portion of SEQ ID NO: 1.

[0024] An "MDM2 inhibitor" comprises any composition that reduces or disrupts MDM2 function in a cell. Described herein is the surprising finding that MDM2 dynamically regulates the protein stability of both HIF1α and HIF2α, which in turn leads to reduced proangiogenic gene expression during a key period of myocardial capillary growth. Accordingly, in some embodiments, reducing or disrupting MDM2 function in a cell refers to reducing or disrupting MDM2 regulation of HIF1α and/or HIF2α. Reducing or disrupting MDM2 function in a cell such as a cardiomyocyte can prevent or reduce a decrease in (or increase) myocardial capillary growth or formation as compared to a control.

[0025] Accordingly, in some embodiments, administration of a composition comprising an MDM2 inhibitor to a subject increases myocardial capillary growth or formation as compared to a control. In those and/or other embodiments, administration of a composition comprising an MDM2 inhibitor to a subject prevents or reduces myocardial microvascular dysfunction as compared to a control. One exemplary control is the subject prior to administration. Another exemplary control is one or more members of a general study population likely to develop myocardial microvascular dysfunction.

[0026] As used herein, "myocardial microvascular dysfunction" refers to a reduction in the blood flow through microvasculature of the myocardium as compared to non-diseased myocardial tissue. Such reduction can be due to blood vessel damage, reduced number of blood vessels, or reduced function of blood vessels. Myocardial microvascular dysfunction can be detected using a coronary or myocardial flow reserve measurement. Reducing or preventing myocardial microvascular dysfunction can in turn also reduce or prevent chronic angina, adverse ventricular remodeling and/or a cardiomyopathy.

[0027] Accordingly, included herein are methods of treating chronic angina, adverse ventricular remodeling or a cardiomyopathy in a subject comprising administering an MDM2 inhibitor to heart cell in the subject. In some embodiments, the heart cell is a cardiomyocyte. In some aspects, the cardiomyopathy is a myocardial hypertrophy or a dilated cardiomyopathy. The myocardial hypertrophy can be a hypertrophic

cardiomyopathy (HCM), a hypertensive heart disease or an aortic stenosis. Accordingly, in some embodiments, the cardiomyopathy is a hypertrophic cardiomyopathy (HCM). In other embodiments, the cardiomyopathy is hypertensive heart disease. In still other embodiments, the cardiomyopathy is aortic stenosis. When the cardiomyopathy is a dilated cardiomyopathy, it can include reduced LV systolic function and/or increased left ventricular dilation.

[0028] Reducing or disrupting MDM2 function for any method described herein (such as increasing myocardial capillary growth or formation, treating myocardial microvascular dysfunction, or treating cardiomyopathy) can be achieved via any means, including, but not limited to, reducing MDM2 expression and reducing MDM2-mediated hypoxia-inducible factor (HIF) signaling. The reduced expression can be reduced MDM2 gene expression and/or reduced MDM2 protein expression. For example, in some embodiments, the MDM2 inhibitor is an RNAi such as a tinyRNA, cityRNA, siRNA, miRNA, or a shRNA. In some aspects, MDM2 expression is reduced by about 10%, about 20%, about 30%, about 40%, about 50%, about 60%, about 70%, about 80%, about 90% or about 100% as compared to a control. In other embodiments, the MDM2 inhibitor is a small molecule chemical composition or protein that either inhibits MDM2 function or reduces MDM2 protein levels.

[0029] As used herein, "MDM2-mediated hypoxia-inducible factor (HIF) signaling" refers to any MDM2-mediated changes in HIF1α and/or HIF2α levels, ratios, stability or activity in a heart cell. Reducing MDM2-mediated HIF signaling refers to reducing MDM2's effect on HIF1α and/or HIF2α levels, ratios, stability or activity in a heart cell. A surprising finding described herein is that MDM2 can regulate the protein stability of HIF1α and/or HIF2α and lead to an imbalance or change in ratio of HIF1α and HIF2α. Accordingly, included herein are methods of administering an MDM2 inhibitor to a heart cell of subject wherein the ratio of HIF1α and HIF2α is changed as compared to prior to treatment or a control or study population having a cardiomyopathy such as a hypertrophic cardiomyopathy.

[0030] It may be advantageous in certain aspects for the MDM2 inhibitor to reduce MDM2 expression or function transiently, or only for a limited time. Accordingly, included herein are methods wherein the inhibition of MDM2 is transient or administration of the MDM2 inhibitor is limited to a particular disease stage. For example, in certain aspects, the MDM2 inhibitor administration occurs during a pre or early left ventricular hypertrophy period of hypertrophic cardiomyopathy.

[0031] The disclosed methods can be performed any time prior to the onset of myocardial microvascular dysfunction, left ventricular hypertrophy, left ventricular dysfunction, or cardiomyopathy. In one aspect, the disclosed methods can be employed 12, 11, 10, 9, 8, 7, 6, 5, 4, 3, 2, or 1 months; 30, 29, 28, 27, 26, 25, 24, 23, 22, 21, 20, 19, 18, 17, 16, 15, 14, 13, 12, 11, 10, 9, 8, 7, 6, 5, 4, or 3 days; 60, 48, 36, 30, 24, 18, 15, 12, 10, 9, 8, 7, 6, 5, 4, 3, or 2 hours; 60, 48, 36, 30, 24, 18, 15, 12, 10, 9, 8, 7, 6, 5, 4, 3, or 2 minutes prior to the onset of myocardial microvascular dysfunction, left ventricular hypertrophy, left ventricular dysfunction, or cardiomyopathy; or 30, 29, 28, 27, 26, 25, 24, 23, 22, 21, 20, 19, 18, 17, 16, 15, 14, 13, 12, 11, 10, 9, 8, 7, 6, 5, 4, or 3 days; 60, 48, 36, 30, 24, 18, 15, 12, 10, 9, 8, 7, 6, 5, 4, 3, or 2 hours; 60, 48, 36, 30, 24, 18, 15, 12, 10, 9, 8, 7, 6, 5, 4, 3, or 2 minutes after onset of myocardial microvascular dysfunction, left ventricular hypertrophy, left ventricular dysfunction, or cardiomyopathy; or 1, 2, 3, 4, 5, 6, 7, 8, 9, 10, 15, 20, 25, 30, 35, 40, 45, 50, 55, 60, 75, 90, 105, 120 minutes; 3, 4, 5, 6, 7, 8, 9, 10, 11, 12, 15, 18, 24, 30, 36, 48, 60 hours; 3, 4, 5, 6, 7, 8, 9, 10, 11, 12, 13, 14, 15, 16, 17, 18, 19, 20, 21, 22, 23, 24, 25, 26, 27, 28, 29, 30, 45, 60, 90 or more days; 4, 5, 6, 7, 8, 9, 10, 11, 12 or more months; 60, 59, 58, 57, 56, 55, 54, 53, 52, 51, 50, 49, 48, 47, 46, 45, 44, 43, 42, 41, 40, 39, 38, 37, 36, 35, 34, 33, 32, 31, 30, 29, 28, 27, 26, 25, 24, 23, 22, 21, 20, 19, 18, 17, 16, 15, 14, 13, 12, 11, 10, 9, 8, 7, 6, 5, 4, 3, 2, 1 years after the onset of myocardial microvascular dysfunction, left ventricular hypertrophy, left ventricular dysfunction, or cardiomyopathy.

[0032] Dosing frequency for the MDM2 inhibitor of any preceding aspects, includes, but is not limited to, at least once every year, once every two years, once every three years, once every four years, once every five years, once every six years, once every seven years, once every eight years, once every nine years, once every ten year, at least once every two months, once every three months, once every four months, once every five months, once every six months, once every seven months, once every eight months, once every nine months, once every ten months, once every eleven months, at least once every month, once every three weeks, once every two weeks, once a week, twice a week, three times a week, four times a week, five times a week, six times a week, daily, two times per day, three times per day, four times per day, five times per day, six times per day, eight times per day, nine times per day, ten times per day, eleven times per day, twelve times per day, once every 12 hours, once every 10 hours, once every 8 hours, once every 6 hours, once every 5 hours, once every 4 hours, once every 3 hours, once every 2 hours, once every hour, once every 40 min, once every 30 min, once every 20 min, or once

every 10 min. Administration can also be continuous and adjusted to maintaining a level of the MDM2 inhibitor within any desired and specified range.

[0033] The pharmaceutically effective amount of the MDM2 inhibitor composition described herein can be determined by one of ordinary skill in the art and includes exemplary dosage amounts for a mammal of from about 0.5 to about 200 mg/kg of body weight of active composition per day, which can be administered in a single dose or in the form of individual divided doses, such as from 1 to 4 times per day. Alternatively, the dosage amount can be from about 0.5 to about 150 mg/kg of body weight of active composition per day, about 0.5 to 100 mg/kg of body weight of active compound per day, about 0.5 to about 75 mg/kg of body weight of active compound per day, about 0.5 to about 50 mg/kg of body weight of active composition per day, about 0.5 to about 25 mg/kg of body weight of active composition per day, about 1 to about 20 mg/kg of body weight of active composition per day, about 1 to about 10 mg/kg of body weight of active composition per day, about 20 mg/kg of body weight of active composition per day, about 10 mg/kg of body weight of active composition per day, or about 5 mg/kg of body weight of active composition per day.

[0034] Those of skill in the art will understand that the specific dose level and frequency of dosage for any particular subject can be varied and will depend upon a variety of factors, including the activity of the specific compound employed, the metabolic stability and length of action of that compound, the species, age, body weight, general health, sex and diet of the subject, the mode and time of administration, rate of excretion, drug combination, and severity of the particular condition.

[0035] It should be understood that the foregoing relates to preferred embodiments of the present invention and that numerous changes may be made therein without departing from the scope of the invention. The invention is further illustrated by the following examples, which are not to be construed in any way as imposing limitations upon the scope thereof. On the contrary, it is to be clearly understood that resort may be had to various other embodiments, modifications, and equivalents thereof, which, after reading the description herein, may suggest themselves to those skilled in the art without departing from the spirit of the present invention and/or the scope of the appended claims. All patents, patent applications, and publications referenced herein are incorporated by reference in their entirety for all purposes.

[0036] EXAMPLES

[0037] Example 1 Methods

[0038] Murine Models

[0039] The generation of the Mybpc3 null model (Mybpc3tm1d) was previously described. The following murine strains were obtained from the Jackson laboratory: Mdm2tm2.1Glo (031614), Hif1atm3Rsjo (007561), Hif2/Epas1tm1Mcs (008407), Myh6:Cre (011038), and Myh6:MerCreMer (005657). All of the mice obtained from Jackson labs were bred to a C57BL/6J genetic background for at least six generations.

[0040] The Myh6R404Q mouse line was generated by first identifying Cas 9 targets using CRISPOR61 and the guide with the lowest potential off target binding sites was chosen (Figure 16). A mutant donor template DNA encoding the R404Q mutation was created with the specific missense mutation necessary to introduce the R404Q amino acid change and silent DNA substitutions were introduced to create diagnostic restriction sites and to block subsequent rounds of CRISPR/Cas9 target sequence cutting (Figure 16). The guide RNA and Myh6-R404Q donor template successfully created a high rate of gene edited founders but they were all homozygote or compound heterozygote for the Myh6 R404Q mutation and/or Myh6 indels and subsequently died within 7-12 days of birth. Therefore, we created a wild type donor template DNA with a CRISPR blocking mutation (Figure 16) which could be co-injected with the Myh6-R404Q mutant template. Fertilized embryos (C57BL/6J, Jackson Laboratory) produced by natural mating were microinjected in the pronuclei stage with a mixture of 0.66 μM EnGen Cas9 protein (New England Biolabs, Cat. No. M0646T), the Cas9 guide RNA (42.5 ng/μl) and two DNA oligonucleotides, Myh6-R404Q and Myh6-WT (0.5 μM each, synthesized by Integrated DNA Technologies). Injected zygotes were cultured overnight, allowed to develop to the 2-cell stage and then were transferred to the oviducts of pseudo pregnant CD1 female surrogates. The founder mice underwent sequencing to confirm the accuracy of Myh6 allele gene editing and to identify if off-target mutations were introduced. Founder mice were backcrossed to wild type C57BL/6J animals to create heterozygote Myh6R404Q/WT mice and were further backcrossed for 5 generations before utilization in the current study (Figure 13A+B).

[0041] mRNA Isolation and Quantitative RT-PCR

[0042] Tissues for RNA analyses were flash-frozen in liquid nitrogen and placed in -80°C. RNA was extracted from LV heart tissue from post-natal (P) day 7 mouse pups using TRIzol reagent (Invitrogen) after column purification (Zymogen). cDNA was generated from RNA using QuantiTect reverse transcription kit (Qiagen). Gene-specific primers were designed and SYBR Green reagent (Applied Biosystems) was used to perform the PCR (QuantStudio). Two technical replicates of each sample were prepared.

Desired genes were normalized to endogenous housekeeping gene Rpl32 using 2 – ΔΔCt method.

[0043] Immunohistochemistry and Immunofluorescence of Heart Sections

[0044] *Hematoxylin & Eosin (H+E) staining of myocardial tissue*: Hearts were embedded in paraffin or optimal cutting temperature (OCT) compound. 5 or 10 μm heart cross sections were obtained from the apex to the base of the heart and H&E staining was then performed.

[0045] *Immunohistochemistry of myocardial tissue*: Cryosections were cut from OCT embedded myocardial tissues at 5-10 μm. The sections were then fixed for 15 minutes with 4% paraformaldehyde (PFA) and washed with phosphate buffered saline (PBS). They were then permeabilized with 0.2% Triton X-100 and again with PBS. Sections were then incubated with 1% Bovine serum albumin (BSA) in PBS for 1 hour at room temperature. Solo or double primary antibody overnight incubation with HIF1α (1:500, Novus Biologicals, nb100-479), HIF2α (1;500, Novus Biologicals, nb100-122), PCM-1 (1:500, Sigma-Aldrich, HPA023370), MDM2 (1:500, Novus Biologicals, NB100-2736), VHL (1:500, Invitrogen, PA5-27322), CD31 (1:100, Invitrogen, 14-0311-82), TIE2 (1:50, R&D Systems, AF762), NG2 (1:1000, Miltenyi Biotec, 130-097-455), CX40 (1:100, Bicellscientific, 00405) and p-Ser139 Histone h2ax (1:500, γh2ax, Millipore Sigma, 05-636-I) at 4°C was performed. After PBS washes, sections were placed in dark incubation for one hour at room temperature with the following fluorescent secondary antibodies: goat anti-rabbit Alexa Fluor 594 (1:500, A-11005), goat anti-mouse Alexa Fluor 488 (1:500, A-10667), donkey anti-goat Alexa Fluor 488 (1:500, A-11055) and/or donkey anti-mouse Alexa Fluor 594 (1:500, A21203) (Thermo Fisher Scientific). After PBS rinses, sections were mounted with ProLong Gold Antifade with DAPI (Thermo Fisher Scientific) and images were acquired at 10x, 20x, 40x or 100x magnification on a fluorescence microscope (Zeiss Axioplan or Nikon Eclipse TI2). Images were analyzed using ImageJ (http://imagej.nih.gov/ij/) and protein expression was calculated by manual counting and/or fluorescence intensity quantification (as noted in the figure legends).

[0046] *Myocardial tissue capillary density quantification*: Immunohistochemistry was performed with CD31 or TIE2 or NG2 antibodies as described above. The sections were then incubated for 10 minutes with Texas Red or Oregon Green 488- conjugated WGA (Thermo Fisher Scientific, W21405/W6748) diluted 1:200 in PBS. After PBS rinses, sections were mounted with ProlongGold Antifade with DAPI. Images with cardiomyocytes in cross-section were taken from the LV free-wall regions at equal intensities under 40x magnification. To obtain capillary count, capillary marker channel

was first merged with WGA channel using ImageJ. Non-specific background was eliminated by equally adjusting minimum and maximum display range values so that no fluorescence was localized inside the cardiomyocyte cytoplasm. Capillary marker channel was split from WGA channel, and capillaries were manually counted using cell counter plugin in ImageJ. Vessels less than 10 μm in size were classified as capillaries and included in the analysis. Cardiomyocytes were counted from WGA channel and capillary cardiomyocyte ratios were then calculated (Figure 8A). Regions where cardiomyocytes and capillaries were not in cross section were excluded from analysis. CD31 or TIE2 fluorescence intensity was calculated by processing images to eliminate non-specific background as described above in ImageJ and then measuring the total fluorescence intensity per field.

[0047] *Coronary artery cross-sectional area*: Immunohistochemistry was performed with CD31 and CX40 antibodies as described above. Large CD31 positive vessels were confirmed as coronary arteries, and not veins, using CX40 which is a marker for endothelial cells of large arteries. Images for left coronary artery in cross-section were taken at mid ventricular level of the heart at 10x or 20x magnification. Arterial walls were manually traced, and coronary artery cross-sectional area were quantified using Image J software.

[0048] *Cardiomyocyte DNA damage quantification*: Immunohistochemistry was performed with DNA damage response marker γH2AX and PCM1 or CD31 antibodies as described above. Images with cardiomyocyte or endothelial nuclei in cross section were taken from LV free-wall regions at 40x magnification. Nuclear γH2AX fluorescence was determined in cardiomyocytes and endothelial cells using the following equation: corrected nuclear fluorescence = integrated density– (area of nuclei × mean fluorescence of background readings), where integrated density is the fluorescence intensity of the defined region of interest (ROI), area of nuclei is the size of the defined ROI and mean fluorescence background is the average intensity of 5 background ROI.

[0049] Tomato Lectin Capillary Staining

[0050] Neonatal and adult mice were sedated by 5% isoflurane. A mix of 100 μg of Dylight 488-conjugated tomato lectin (Thermo Fisher Scientific, L32470) in 100 μl volume and 100 μl of PBS (total of 200 μl) was directly injected into the LV cavity in adult mice. A total of 100 μl was injected via retroorbital route in neonatal mice. After waiting for two minutes, the hearts were excised and embedded in OCT and 50 μm sections were obtained, slides were mounted and images were acquired for LV free-wall regions. When immunohistochemistry for CD31 or NG2 was performed

[0051] in combination with lectin staining, the sections were fixed using the method for

[0052] immunohistochemistry described above.

[0053] Tissue Hypoxia Assessment

[0054] Mice were injected intraperitoneally with 60 mg/kg of pimonidazole (HP2, Hypoxyprobe Inc) and then euthanized 1hr later. The hearts were harvested and embedded in OCT. 5 μm tissue sections were obtained and fixed with 4% PFA. Sections were permeabilized with 0.2% Triton X-100 and incubated with 1% BSA in PBS for 1 hour at room temperature. Sections were then incubated with a fluorescein-conjugated, anti-pimonidazole, mouse IgG1 monoclonal antibody (Hypoxyprobe Inc) for 1 hour at room temperature in darkness. After PBS washes, sections were counterstained and mounted with ProLong Gold Antifade with DAPI (Thermo Fisher Scientific) and allowed to cure for 30 min in the dark. Slides were imaged at 5x, 20x and 40x magnification (Zeiss Axioplan). Images were processed in ImageJ (http://imagej.nih.gov/ij/) to measure green fluorescence intensity. Multiple images were acquired and stitched together to reconstruct the contour of the heart using the Fiji ImageJ plugin for pairwise-stitching.

[0055] Coronary Flow Reserve Measurement

[0056] Echocardiography and doppler measurement of myocardial blood flow (MBF) was performed using previously described methods.65,66 In brief, transthoracic echocardiography on anesthetized mice at P25 and P60 was performed using a Vevo 3100 (VisualSonics Inc). Short axis B-mode images were acquired, and color Doppler was used to identify the left coronary artery (LCA) and measure the internal LCA diameter (Figure 9J). Baseline LCA velocity was obtained using doppler (Figure 9K) and heart rate was recorded. Mice were then injected with adenosine (0.2 mg/mouse diluted in PBS) retro-orbitally to achieve maximal coronary vasodilation. Maximal hyperemia was achieved after 2 minutes of adenosine injection. Internal LCA diameter and coronary flow velocity were then remeasured, and heart rate was recorded. Velocity time interval (VTI) was then obtained by measuring the area within LCA diastolic flow velocity curve (Figure 9L). Myocardial blood flow (MBF) was then calculated using the formula MBF(ml/min) = $((\pi/4) \times D2 \times VTI \times HR)$ where D is the internal LCA diameter (mm), VTI (velocity time integral) and HR is the heart rate. Myocardial blood flow (MBF) was then indexed to total heart mass by dividing the MBF by heart weight (mg). Coronary flow reserve (CFR) was defined as the ratio of postadenosine MBF divided by baseline MBF (CFR= MBFpost-adenosine/MBFbaseline).

[0057] Immunoblotting and Antibodies

[0058] LV tissue lysates were homogenized in chilled RIPA buffer containing protease and phosphatase inhibitors (Thermo Fisher Scientific, 78430). Proteins were then separated by SDS-PAGE utilizing 10% Criterion TGX precast gel (Bio-Rad) and transferred to 0.45 μm pore size PVDF (Millipore Sigma) or nitrocellulose membrane (Bio-Rad) at 100 V for 60 minutes in 4 degrees. Membranes were blocked for one hour at room temperature with 5% BSA or nonfat dry milk in TBS containing 0.1% Tween-20 (TBST). Blots were incubated with the following primary antibodies: HIF1α (Novus Biologicals, NB100-479 and Figure S5C NB100-105), HIF2α (Novus Biologicals, NB100-122), MDM2 [SMP14 (Novus Biologicals, NB100-2736), Figure 10M Ab-3/4B11 (Sigma-Aldrich, OP143) and 42BC1.11 (Sigma-Aldrich, MABE331)], VHL (Invitrogen, PA5-27322), MYBPC3 (SCBT, sc-137180), K48-linked ubiquitin (CST, 8081), Ubiquitin (SCBT, sc8017), p53 (CST, 2524) or β-actin (CST, 8457) overnight at 4°C. For chemiluminescent immunoblot detection, membranes were incubated with goat anti-rabbit or anti-mouse horseradish peroxidase (HRP)-linked secondary antibodies for 1 hour at room temperature. The membranes were then developed with Clarity ECL Western substrate (Bio-Rad) or ultra-sensitive Supersignal West Femto Substrate (Thermo Scientific). Images were captured under ChemiDoc MP Imager (BioRad) by highlighting saturated pixels to control for overexposure. For fluorescent immunoblot detection, goat anti-mouse 680LT or goat anti-rabbit 800CW IRDye (Licor Biotech) was utilized, and the membrane was then imaged using an Odyssey CLx Infrared imager (Licor Biotech). Densitometric analyses were performed using Image J, Image Lab (Bio-Rad) or Image Studio Lite software (LI-COR Biosciences). To control for loading differences between samples, β-actin or a total protein stain (Revert LI-COR) was utilized as delineated in the figure legends.

[0059] Co-Immunoprecipitation

[0060] Protein extraction from LV tissue was carried out using chilled Pierce IP lysis buffer (Thermo Fisher Scientific, 87788) with protease and phosphatase inhibitors. For co-immunoprecipitation, MDM2 antibody (1 μg/ml) was incubated with 100 μl of pre-washed SureBeads Magnetic Beads (Bio-Rad, 161-4013) for 1 hour on a rocking platform. Next, antibody-conjugated beads were collected by magnetization, washed in PBST, and then incubated with 500 μg of cardiac tissue lysate for 2 hours on a rocking platform. Samples were then collected by magnetization and washed a minimum of three times with IP lysis buffer containing protease/phosphatase inhibitors. After removing the supernatant, proteins were eluted with 2X Laemmli sample buffer followed by heating at 95°C for 5 min and western blots for MDM2 and VHL were performed. A measure of

10% of the co-IP homogenate was taken for examination of the input and loading control.

[0061] Immunoprecipitation

[0062] Protein extraction from LV tissue was carried out using chilled RIPA buffer containing SDS (Thermo 78430) with protease/phosphatase inhibitor (Thermo 78440) and deubiquitinase (DUB) inhibitor PR-619 (Apexbio, A8212, 50 μM). For immunoprecipitation, the following primary antibodies (MDM2 1 μg/ml, HIF1α 1 μg/ml, HIF2α 1 μg/ml, VHL 1 μg/ml) were incubated as described section in co-immunoprecipitation. Western blots for K48-linked poly-ubiquitin (CST, 8081) and protein of interest were performed. A measure of 10% of the co-IP homogenate was used for examination of the input and loading control.

[0063] Proximity Ligation Assay

[0064] In situ protein-protein complexes and post-translational modifications (ubiquitination, neddylation) were measured using a proximity ligation assay (PLA, Duolink Sigma Aldrich). OCT embedded myocardial tissue sections of 5 μm were obtained and fixed with 4% PFA. Rabbit PLUS and mouse MINUS Duolink probes (Sigma Aldrich) were utilized to detect complexes using the antibodies targeting HIF1α (Novus Biologicals, NB100-479), HIF2α (Novus Biologicals, NB100-122), MDM2 (Novus Biologicals, NB100-2736), VHL (Invitrogen, PA5-27322), Ubiquitin mouse (SCBT, sc8017), Ubiquitin rabbit (CST, 3933) and NEDD8 (CST, 2754). Uniform antibody concentrations were maintained across different PLA experiments. Control experiments were performed using single antibody combinations and PLA probes alone to confirm that there was minimal non-selective detection at the antibody concentrations utilized (Figure 10A-B, 10N, 11AB, 11E, 11H). Images were obtained at 20x and 40x magnification using fluorescence microscopy (Zeiss Axioplan). Images were analyzed in ImageJ to calculate the protein-protein complexes and nuclei per field.

[0065] In vivo Pharmacological Studies

[0066] For administration of the proteasome inhibitor Bortezomib (MCE, HY-10227, 0.1 mg/kg, daily injections from P1 to P6), pan PHD Inhibitor Molidustat (MCE, BAY 85-3934, 10 mg/kg, daily injections from P1 to P6) and MDM2 degrader MD-224(Adooq, A18712, 10 mg/kg, daily injections from P1 to P6 or P1 to P24), the drugs were dissolved in 1% DMSO and administered via subcutaneous route. Tamoxifen (50 mg/kg, injections at P1 and P4) was dissolved in warm sesame oil and administered via subcutaneous route. For information on frequency and interval, please refer to figure legends.

[0067] Echocardiography

[0068] Murine cardiac structure and function were assessed by transthoracic echocardiography using a Vevo 3100 (VisualSonics Inc) without anesthesia. LV M-mode images were acquired to measure interventricular septal thickness at end diastole (IVSd, mm), LV posterior wall thickness at end diastole (LVPWd, mm), LV internal diameter at end diastole (LVIDd, mm) and LV internal diameter at end systole (LVIDs, mm). LV fractional shortening (FS, %) was calculated using the following formula: [(LVIDd–LVIDs)/ LVIDd] x100. Quantification was performed in a blinded fashion using Vevo Lab or ImageJ/Fiji software.

[0069] Cardiomyocyte Size

[0070] OCT embedded myocardial tissue sections of 5 µm were obtained and fixed with 4% PFA. Following PBS washes, slides were incubated with Oregon Green 488–conjugated WGA (Thermo Fisher Scientific, W6748) diluted 1:200 in PBS. After PBS rinses, slides were mounted with ProlongGold Antifade with DAPI and LV tissue imaged at 40x magnification. Cardiomyocyte cross sectional area was then calculated using regions of interest (ROI) function in ImageJ software and the average cardiomyocyte cross-sectional area for each region was tabulated.

[0071] Example 2 Reduced Postnatal Capillary Formation in Mybpc3-/- Myocardium Is Associated With MVD and Tissue Hypoxia

[0072] We previously found that deletion of the sarcomere protein MYBPC3 leads to early postnatal LV hypertrophy (LVH). Therefore, we wanted to determine whether there was evidence of MVD in this model. First, we measured capillary-to-cardiomyocyte ratios in wild-type (WT) and Mybpc3-/- LV tissue by staining for the endothelial cell marker CD31 (cluster of differentiation 31). We discovered that capillary density was reduced in Mybpc3-/- LV tissue beginning at postnatal day 7 (Figure 1A and 1B; Figure 8A and 8B). Both male and female Mybpc3-/-mice had similar reductions in LV capillary density (Figure 8C). We then performed immunohistochemistry for an alternative endothelial cell marker, angiopoietin-1 receptor TIE2 (aka, TEK [tyrosine kinase]), and again found that capillary density was reduced at postnatal day 7 (Figure 1A and 1B; Figure 8D). We confirmed that CD31 and TIE2 detect the same cell population in the myocardium (Figure 8E and 8F). In addition to endothelial cells, pericytes are a critical cell population for proper capillary development. Therefore, we performed immunohistochemistry for the pericyte marker NG2 (neural/glial antigen 2) and found that Mybpc3-/- mice also had reduced LV pericytes (Figure 1C and 1D; Figure 9A).

[0073] To complement the immunohistochemistry-based methods, we then injected fluorescently labeled tomato lectin which binds to vascular endothelial cells. This allowed better visualization of the capillary lumens and confirmed that Mybpc3-/- mice had a significant reduction in LV capillaries (Figure 1E and 1F; Figure 9B and 9C). We confirmed that tomato lectin, CD31, and NG2 could detect the same myocardial capillaries (Figure 9D and 9E). In addition to reduced LV capillaries, we discovered that postnatal day 7 Mybpc3-/-mice had increased left coronary artery (LCA) dilation compared with WT control mice. However, LCA size was similar in both groups of mice after birth at postnatal day 2 arguing against a difference in embryonic coronary development between the groups (Figure 9F through 9I). Overall, these results show that LV capillary formation is reduced in the early postnatal period in Mybpc3-/- mice.

[0074] Next, we wanted to determine whether the reduction of LV capillaries in Mybpc3-/- mice led to microvasculature dysfunction. We measured blood flow in the LCA before and after the administration of the vasodilator adenosine to calculate the coronary flow reserve which is dependent on myocardial capillary blood flow (Figure 1G; Figure 9J through 9L). Baseline myocardial blood flow was increased in Mybpc3-/- animals which was partly driven by the increased LCA size in these mice (Figure 1G and 1H). However, myocardial blood flow minimally increased after adenosine administration (Figure 1H). Therefore, the coronary flow reserve was reduced in Mybpc3-/- animals (Figure 1I). Next, we wanted to determine whether the MVD in Mybpc3-/- myocardium was associated with tissue hypoxia. We used the tissue hypoxia marker pimonidazole and detected a large increase in LV tissue hypoxia in Mybpc3-/- heart tissue (Figure 1J and 1K). Overall, these results show that the reduction of myocardial capillary formation in Mybpc3-/- mice leads to MVD and LV tissue hypoxia.

[0075] **Example 3 Dynamic Changes in HIF1α and HIF2α Occur During Early Postnatal Period in the Mybpc3-/- Myocardium**

[0076] Since we detected tissue hypoxia in the Mybpc3-/- myocardium, we measured the protein levels of the hypoxia regulated transcriptions factors HIF1α (hypoxia-inducible factor 1 alpha) and HIF2α (hypoxia-inducible factor 2 alpha)/EPAS1 (endothelial PAS domain protein 1). We detected no differences in the protein levels at postnatal day 2 (Figure 2A and 2B). In contrast, there was a reduction of HIF1α protein and an increase of HIF2α in the Mybpc3-/- LV tissue at postnatal day 7 (Figure 2A and 2B). However, by postnatal day 25, the HIF1α and HIF2α LV protein levels were similar between WT and Mybpc3-/- mice (Figure 2A and 2B). We compared protein levels across the different ages and discovered that myocardial HIF1α protein levels do not increase at

postnatal day 7 in the Mybpc3-/- LV tissue when compared with WT LV tissue (Figure 2C). In contrast, HIF2α protein levels increase at postnatal day 7 in Mybpc3-/- LV tissue and then return to control levels by postnatal day 25 (Figure 2D). We then performed immunohistochemistry to confirm that the changes in HIF1α and HIF2α protein levels were cardiomyocyte-specific (Figure 2E through 2G). Overall, these results show that during the early postnatal time period when myocardial capillary formation is reduced in the Mybpc3-/- mice, there are dynamic changes in cardiomyocyte HIF1α and HIF2α protein levels.

[0077] **Example 4 Noncanonical Degradation of HIF1α in the Mybpc3-/- Myocardium Is Regulated by Cardiomyocyte MDM2**

[0078] We identified a reduction in HIF1α protein in the Mybpc3-/- myocardium at postnatal day 7. However, it was unclear whether the reduction of HIF1α protein was secondary to a reduction in gene expression or increased protein degradation. We found that despite the reduction of HIF1α protein at postnatal day 7, there was increased Hif1α mRNA in Mybpc3-/- LV tissue (Figure 3A). Therefore, we hypothesized that there was increased degradation of HIF1α in the Mybpc3-/- myocardium. We administered the proteasomal inhibitor bortezomib and this normalized HIF1α protein (Figure 3B and 3C). We then performed an in situ proximity ligation assay to measure the amount of ubiquitinated HIF1α in the groups of mice that had been administered bortezomib. We discovered a robust increase in ubiquitinated HIF1α in the Mybpc3-/- LV tissue (Figure 3D and 3E; Figure 10A). These data show that the reduction of HIF1α in Mybpc3-/-LV tissue is secondary to increased ubiquitination and proteasomal degradation of HIF1α.

[0079] The canonical HIF1α ubiquitination and proteasomal degradation pathway require oxygen-dependent PHD (prolyl hydroxyl domain) enzymes to hydroxylate HIF1α which then allows the E3 ligase VHL (Von Hippel-Lindau) to ubiquitinate HIF1α. To determine whether the canonical HIF1α degradation pathway was regulating HIF1α degradation we first measured VHL protein levels. Surprisingly, VHL protein levels were reduced in Mybpc3-/- (Figure 3F and 3G). We then measured in situ HIF1α–VHL protein complexes and found that HIF1α–VHL complexes were significantly reduced in Mybpc3-/- LV tissue (Figure 3H and 3I; Figure 10B). In addition, Phd gene expression was unchanged and the pan-PHD inhibitor molidustat did not increase HIF1α protein levels in Mybpc3-/- mice (Figure 10C through 10F). This data shows that the canonical oxygen-dependent PHD–VHL degradation pathway is not regulating the increased proteasomal degradation of HIF1α in the Mybpc3-/- LV tissue.

[0080] In addition to the oxygen-dependent canonical HIF degradation pathway, oxygen-independent noncanonical HIF degradation pathways have been identified. The E3 ligase MDM2 (murine double minute 2) has been shown to ubiquitinate HIF1α.33 Therefore, we wanted to determine whether MDM2 was regulating the ubiquitination of HIF1α in Mybpc3-/- cardiomyocytes. First, we measured MDM2 protein levels and discovered that MDM2 protein levels were increased in Mybpc3-/- LV tissue during the same time point (postnatal day 7) when HIF1α protein was decreased (Figure 3J and 3K). Next, we selectively reduced cardiomyocyte MDM2 levels in vivo using a transgenic strategy that used a cardiomyocyte-selective Cre line (Myh6 [myosin heavy chain 6]:Cre) (Figure 3L). This strategy successfully reduced MDM2 protein levels (Figure 3M; Figure 10M). Selective reduction of cardiomyocyte MDM2 led to the normalization of HIF1α and HIF2α protein levels in Mybpc3-/- LV tissue (Figure 3M; Figure 10M).

[0081] We previously discovered that Mybpc3-/- cardiomyocytes develop increased DNA damage and increased gene expression of MDM2 at postnatal day 25. Therefore, we measured MDM2 mRNA levels at postnatal day 7 to determine if increased MDM2 gene expression was the reason for the elevated MDM2 protein levels at postnatal day 7 in Mybpc3-/- mice. Interestingly, we found that MDM2 mRNA was reduced in the Mybpc3-/- mice at postnatal day 7 but was increased at postnatal day 25 (Figure 10G). It was previously shown that MDM2 can serve as a negative regulator of its own gene expression through inhibiting p53.34 Indeed, we detected a rebound in MDM2 mRNA levels when cardiomyocyte MDM2 protein levels were reduced in Mybpc3-/- mice at postnatal day 7 (Figure 10H). Likewise, MDM2 mRNA increased at postnatal day 25 when levels of MDM2 protein declined (Figure 10G and 10I). These results suggested that cardiomyocyte MDM2 gene expression was not the primary cause of increased MDM2 protein levels at postnatal day 7 and suggested that MDM2 protein stability was altered in the Mybpc3-/- mice. Indeed, we found that MDM2 protein ubiquitination was reduced in postnatal day 7 Mybpc3-/- LV tissue (Figure 10J and 10K). In addition, we found that MDM2 and MDM4 (aka MDMX) protein complexes were reduced in Mybpc3 LV tissue (Figure 10L). It was previously shown that MDM4 can stimulate MDM2 autoubiquitination and degradation. Importantly, when MDM2 protein levels decrease at postnatal day 25 in the Mybpc3-/- mice (Figure 10I), this is associated with a normalization of myocardial levels of HIF1α and HIF2α (Figure 2A and 2B). Overall, these results suggest that MDM2 protein is increased at postnatal day 7 in the Mybpc3-/- myocardium secondary changes in its protein stability.

[0082] Next, we measured in situ HIF1α-MDM2 protein complexes and discovered that they were robustly increased in Mybpc3-/- LV tissue and greatly reduced by selective cardiomyocyte reduction of MDM2 (Figure 3N and 3O; Figure 10N). We then measured in situ HIF1α ubiquitination in LV tissue and found that a reduction of cardiomyocyte MDM2 led to a corresponding reduction in HIF1α ubiquitination (Figure 3P and 3Q). We confirmed our in situ proximity ligation assay results by performing immunoprecipitation of LV tissue lysates using a HIF1α antibody and then immunoblotting with a K48 ubiquitin selective antibody (Figure 3R). Finally, the E3 ligase function of MDM2 is a well-described inducer of p53 protein degradation. Therefore, we wanted to determine whether reducing cardiomyocyte MDM2 led to a surge of p53 protein levels. However, this did not occur, and LV p53 protein levels decreased in parallel with a reduction of cardiomyocyte MDM2 protein (Figure 10O). Overall, these results show that cardiomyocyte MDM2 is facilitating the noncanonical ubiquitination and degradation of HIF1α in Mybpc3-/- LV tissue.

[0083] Example 5 Increased HIF2α in the Mybpc3-/- Myocardium Occurs Secondary to MDM2 Facilitated Degradation of VHL

[0084] Although we identified the molecular mechanisms regulating the increased degradation of HIF1α in Mybpc3-/- cardiomyocytes, it remained unclear why HIF2α protein levels were increased. We hypothesized that the reduced VHL protein levels may be contributing to the increased levels of HIF2α (Figure 3F). We first measured Vhl gene expression and detected no difference between the groups (Figure 4A). This result suggested the reduction of VHL protein in Mybpc3-/- LV tissue was secondary to increased proteasomal degradation. Indeed, we found that VHL protein levels rebounded to normal levels when a proteasome inhibitor was administered to the Mybpc3-/- mice (Figure 4B and 4C). Next, we performed a coimmunoprecipitation assay to determine whether MDM2 bound to VHL and discovered that there was increased VHL binding to MDM2 in Mybpc3-/- LV tissue lysates (Figure 4D). In situ MDM2–VHL protein complexes were also increased in Mybpc3-/- LV tissue and were reduced with the selective reduction of cardiomyocyte MDM2 (Figure 4E and 4F; Figure 11A). Next, we discovered that in situ VHL ubiquitination was increased in Mybpc3-/- LV tissue and this increase was eliminated with reduction of cardiomyocyte MDM2. (Figure 4G and 4H; Figure 11B). We confirmed our in situ proximity ligation assay results by performing immunoprecipitation of LV tissue lysates using a VHL antibody and then immunoblotting with a K48 ubiquitin selective antibody (Figure 4I). In contrast to VHL ubiquitination, the neddylation of VHL was unchanged (Figure 11C and 11D). Taken

together, these results show that MDM2 regulates the ubiquitination and degradation of VHL in Mybpc3-/- cardiomyocytes.

[0085] We identified a novel role for cardiomyocyte MDM2 in the regulation of VHL ubiquitination and VHL protein stability. Therefore, we hypothesized that the increase in HIF2α protein levels in Mybpc3-/- LV tissue was related to the changes we identified in VHL. First, we confirmed that Hif2α expression was unchanged in the groups (Figure 4J). However, in situ VHL-HIF2α protein complexes were greatly reduced in the Mybpc3-/- LV tissue but were normalized with the reduction of MDM2 (Figure 4K and 4L; Figure 11E). Importantly, we confirmed that there were minimal MDM2 and HIF2α protein complexes in LV tissue (Figure 11F and 11G). We then measured in situ HIF2α ubiquitination and found that HIF2α ubiquitination was reduced in Mybpc3-/- LV tissue and was normalized by the cardiomyocyte selective reduction of MDM2 (Figure 4M and 4N; Figure 11H). Again, we confirmed our in situ proximity ligation assay results by performing immunoprecipitation of LV tissue lysates using a HIF2α antibody and then immunoblotting with a K48 ubiquitin selective antibody (Figure 4O). Overall, these results show that cardiomyocyte MDM2 facilitates the degradation of VHL which leads to dynamic increases in HIF2α protein levels.

[0086] **Example 6 Reduction of Cardiomyocyte MDM2 in Mybpc3-/- Mice Increases Myocardial Capillary Formation and Proangiogenic Gene Expression**

[0087] We identified a role for cardiomyocyte MDM2 in regulating the protein stability of both HIF1α and HIF2α. Therefore, we wanted to determine whether selective reduction of cardiomyocyte MDM2 would impact capillary formation in Mybpc3-/- mice. Indeed, we found that the reduction of cardiomyocyte MDM2 led to increased LV capillaries in Mybpc3-/- mice (Figure 5A and 5B). Likewise, pericytes were also increased with selective reduction of cardiomyocyte MDM2 in Mybpc3-/- mice (Figure 12A and 12B). We wanted to determine whether the reduction of LV capillary density in the Mybpc3-/- myocardium was associated with reduced expression of angiogenic genes. Indeed, we found that Mybpc3-/- LV tissue had reduced expression of multiple proangiogenic genes (Figure 5C). Importantly, the selective cardiomyocyte reduction of MDM2 could reverse these gene expression changes (Figure 5C).

[0088] We next investigated whether reduction of capillary density in the Mybpc3-/- myocardium was secondary to the reduction of HIF1α or the increase of HIF2α protein at postnatal day 7. Selective reduction of cardiomyocyte HIF1α during the postnatal day 2 to postnatal day 7 postnatal time period in WT mice led to a reduction in LV capillary formation (Figure 5D and 5E; Figure 12C). In contrast, the reduction of cardiomyocyte

HIF2α in Mybpc3-/- mice resulted in a partial increase of capillary density in Mybpc3-/- mice but had no impact on WT LV capillary density (Figure 5G and 5H; Figure 12D). These results show that the transient imbalance of both HIF1α and HIF2α are contributing to the capillary formation abnormality in Mybpc3-/- mice.

[0089] Mybpc3-/- mice rapidly develop LVH and LV dysfunction in the early postnatal time period. Therefore, we measured cardiac structure and function in Mybpc3-/- mice with reduction of cardiomyocyte MDM2. We discovered that selective reduction of cardiomyocyte MDM2 did reduce LVH and improve systolic function in Mybpc3-/- mice during the early postnatal time period (Figure12E through 12G). In contrast, targeted elimination of cardiomyocyte HIF1α and HIF2α did not cause significant changes in cardiac structure or function in the early postnatal time period (Figure 12H through 12M). These results show that the MDM2-induced HIF imbalance selectively alters LV capillary formation during the early postnatal time period in Mybpc3-/- mice.

[0090] **Example 7 MDM2 Regulates Capillary Formation Before the Development of Ventricular Hypertrophy in Myh6R404Q/WT Mice**

[0091] We discovered that Mybpc3-/- mice have reduced LV capillary formation during the early postnatal time period and that MDM2 plays a critical role in this process. However, it remained unclear whether LV capillary formation defects could occur independently of LVH and whether other sarcomere gene mutations had shared pathophysiologic responses to the Mybpc3-/- mice. To address these questions, we used genetic editing to create a murine model with a point mutation in the Myh6 gene (Myh6R404Q/WT) (Figure 13A and 13B) to model the human MYH7 R403Q mutation, which is a well described cause of HCM in humans. The murine MYH6 protein is targeted because it is the dominant myosin heavy chain protein in the adult mouse LV versus MYH7 in the adult human LV and this strategy was successfully used in the past with homologous recombination methods. In contrast to Mybpc3-/- mice that rapidly develop LVH by postnatal day 7, heterozygote Myh6R404Q/WT mice had normal LV wall thickness through postnatal day 25 but developed LVH by postnatal day 60 without systolic dysfunction (Figure 6A through 6C; Figure 13C). Male and female Myh6R404Q/WT mice developed similar levels of LVH by postnatal day 60 but male mice had slightly more LVH by 6 months of age (Figure 13D through 13G). Similar to the development of myocardial hypertrophy, the heterozygote Myh6R404Q/WT mice developed cardiomyocyte hypertrophy by postnatal day 60 (Figure 6D and 6E). Therefore, this HCM model of adult onset LVH allowed us to determine whether

sarcomere protein dysfunction impacted myocardial capillary formation before the development of LVH.

[0092] We analyzed LV capillary density in the Myh6R404Q/WT mice and discovered that capillary formation was reduced (Figure 6F through 6I). Similar to Mybpc3-/- mice, both male and female Myh6R404Q/WT mice had similar reductions in capillary density (Figure 13H). However, in contrast to Mybpc3-/- mice, LCA size of Myh6R404Q/WT mice was similar to WT mice at postnatal day 7 (Figure 13I and 13J). We then wanted to determine whether the changes in LV capillary formation in Myh6R404Q/WT mice were related to changes in MDM2-HIF signaling. We found that Myh6R404Q/WT myocardium had an increase in MDM2 protein (Figure 6J and 6K). Similar to Mybpc3-/- mice, the increase in MDM2 in the Myh6R404Q/WT mice was associated with increased cardiomyocyte DNA damage (Figure 13K and 13L). Importantly, we found no evidence of increased endothelial cell DNA damage (Figure 13M and 13N). We then measured HIF1α and HIF2α protein levels and discovered that postnatal day 7 Myh6R404Q/WT myocardium had reduced HIF1α and increased HIF2α protein levels (Figure 6J, 6L, and 6M). In addition, VHL protein levels were also reduced in postnatal day 7 Myh6R404Q/WT myocardium Figure 13O and 13P). Next, we wanted to determine whether selective reduction of cardiomyocyte MDM2 would increase capillary density and prevent MVD in Myh6R404Q/WT mice in the pre-LVH period. Indeed, we found that genetic reduction of cardiomyocyte MDM2 in Myh6R404Q/WT mice led to increased LV capillary formation and normalization of coronary flow reserve (Figure 6N and 6O; Figure 14A through 14C). In contrast to the Mybpc3-/- model that had LVH at postnatal day 7, we did not detect evidence of myocardial tissue hypoxia in the Myh6R404Q/WT model at postnatal day 7 (Figure 14D). Therefore, despite the absence of myocardial tissue hypoxia in the Myh6R404Q/WT model, the abnormalities in the microvasculature and molecular alterations in MDM2, HIF1/2, and VHL were conserved with the Mybpc3-/- model. Overall, these results show that myocardial capillary formation precedes the development of ventricular hypertrophy in Myh6R404Q/WT mice and MVD can be prevented by genetic reduction of cardiomyocyte MDM2.

[0093] Example 8 Chemical Inhibition of MDM2 Prevents MVD in Two Distinct HCM Models

[0094] We discovered that cardiomyocyte MDM2 regulates the development of MVD in both the Mybpc3-/- and Myh6R404Q/WT mouse lines. Therefore, we wanted to determine whether chemically targeting MDM2 could prevent the development of MVD in these models. We used MD-224, a chemical proteolysis targeting chimeric compound,

to selectively degrade MDM2 in the early postnatal time period (Figure 7A). Chemical targeting of MDM2 led to the normalization of HIF1α and HIF2α levels in both Mybpc3-/- (Figure 7B) and Myh6R404Q/WT mice (Figure 7C). Likewise, chemical MDM2 degradation led to an increase in LV capillary density in both Mybpc3-/- and Myh6R404Q/WT mice (Figure 7D and 7E).

[0095] Similar to genetic reduction of MDM2, chemical targeting of MDM2 using MD-224 reduced myocardial hypertrophy and improved LV systolic function in Mybpc3-/- mice (Figure 15A through 15F). Next, we wanted to determine whether transient targeting of MDM2 during the pre-hypertrophic period of Myh6R404Q/WT mice would lead to persistent improvement in LV capillary density and coronary flow reserve in the adult animal (Figure 7F). We found that transient chemical targeting of MDM2 during the early postnatal time period led to a persistent increase in LV capillary density and normalized coronary flow reserve in adult Myh6R404Q/WT mice (Figure 7G through 7I; Figure 15G). In addition, transient chemical targeting of MDM2 prevented the development of LVH in the Myh6R404Q/WT model at postnatal day 60 (Figure 15H through 15M). In summary, these findings show that transient chemical targeting of MDM2 prevents the HIF imbalance and myocardial capillary dysfunction in 2 unrelated models of HCM.

[0096] Example 9 Discussion

[0097] Myocardial MVD has been identified in multiple different forms of human cardiomyopathy and is often thought to occur as a consequence of the pathologic myocardial remodeling process. Myocardial MVD has been demonstrated in humans with hypertrophic cardiomyopathy (HCM) and is thought to be a significant contributor to disease pathogenesis. However, it remains unclear when MVD develops in HCM and the molecular mechanisms regulating this pathologic process. Using 2 distinct animal models of HCM, we discovered that early postnatal myocardial capillary formation is impaired, and this leads to MVD in adult animals. The reduction in myocardial capillary formation in HCM is caused by the E3 ligase MDM2 inducing an imbalance of cardiomyocyte HIF1α and HIF2α protein levels during the early postnatal time period. Importantly, myocardial MVD can precede the development of myocardial hypertrophy in HCM and selective targeting of MDM2 prevents myocardial MVD from developing. This study identified a key regulatory mechanism controlling the development of myocardial MVD and provides unique insights into molecular pathways contributing to the pathophysiology of HCM.

[0098] We have identified a unique role for MDM2 as a critical regulator of MVD in HCM by reducing myocardial angiogenesis in the early postnatal heart. MDM2 has not been previously shown to regulate MVD in the heart or other organ systems. In contrast, increased expression of MDM2 has been shown to play a proangiogenic role in malignant tissues. The divergent pro- and antiangiogenic properties of MDM2 appear to be partially explained by the acute versus chronic overexpression of the protein. For example, the chronic overexpression of MDM2 in malignant tissues can lead to increased p53 degradation which facilitates proangiogenic gene expression. In contrast, the acute increase in cardiomyocyte MDM2 in our HCM models led to an antiangiogenic role for this protein through its role in simultaneously regulating the protein stability of HIF1α and HIF2α.

[0099] We found that MDM2 concurrently regulated the noncanonical degradation of HIF1α and the canonical degradation of HIF2α leading to an imbalance in these proteins. Previously it was shown that MDM2 can regulate HIF1α ubiquitination in cancer cell lines, but our data indicates this noncanonical mechanism of HIF1α degradation is important in vivo in a nonmalignant context. In addition, we discovered that in-vivo cardiomyocyte MDM2 can bind and regulate the ubiquitination of VHL leading to a reduction in the canonical degradation of HIF2α. Our results identified MDM2 as a specific regulator of HIF and VHL protein stability in the early stages of HCM and reinforces the increasing evidence that the ubiquitin–proteosome system is an important regulator in HCM. Interestingly it was previously shown that MDM2 can also regulate VHL neddylation in cancer cell lines. However, in contrast to the effect that MDM2 has on VHL ubiquitination, we found no evidence that MDM2 dynamically regulated VHL neddylation in vivo in our disease model. Interestingly, we discovered that HIF1α and HIF2α have opposing roles in regulating myocardial capillary formation in the postnatal mammalian heart, with HIF1α serving a proangiogenic role and HIF2α serving an antiangiogenic role. This is in contrast to tumor angiogenesis, where HIF1α and HIF2α are more often reported to have synergistic roles in promoting angiogenesis. Our data shows that the regulation of organ angiogenesis by HIF1α and HIF2α is highly dependent on cell type and tissue environment. This study adds to the growing data that cardiomyocyte HIF signaling has distinct roles in regulating myocardial growth and maturation depending on the developmental time point when they are expressed.

[0100] Another important result from this study is that MVD can develop before cardiomyocyte hypertrophy. Using our Myh6R404Q HCM model that develops LVH in the adolescent period of mouse development, we identified early postnatal capillary

defects before the development of LVH. These results suggest that myocardial MVD and myocardial hypertrophy in HCM can occur through distinct molecular mechanisms. Supporting this conclusion are the results from our targeted cardiomyocyte deletion of the MDM2 target proteins HIF1α and HIF2α. Selective reduction of cardiomyocyte HIF1α and HIF2α had opposing effects on myocardial capillary growth but had no measurable impact on myocardial hypertrophic growth in the early postnatal time period. Likewise, we found that targeting MDM2 activity in the early postnatal time period in the Myh6R404Q model prevented myocardial MVD well before the onset of LVH. Our results are further supported by clinical studies in human carriers of pathogenic sarcomere gene mutations which identified evidence of MVD even before the development of myocardial hypertrophy. Although we have defined a unique role of MDM2 in regulating myocardial HIF signaling and capillary growth in 2 distinct HCM models, it remains unknown how alterations in MDM2 signaling lead to changes in cardiomyocyte hypertrophy in HCM.

[0101] In contrast to this study which is focused on how a lifelong genetic hypertrophic stimulus leads to MVD, acquired forms of LVH secondary to hypertension or aortic stenosis typically occur during adulthood. MVD in acquired forms of LVH is thought to be from capillary regression leading to microvascular rarefaction. Therefore, it would be assumed that MVD in genetic and acquired forms of hypertrophy may have divergent mechanisms. However, capillary rarefaction in pressure overload was also shown to occur before the development of LVH. Likewise, alterations in p53 activity were previously identified to regulate capillary regression in a pressure overload LVH model.16 Therefore, it will be important determine how dynamic changes in MDM2 signaling impacts capillary rarefaction in acquired forms of LVH.

[0102] Our results show that MVD can be prevented by partial genetic or chemical reduction of MDM2 in 2 different mouse models of HCM. Importantly, we found that partial chemical or genetic reduction of MDM2 in our models did not lead to an increase in myocardial p53 protein levels. In contrast, previous studies have shown that complete ablation of cardiomyocyte MDM2 during the embryonic or adult period leads to cardiomyopathy and lethality secondary to elevated myocardial p53 levels. Likewise, the overexpression of a negative regulator of Mdm2 mRNA stability, ZFP36L2, was found to facilitate the development of peripartum cardiomyopathy secondary to increased cardiomyocyte p53 activity leading to a reduction of mTorc1. The divergent phenotypic responses in models with partial versus complete ablation of MDM2 is at least somewhat

explained by these divergent p53 responses. However, the type and timing of the pathogenic stimulus may also be an important contributor.

[0103] Our data demonstrating that MDM2 regulates a critical stage of HCM disease development further reinforces that the pre- or early LVH period of HCM is important in establishing the long-term disease. We show that targeting MDM2 during this key period can modify long-term HCM pathologic remodeling. Therefore, it may be possible to target MDM2 or related pathways during the earliest stages of HCM disease development and positively impact long-term remodeling while avoiding the potential negative consequences of chronic MDM2 inhibition. The pre-LVH period in mouse HCM models is measured in days to months after birth but in humans this period is typically years in duration. Therefore, the window for targeting disease modifying pathways in human HCM may be much larger. Supporting the strategy of early disease modification in HCM was a recent clinical trial administering an angiotensin receptor blocker during the earliest stages of hypertrophic growth which successfully modified pathologic structural remodeling in HCM patients.

[0104] In conclusion, our results show that sarcomere mutations cause abnormal cardiomyocyte MDM2 signaling which can occur even before the development of cardiomyocyte hypertrophy. Importantly, the early postnatal pathologic changes in cardiomyocyte MDM2 signaling led to persistent changes in the myocardial microenvironment of the adult animals. This study reinforces the importance of targeting HCM during the earliest periods of disease development in order to successfully prevent the long-term pathologic remodeling of the myocardium in this disease.

CLAIMS

1. A method of treating a cardiomyopathy in a subject in need thereof comprising administering an E3 ubiquitin-protein ligase MDM2 polypeptide (MDM2) inhibitor to a heart cell in the subject.
2. The method of claim 1, wherein the cardiomyopathy is a myocardial hypertrophy or a dilated cardiomyopathy.
3. The method of claim 1 or claim 2, wherein the cardiomyopathy is a myocardial hypertrophy.
4. The method of claim 2 or claim 3, wherein the myocardial hypertrophy is selected from the group consisting of hypertrophic cardiomyopathy, hypertensive heart disease and aortic stenosis.
5. The method of any one of claims 2-4, wherein the myocardial hypertrophy is a hypertrophic cardiomyopathy.
6. The method of claim 5, wherein the administration occurs during a pre or early left ventricular hypertrophy period of the hypertrophic cardiomyopathy.
7. The method of claim 2, wherein the dilated cardiomyopathy comprises reduced LV systolic function and increased left ventricular dilation.
8. The method of any one of claims 1-7, wherein the administration reduces myocardial microvascular dysfunction in the subject.
9. The method any one of claims 1-8, wherein the administration reduces myocardial hypertrophy in the subject.
10. The method of any one of claims 1-9, wherein the administration increases left ventricular function in the subject.
11. The method of any one of claims 1-10, wherein the heart cell is a cardiomyocyte.
12. The method of any one of claims 1-11, wherein the subject is a human.
13. The method of any one of claims 1-12, wherein the MDM2 inhibitor reduces expression of MDM2.
14. The method of claim 13, wherein MDM2 expression is reduced by between about 10% and about 90% as compared to an untreated heart cell.
15. The method of claim 13, wherein MDM2 expression is reduced by between about 30% and about 70% as compared to an untreated heart cell.
16. The method of claim 13, wherein MDM2 expression is reduced by about 50% as compared to an untreated heart cell.

17. The method of any one of claims 1-12, wherein the MDM2 inhibitor reduces MDM2-mediated hypoxia-inducible factor (HIF) signaling.
18. The method of any one of claims 1-17, wherein the inhibition of MDM2 is transient.
19. A method of treating a myocardial microvascular dysfunction in a subject in need thereof comprising administering an E3 ubiquitin-protein ligase MDM2 polypeptide (MDM2) inhibitor to a heart cell in the subject.
20. A method of increasing myocardial capillary growth in a subject comprising administering an E3 ubiquitin-protein ligase MDM2 polypeptide (MDM2) inhibitor to a heart cell in the subject.
21. The method of claim 19 or claim 20, wherein the heart cell is a cardiomyocyte.
22. The method of any one of claims 19-21, wherein the subject is a human.
23. The method of any one of claims 19-22, wherein the MDM2 inhibitor reduces expression of MDM2.
24. The method of claim 23 wherein MDM2 expression is reduced by between about 10% and about 90% as compared to an untreated heart cell.
25. The method of claim 23, wherein MDM2 expression is reduced by between about 30% and about 70% as compared to an untreated heart cell.
26. The method of claim 23, wherein MDM2 expression is reduced by about 50% as compared to an untreated heart cell.
27. The method of any one of claims 19-22, wherein the MDM2 inhibitor reduces MDM2-mediated hypoxia-inducible factor (HIF) signaling.
28. The method of any one of claims 19-27, wherein the inhibition of MDM2 is transient.
29. The method of any one of claims 1-28, wherein the administration decreases chronic angina.
30. The method of any one of claims 1-29, wherein the administration decreases adverse ventricular remodeling.

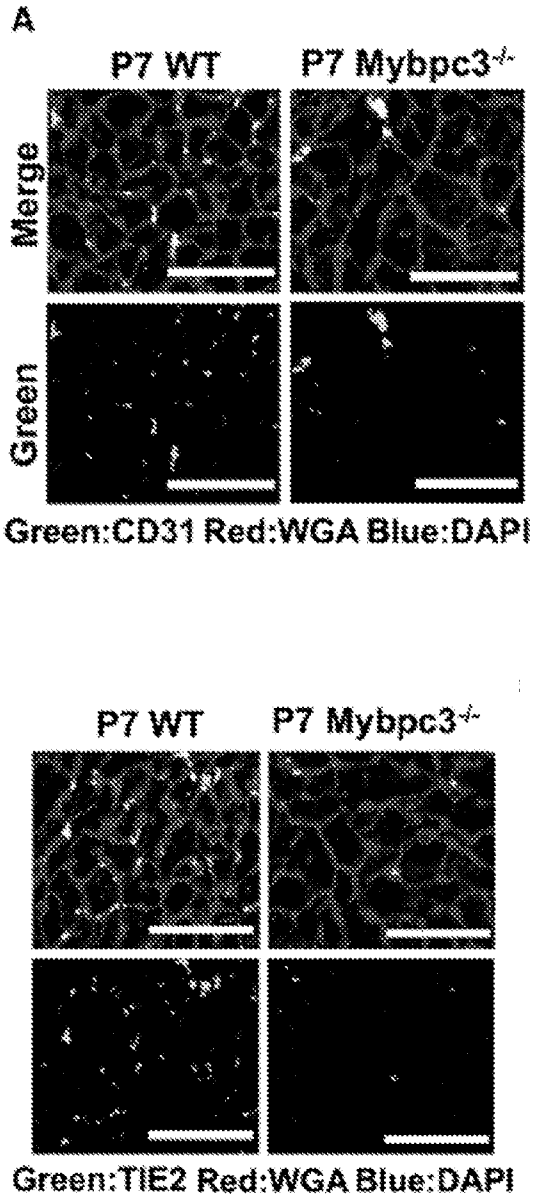
A
P7 WT
P7 Mybpc3-/-
Merge
Green
Green:CD31 Red:WGA Blue:DAPI
P7 WT
P7 Mybpc3-/-
Green:TIE2 Red:WGA Blue:DAPI

FIG. 1A

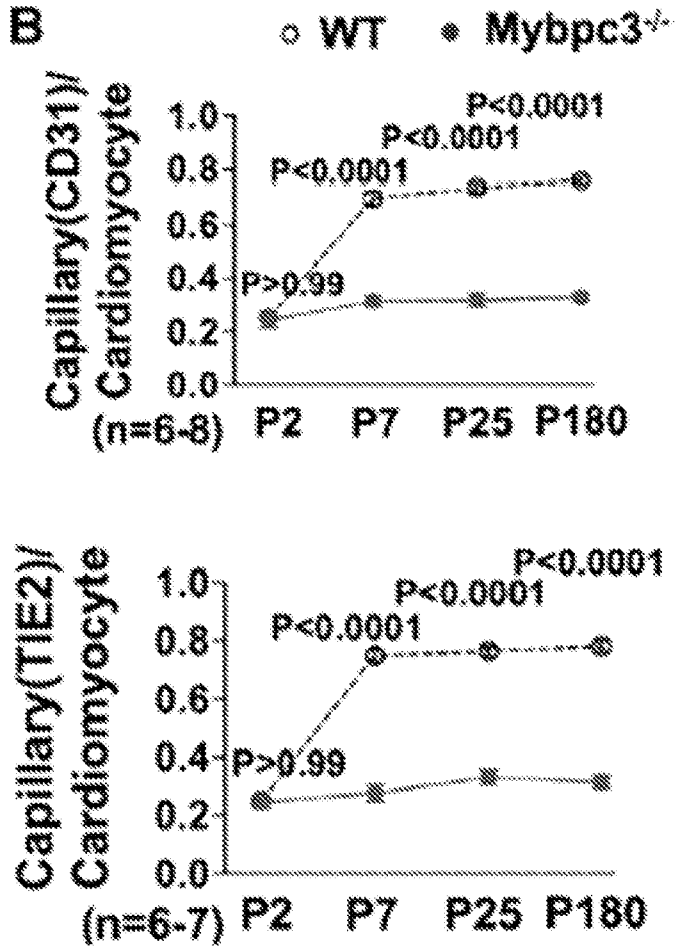
B
WT
Mybpc3-/-
Capillary(CD31)/ Cardiomyocyte
1.0
0.8
0.6
0.4
0.2
0.0
P<0.0001
P<0.0001
P<0.0001
P>0.99
(n=6-8)
P2
P7
P25
P180
Capillary(TIE2)/ Cardiomyocyte
1.0
0.8
0.6
0.4
0.2
0.0
P<0.0001
P<0.0001
P<0.0001
P>0.99
(n=6-7)
P2
P7
P25
P180

FIG. 1B

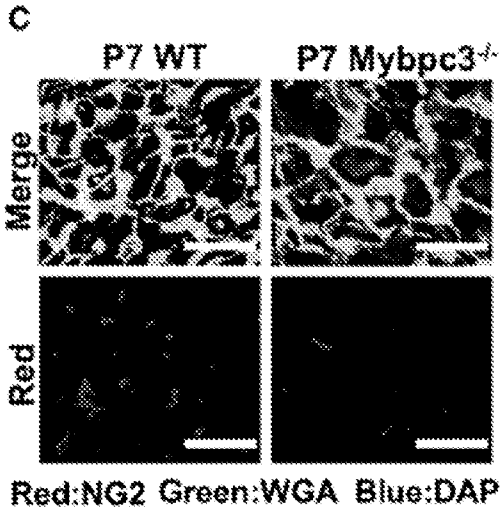

FIG. 1C

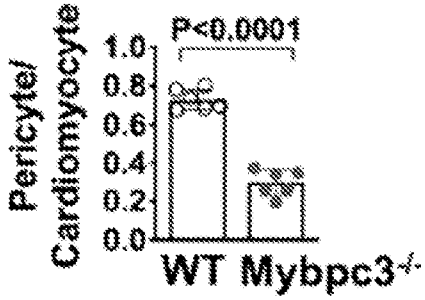

FIG. 1D

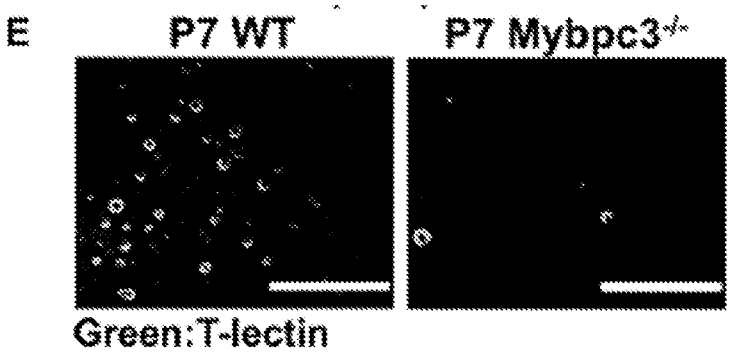

FIG. 1E

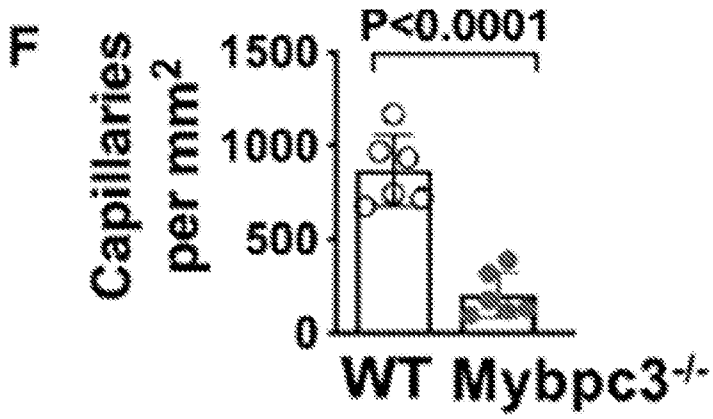
F
Capillaries per mm2
1500
1000
500
0
P<0.0001
WT
Mybpc3-/-

FIG. 1F

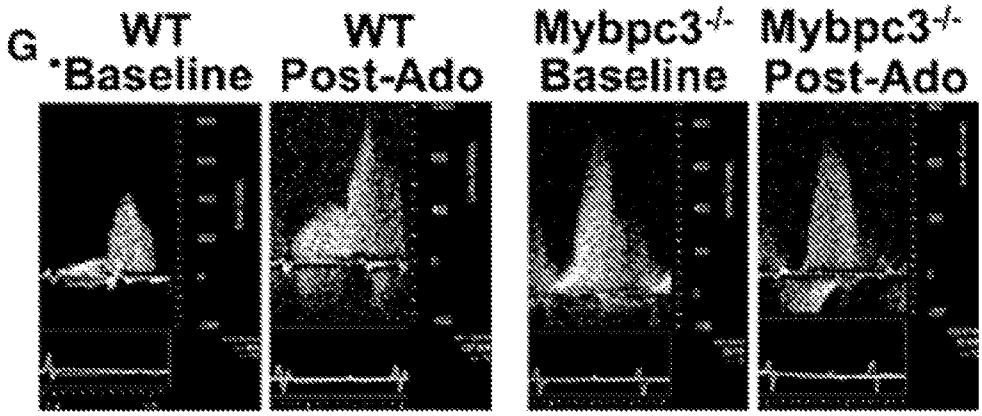
G
WT
Baseline
WT
Post-Ado
Mybpc3-/-
Baseline
Mybpc3-/-
Post-Ado

FIG. 1G

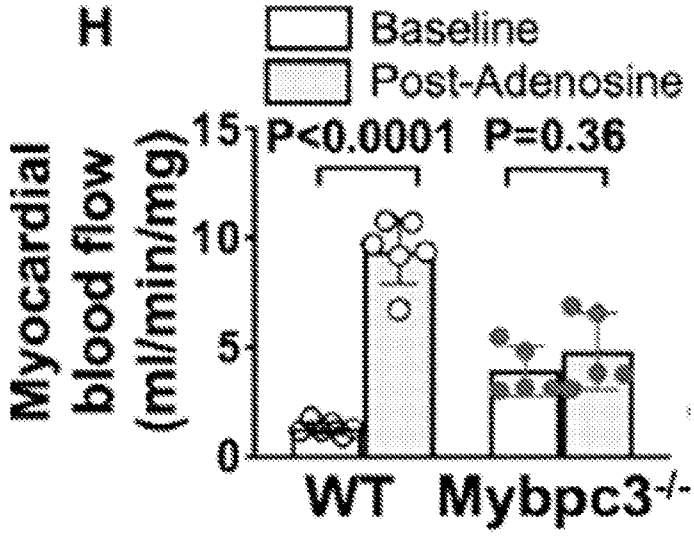
H
Baseline
Post-Adenosine
Myocardial blood flow (ml/min/mg)
15
10
5
0
P<0.0001
P=0.36
WT
Mybpc3-/-

FIG. 1H

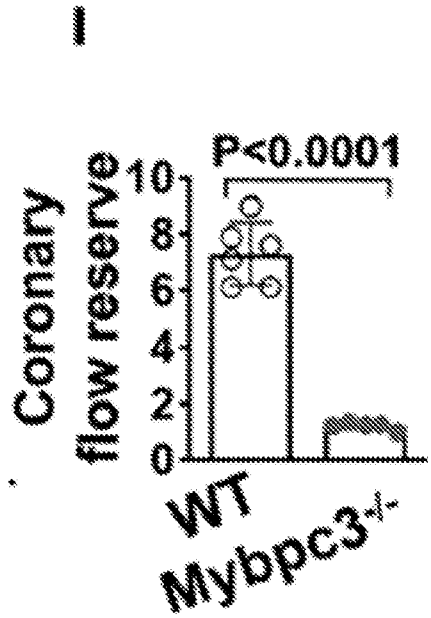
I
Coronary flow reserve
10
8
6
4
2
0
P<0.0001
WT
Mybpc3-/-

FIG. 1I

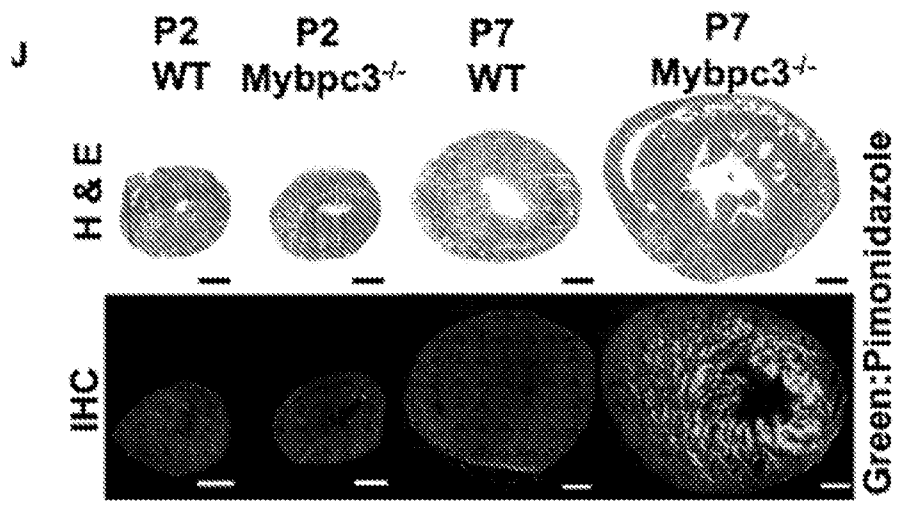
J
P2 WT
P2 Mybpc3-/-
P7 WT
P7 Mybpc3-/-
H & E
IHC
Green:Pimonidazole

FIG. 1J

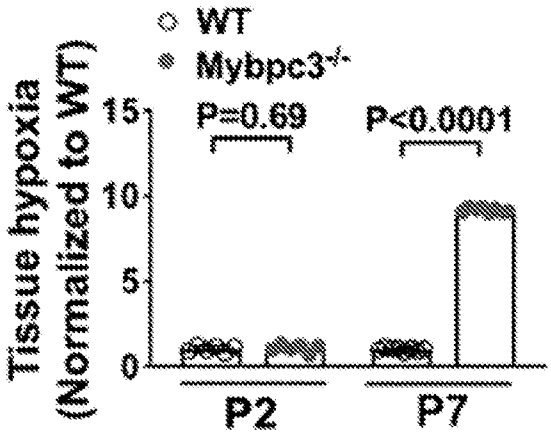
WT
Mybpc3-/-
P=0.69
P<0.0001
Tissue hypoxia (Normalized to WT)
15
10
5
0
P2
P7

FIG. 1K

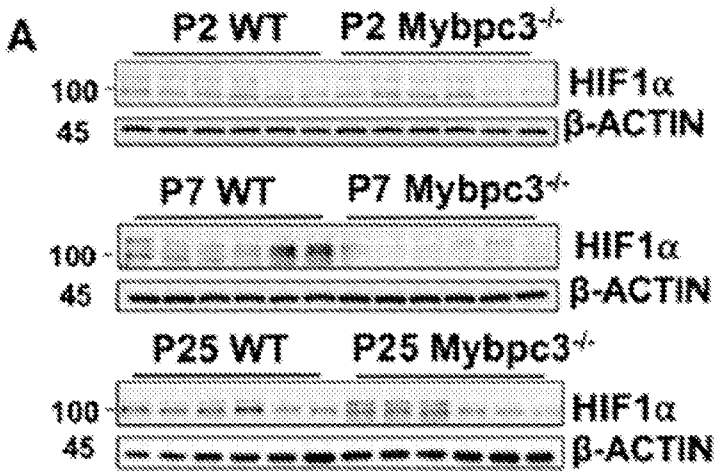
A
P2 WT
P2 Mybpc3-/-
100
HIF1α
45
β-ACTIN
P7 WT
P7 Mybpc3-/-
100
HIF1α
45
β-ACTIN
P25 WT
P25 Mybpc3-/-
100
HIF1α
45
β-ACTIN

FIG. 2A

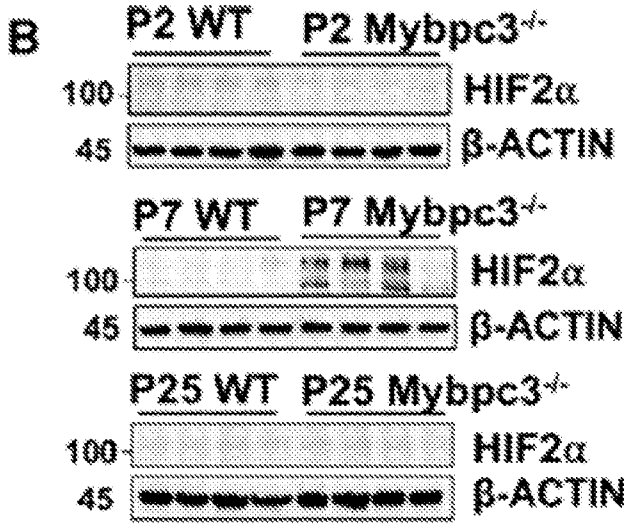
B
P2 WT
P2 Mybpc3-/-
100
HIF2α
45
β-ACTIN
P7 WT
P7 Mybpc3-/-
100
HIF2α
45
β-ACTIN
P25 WT
P25 Mybpc3-/-
100
HIF2α
45
β-ACTIN

FIG. 2B

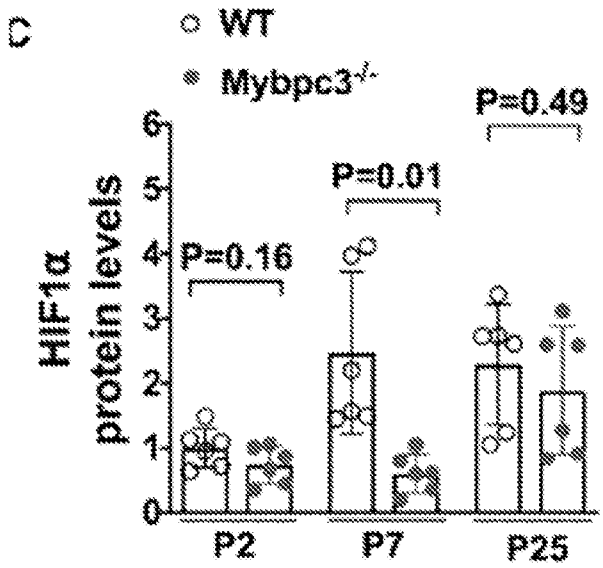
C
WT
Mybpc3-/-
HIF1α protein levels
P=0.16
P=0.01
P=0.49
0
1
2
3
4
5
6
P2
P7
P25

FIG. 2C

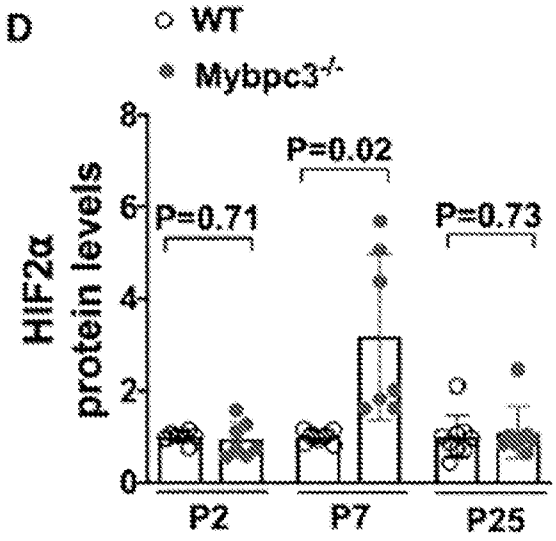
D
WT
Mybpc3-/-
HIF2α protein levels
P=0.71
P=0.02
P=0.73
0
2
4
6
8
P2
P7
P25

FIG. 2D

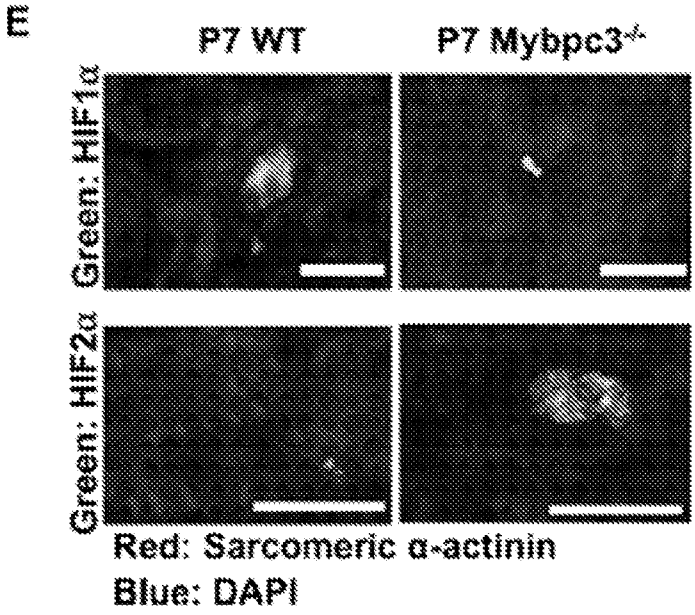

FIG. 2E

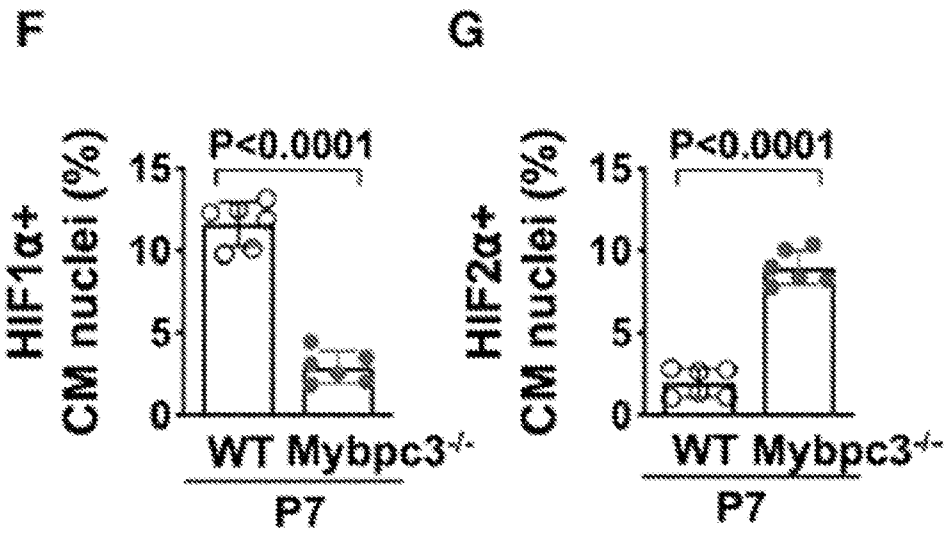

FIG. 2F, 2G

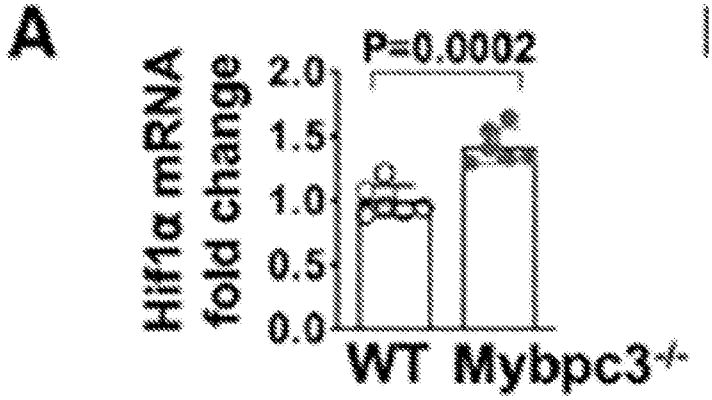
A
P=0.0002
Hif1α mRNA fold change
2.0
1.5
1.0
0.5
0.0
WT
Mybpc3-/-

FIG. 3A


B
100
150
45
HIF1α
MYBPC3
β-ACTIN
WT
Mybpc3-/-
Mybpc3-/-
BTZ

FIG. 3B

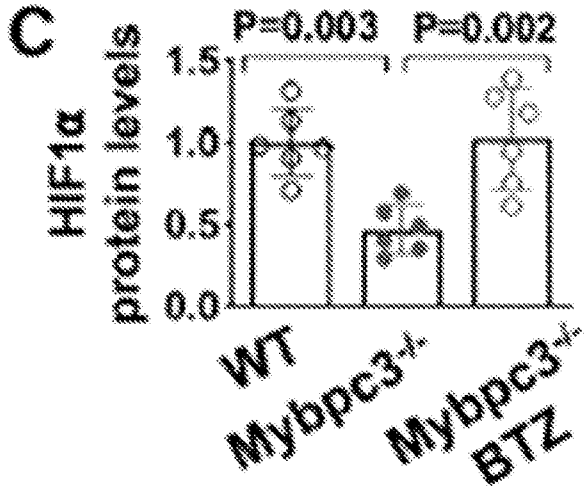
C
HIF1α protein levels
P=0.003
P=0.002
1.5
1.0
0.5
0.0
WT
Mybpc3-/-
Mybpc3-/- BTZ

FIG. 3C

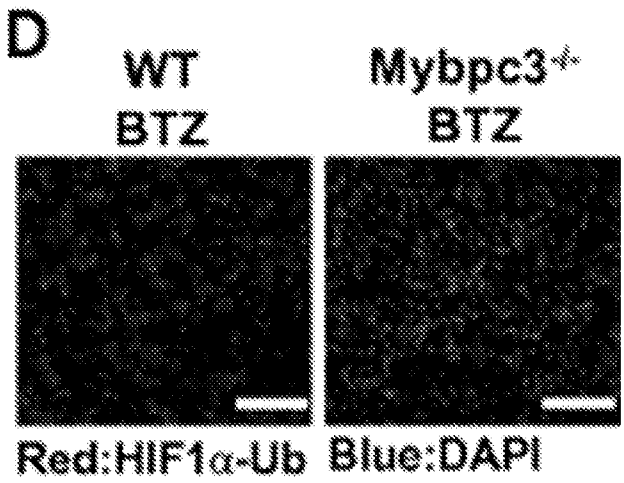
D
WT BTZ
Mybpc3-/- BTZ
Red:HIF1α-Ub
Blue:DAPI

FIG. 3D

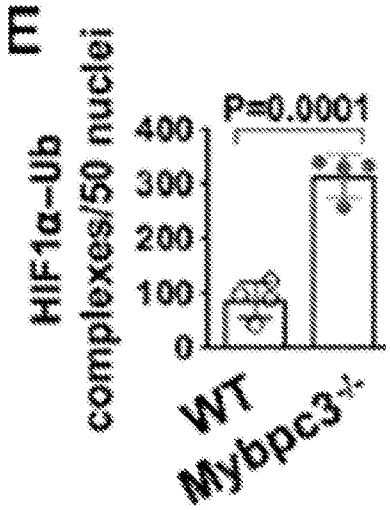
E
HIF1α–Ub complexes/50 nuclei
P=0.0001
400
300
200
100
0
WT
Mybpc3-/-

FIG. 3E

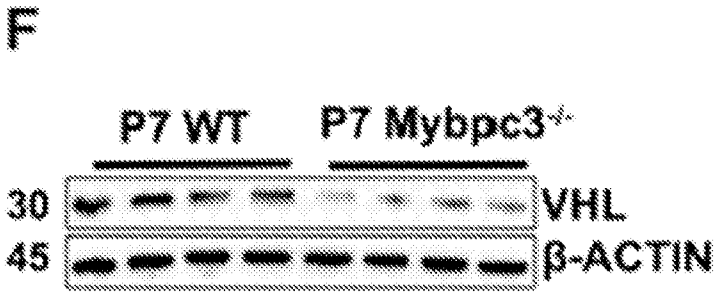
F
P7 WT
P7 Mybpc3-/-
30
45
VHL
β-ACTIN

FIG. 3F

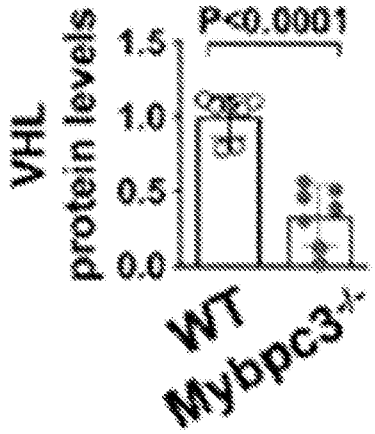
P<0.0001
VHL protein levels
1.5
1.0
0.5
0.0
WT
Mybpc3-/-

FIG. 3G

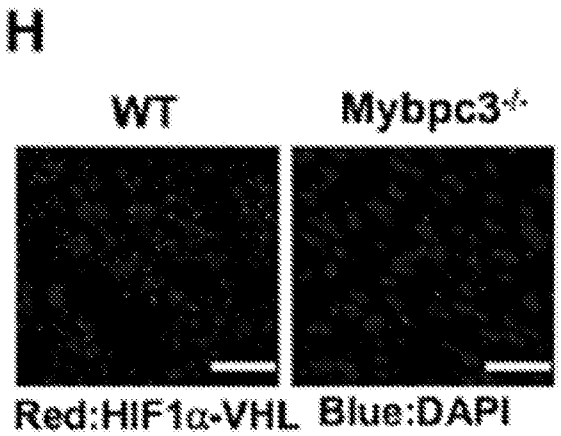
H
WT
Mybpc3-/-
Red:HIF1α-VHL
Blue:DAPI

FIG. 3H

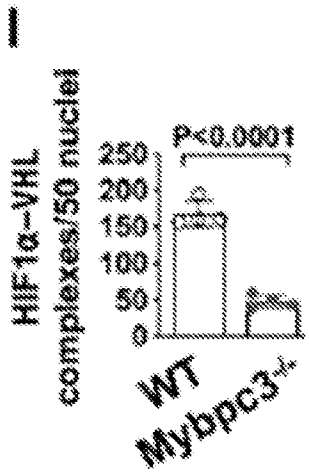
I
HIF1α–VHL complexes/50 nuclei
250
200
150
100
50
0
P<0.0001
WT
Mybpc3-/-

FIG. 3I

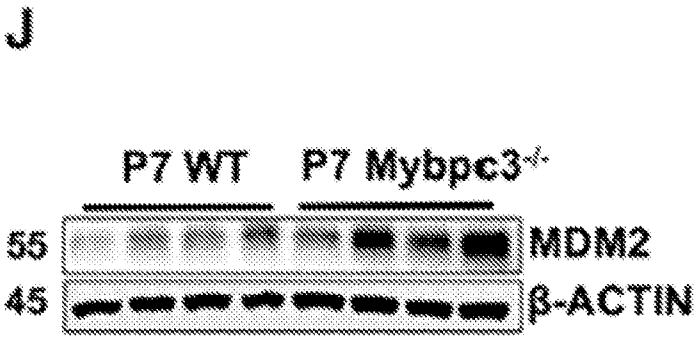
J
P7 WT
P7 Mybpc3-/-
55
45
MDM2
β-ACTIN

FIG. 3J

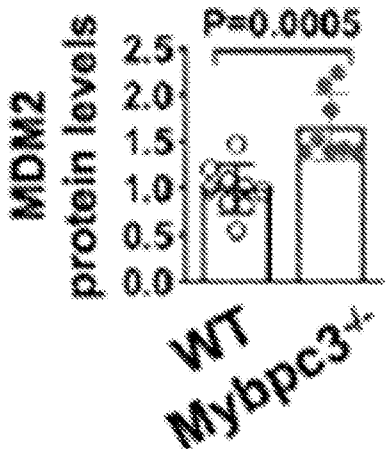

FIG. 3K

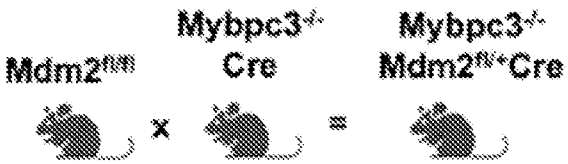

FIG. 3L

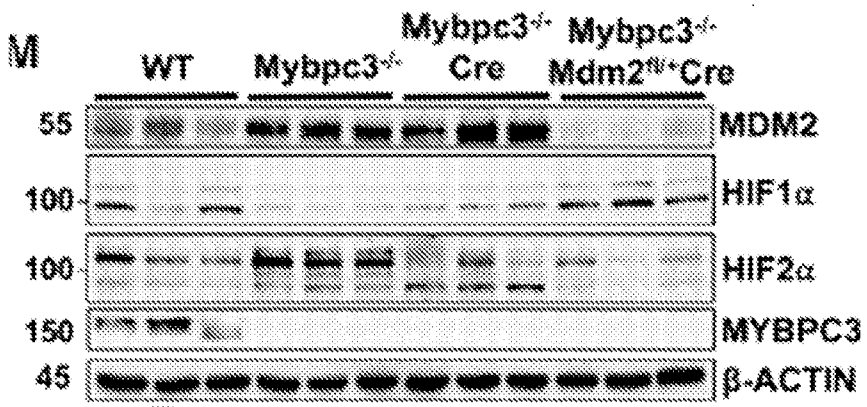

FIG. 3M

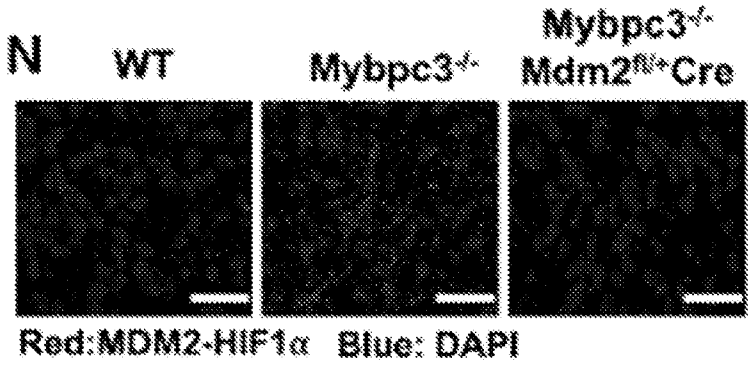
N
WT
Mybpc3-/-
Mybpc3-/-
Mdm2fl/+Cre
Red:MDM2-HIF1α Blue: DAPI

FIG. 3N

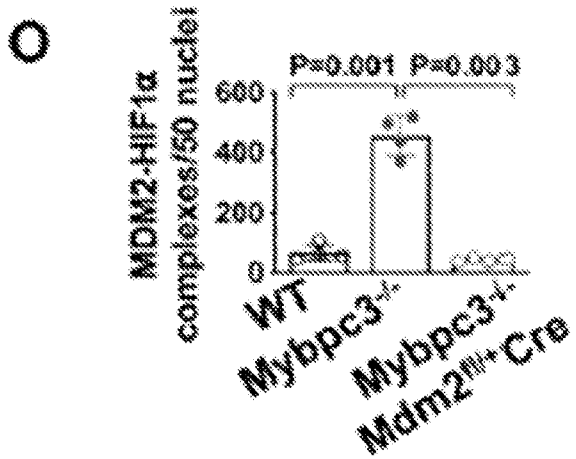
O
MDM2-HIF1α
complexes/50 nuclei
P=0.001 P=0.003
600
400
200
0
WT
Mybpc3-/-
Mybpc3-/-
Mdm2fl/+Cre

FIG. 3O

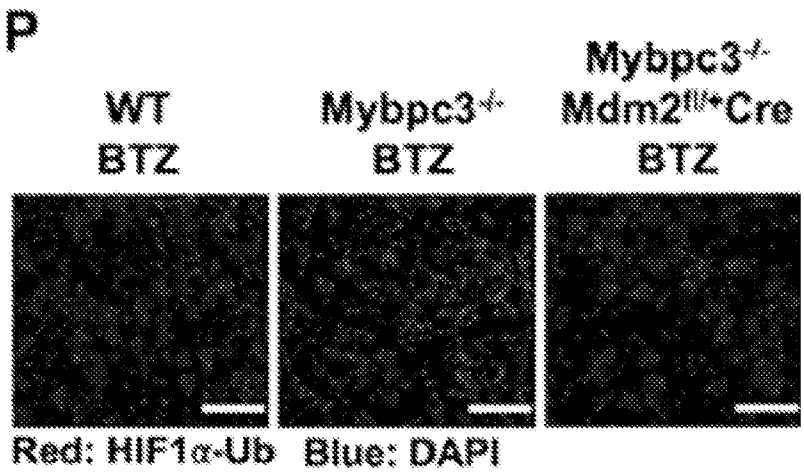
P
WT
BTZ
Mybpc3-/-
BTZ
Mybpc3-/-
Mdm2fl/+Cre
BTZ
Red: HIF1α-Ub
Blue: DAPI

FIG. 3P

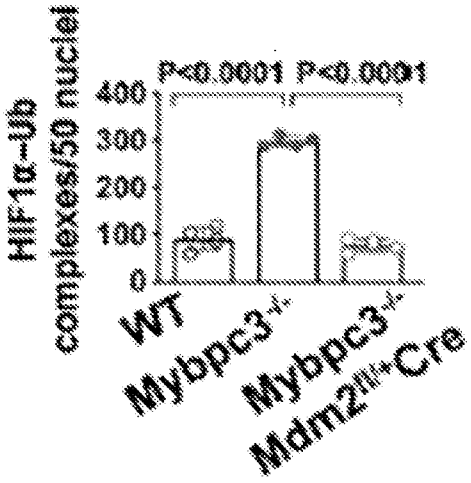
HIF1α–Ub
complexes/50 nuclei
400
300
200
100
0
P<0.0001
P<0.0001
WT
Mybpc3-/-
Mybpc3-/-
Mdm2fl/+Cre

FIG. 3Q

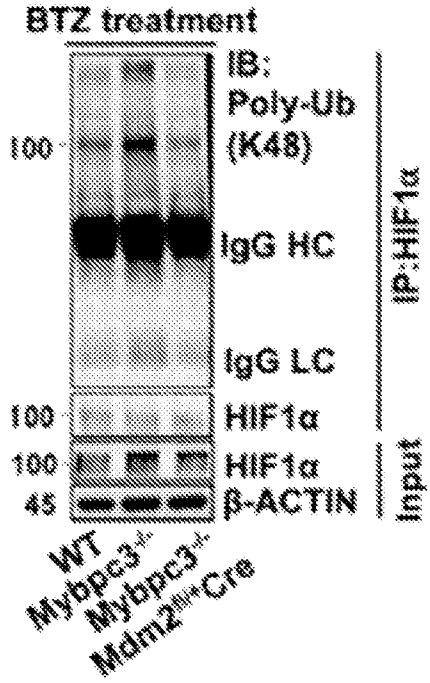
BTZ treatment
IB:
Poly-Ub
(K48)
100
IgG HC
IgG LC
IP:HIF1α
100
HIF1α
100
HIF1α
45
β-ACTIN
Input
WT
Mybpc3-/-
Mybpc3-/-
Mdm2fl/+Cre

FIG. 3R

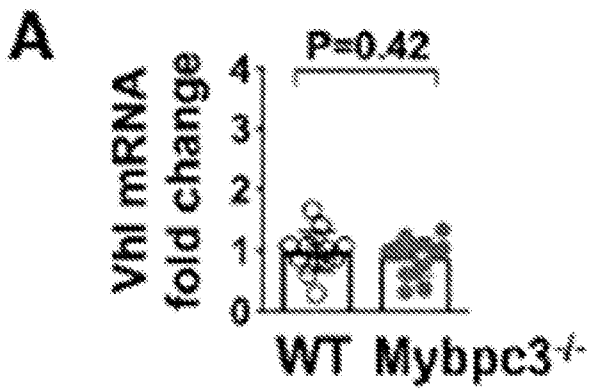
A
P=0.42
Vhl mRNA
fold change
4
3
2
1
0
WT Mybpc3-/-

FIG. 4A


B
30
150
45
VHL
MYBPC3
β-ACTIN
WT
Mybpc3-/-
Mybpc3-/-
BTZ

FIG. 4B

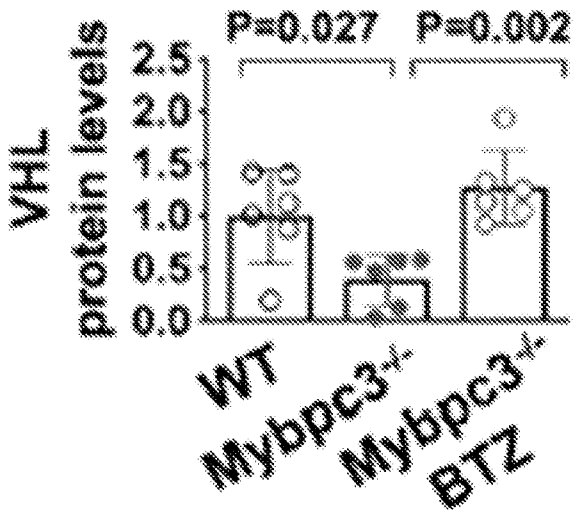
P=0.027
P=0.002
VHL
protein levels
2.5
2.0
1.5
1.0
0.5
0.0
WT
Mybpc3-/-
Mybpc3-/-
BTZ

FIG. 4C

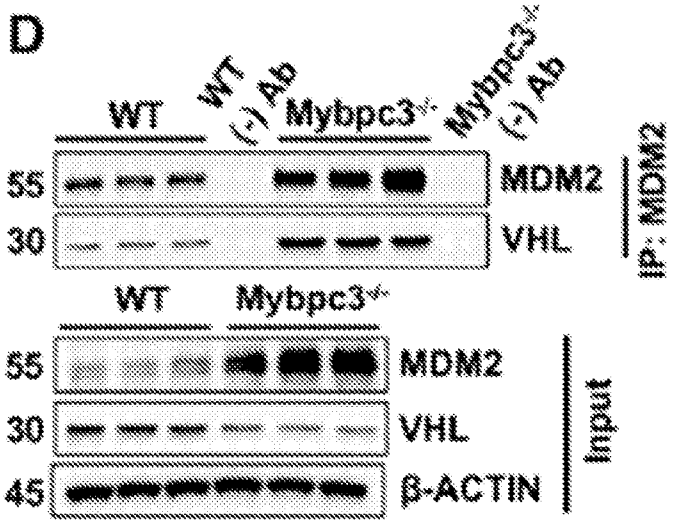
D
WT
WT (-) Ab
Mybpc3-/-
Mybpc3-/- (-) Ab
55
MDM2
30
VHL
IP: MDM2
WT
Mybpc3-/-
55
MDM2
30
VHL
45
β-ACTIN
Input

FIG. 4D

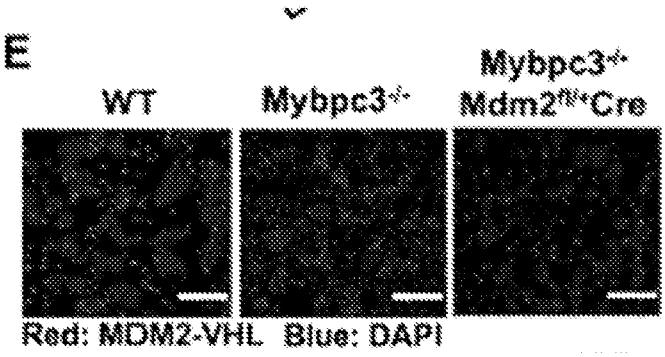
E
WT
Mybpc3-/-
Mybpc3-/-
Mdm2fl/fl Cre
Red: MDM2-VHL Blue: DAPI

FIG. 4E

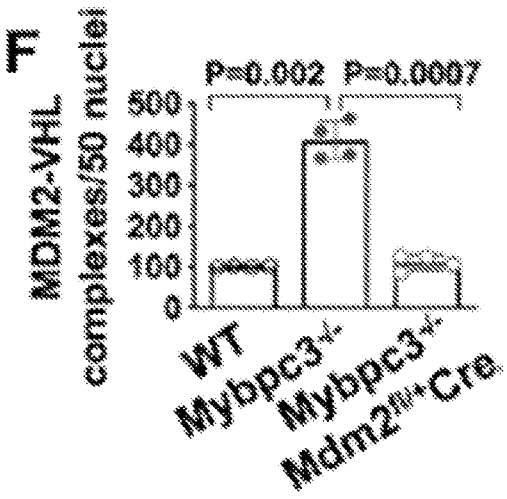
F
MDM2-VHL complexes/50 nuclei
P=0.002
P=0.0007
500
400
300
200
100
0
WT
Mybpc3-/-
Mybpc3-/- Mdm2fl/+Cre

FIG. 4F

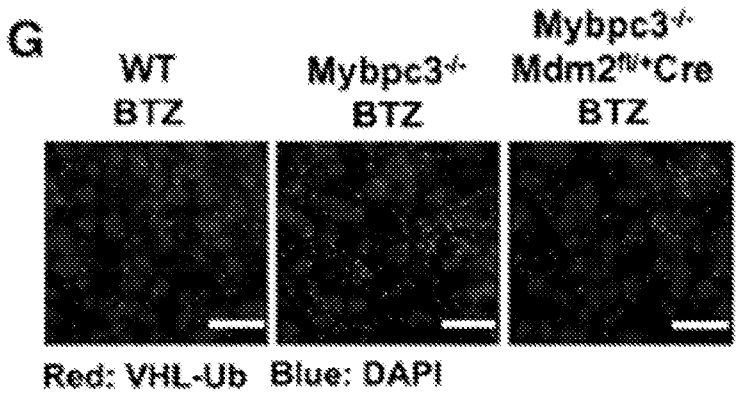
G
WT
BTZ
Mybpc3-/-
BTZ
Mybpc3-/-
Mdm2fl/+Cre
BTZ
Red: VHL-Ub Blue: DAPI

FIG. 4G

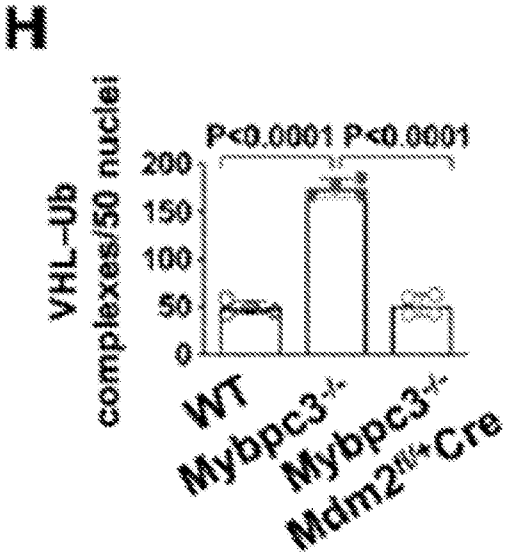
H
VHL–Ub complexes/50 nuclei
P<0.0001 P<0.0001
200
150
100
50
0
WT
Mybpc3-/-
Mybpc3-/- Mdm2fl/fl+Cre

FIG. 4H

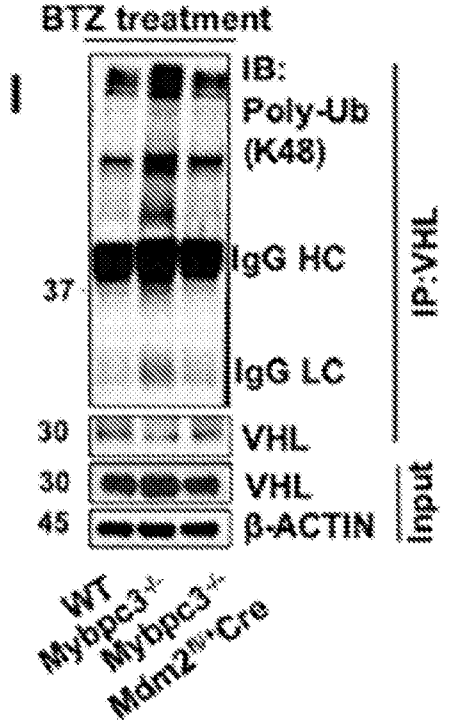
BTZ treatment
I
IB:
Poly-Ub (K48)
IgG HC
IgG LC
IP:VHL
37
30
VHL
30
VHL
45
β-ACTIN
Input
WT
Mybpc3-/-
Mybpc3-/- Mdm2fl/fl+Cre

FIG. 4I

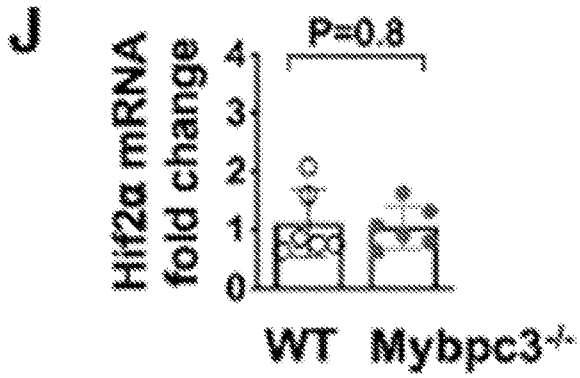

FIG. 4J

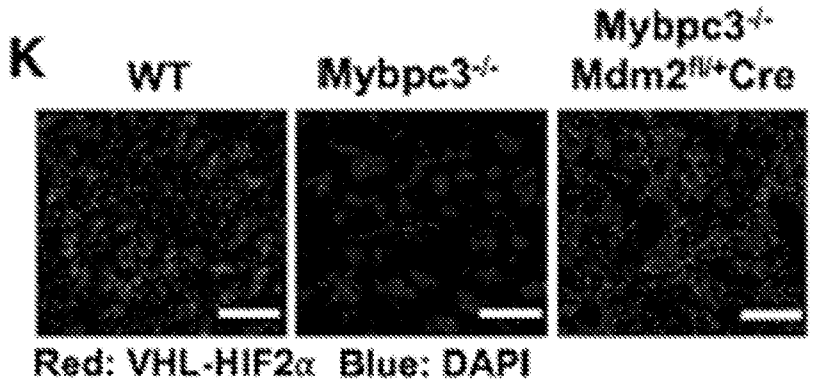

FIG. 4K

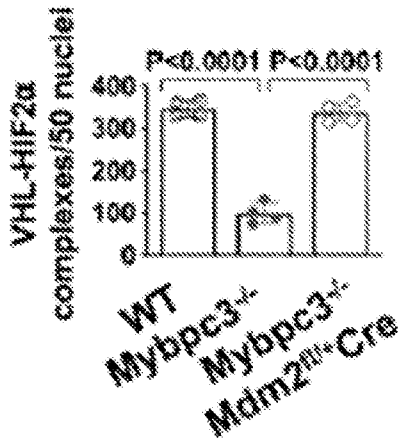

FIG. 4L

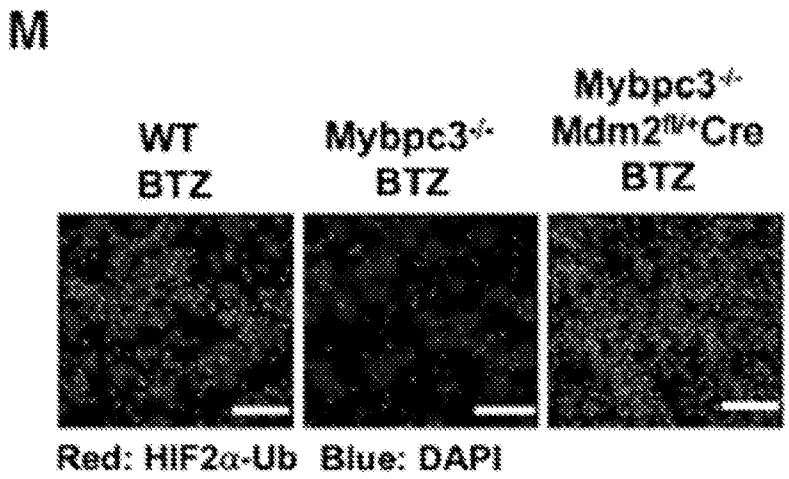
M
WT
BTZ
Mybpc3-/-
BTZ
Mybpc3-/-
Mdm2fl/+Cre
BTZ
Red: HIF2α-Ub
Blue: DAPI

FIG. 4M

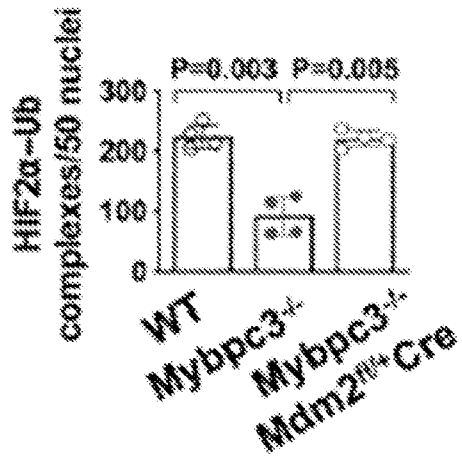
HIF2α-Ub
complexes/50 nuclei
300
200
100
0
P=0.003
P=0.005
WT
Mybpc3-/-
Mybpc3-/-
Mdm2fl/+Cre

FIG. 4N

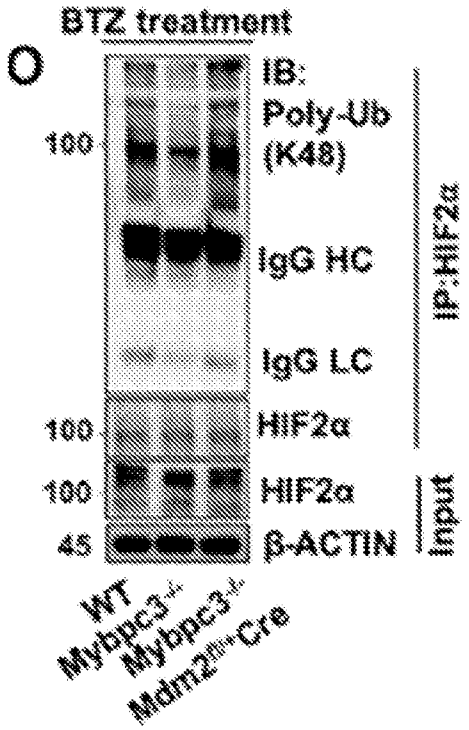
O
BTZ treatment
IB:
Poly-Ub
(K48)
IgG HC
IgG LC
HIF2α
HIF2α
β-ACTIN
IP:HIF2α
input
100
100
100
45
WT
Mybpc3-/-
Mybpc3-/-
Mdm2fl/+Cre

FIG. 4O

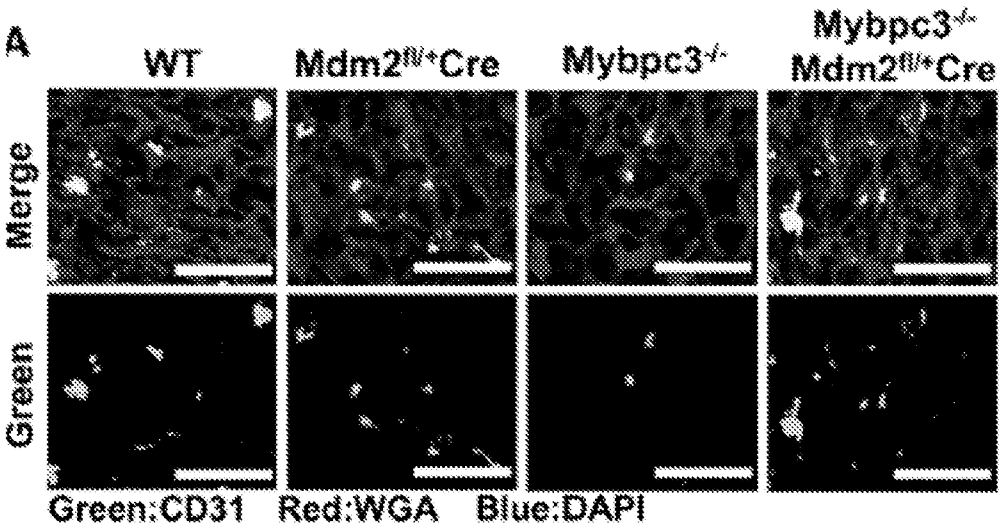
A
WT
Mdm2fl/+Cre
Mybpc3-/-
Mybpc3-/-
Mdm2fl/+Cre
Merge
Green
Green:CD31 Red:WGA Blue:DAPI

FIG. 5A

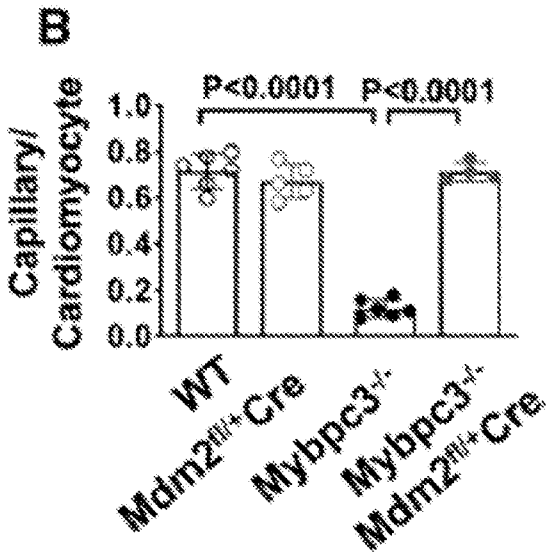
B
Capillary/ Cardiomyocyte
1.0
0.8
0.6
0.4
0.2
0.0
P<0.0001
P<0.0001
WT
Mdm2fl/+Cre
Mybpc3-/-
Mybpc3-/- Mdm2fl/+Cre

FIG. 5B

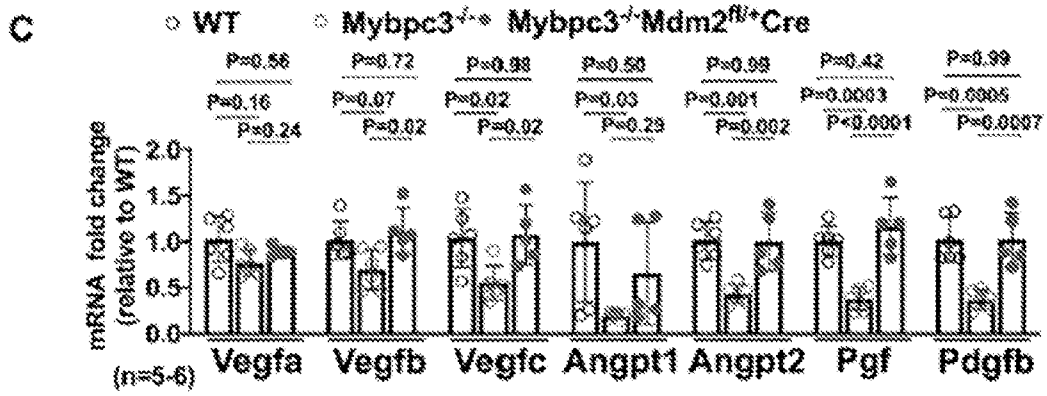
C
WT
Mybpc3-/-
Mybpc3-/-Mdm2fl/+Cre
mRNA fold change (relative to WT)
(n=5-6)
Vegfa
Vegfb
Vegfc
Angpt1
Angpt2
Pgf
Pdgfb

FIG. 5C

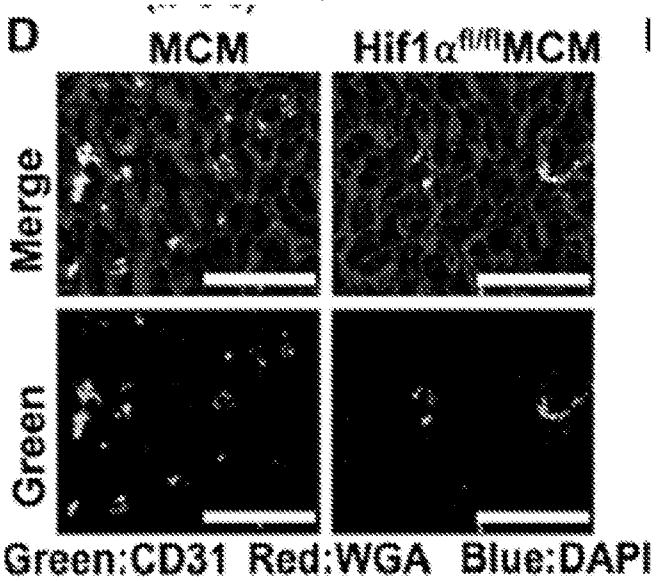
D
MCM
Hif1α^fl/fl MCM
Merge
Green
Green:CD31 Red:WGA Blue:DAPI

FIG. 5D

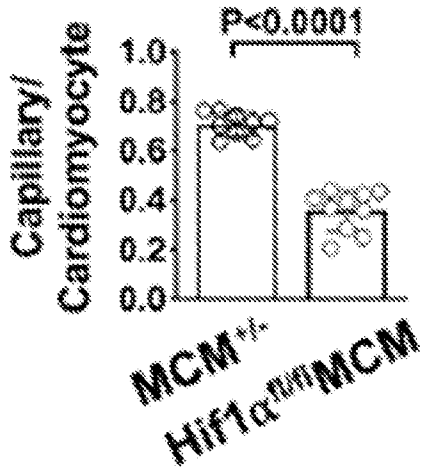
P<0.0001
Capillary/ Cardiomyocyte
1.0
0.8
0.6
0.4
0.2
0.0
MCM+/+
Hif1α fl/fl MCM

FIG. 5E

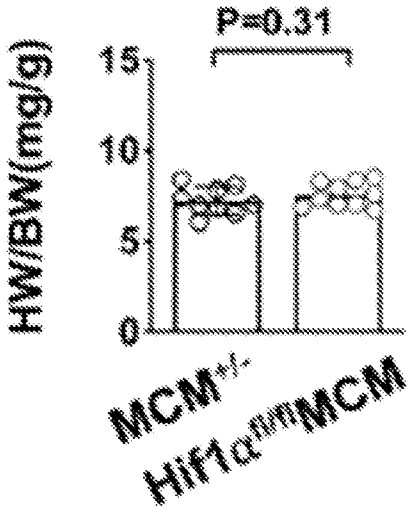
P=0.31
HW/BW(mg/g)
15
10
5
0
MCM+/-
Hif1α fl/flMCM

FIG. 5F

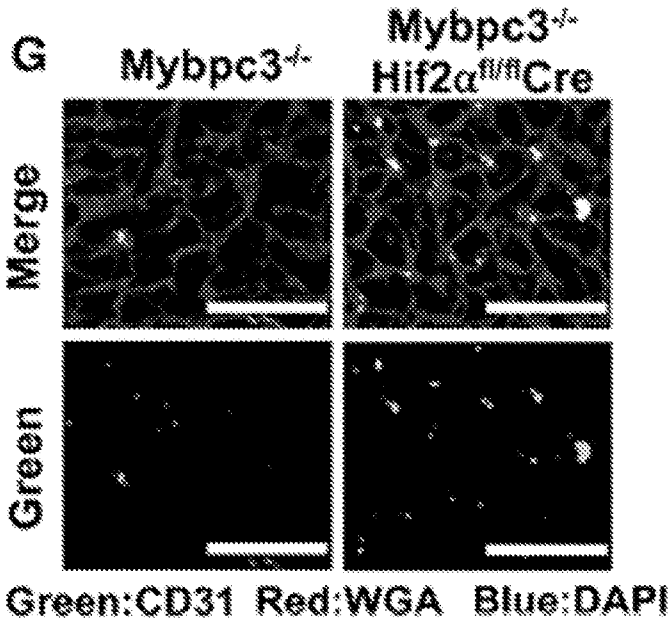
G
Mybpc3-/-
Mybpc3-/-
Hif2α fl/flCre
Merge
Green
Green:CD31 Red:WGA Blue:DAPI

FIG. 5G

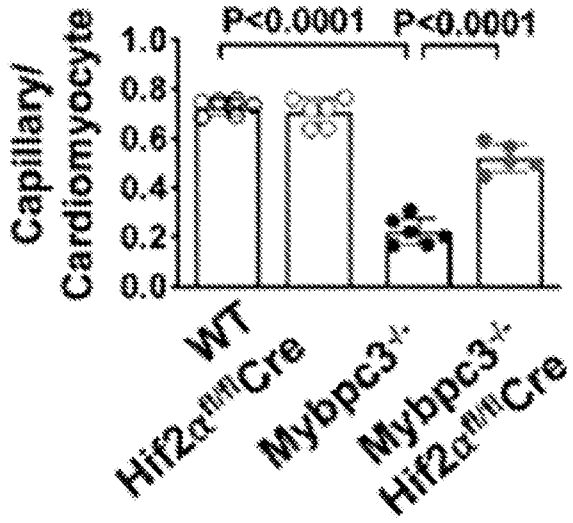
P<0.0001
P<0.0001
Capillary/ Cardiomyocyte
1.0
0.8
0.6
0.4
0.2
0.0
WT
Hif2α^fl/flCre
Mybpc3^-/-
Mybpc3^-/- Hif2α^fl/flCre

FIG. 5H

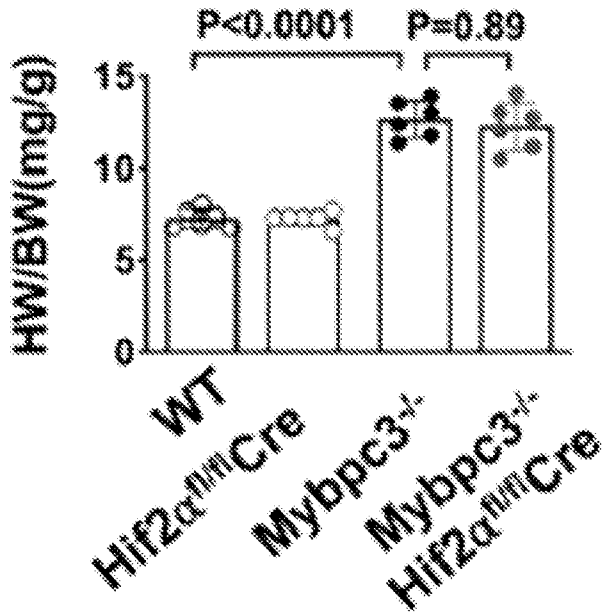
P<0.0001
P=0.89
HW/BW(mg/g)
15
10
5
0
WT
Hif2α^fl/flCre
Mybpc3^-/-
Mybpc3^-/- Hif2α^fl/flCre

FIG. 5I

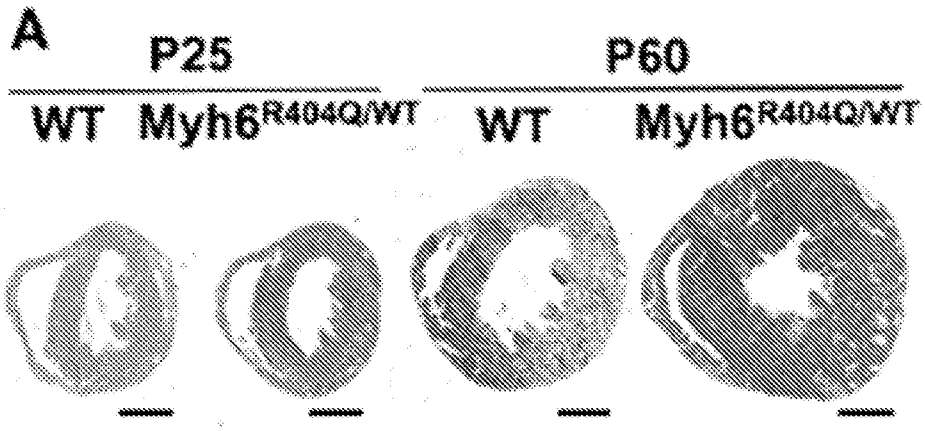
A
P25
P60
WT
Myh6R404Q/WT
WT
Myh6R404Q/WT

FIG. 6A

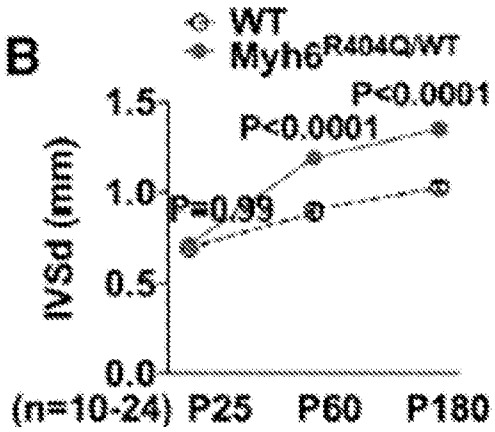
B
WT
Myh6R404Q/WT
P<0.0001
P<0.0001
P=0.99
IVSd (mm)
1.5
1.0
0.5
0.0
(n=10-24)
P25
P60
P180

FIG. 6B

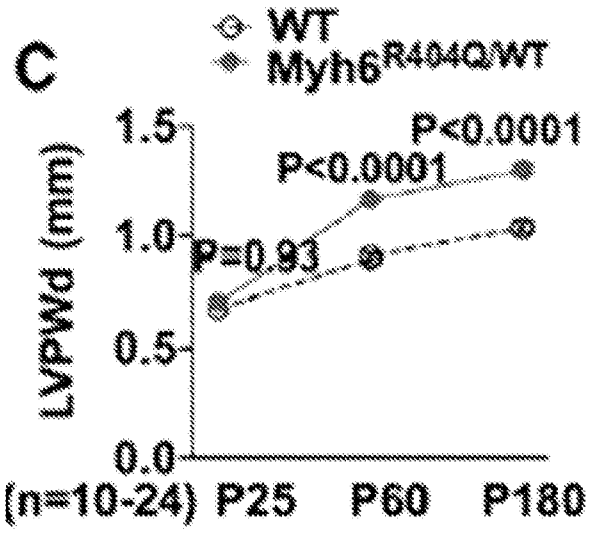
C
WT
Myh6R404Q/WT
LVPWd (mm)
1.5
1.0
0.5
0.0
P<0.0001
P<0.0001
P=0.93
(n=10-24) P25 P60 P180

FIG. 6C

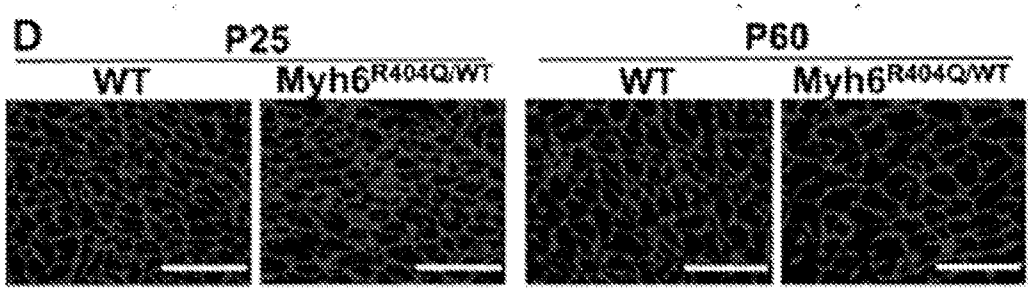
D
P25
P60
WT
Myh6R404Q/WT
WT
Myh6R404Q/WT

FIG. 6D

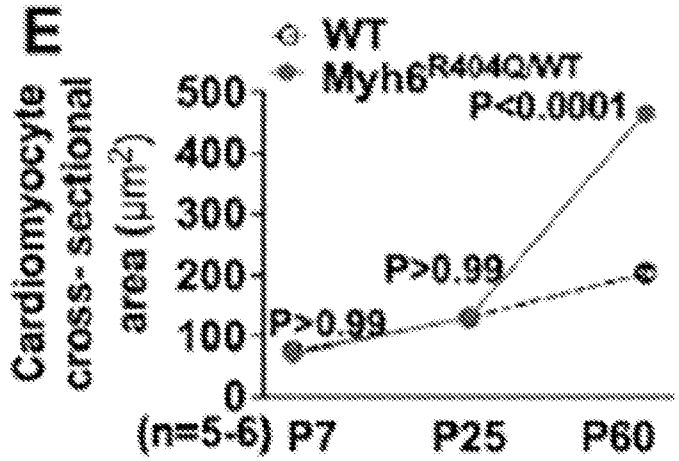
E
WT
Myh6R404Q/WT
P<0.0001
P>0.99
P>0.99
Cardiomyocyte cross- sectional area (μm2)
500
400
300
200
100
0
(n=5-6) P7
P25
P60

FIG. 6E

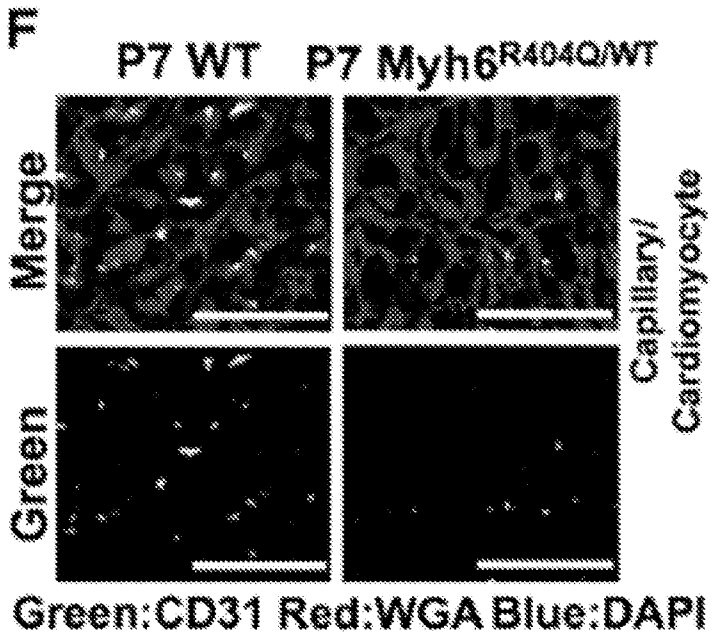
F
P7 WT
P7 Myh6R404Q/WT
Merge
Green
Capillary/ Cardiomyocyte
Green:CD31 Red:WGA Blue:DAPI

FIG. 6F

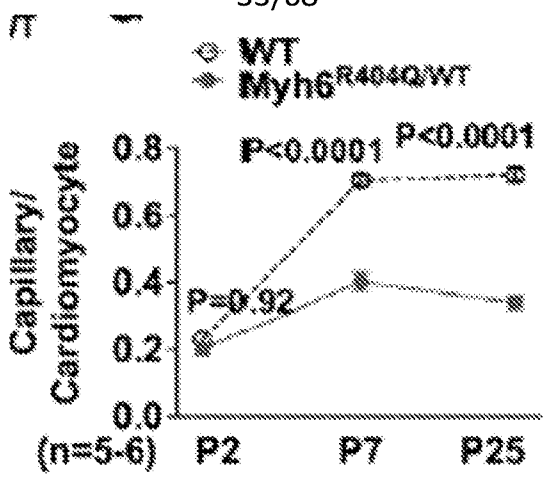

FIG. 6G

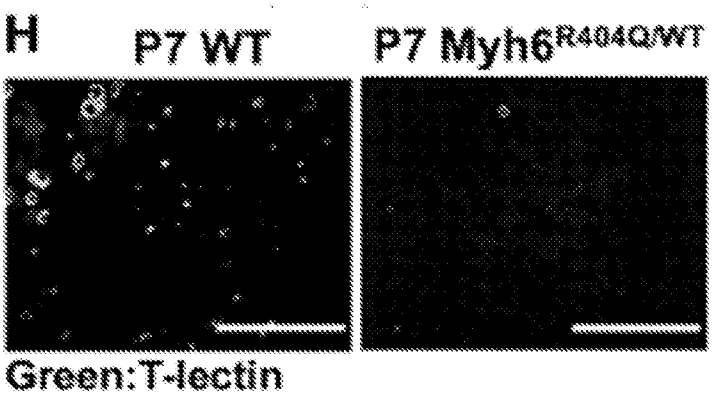

FIG. 6H

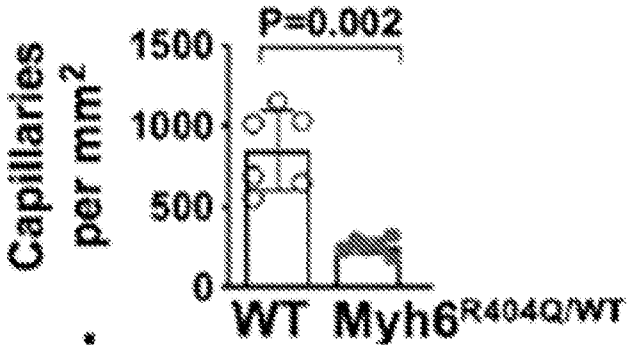

FIG. 6I

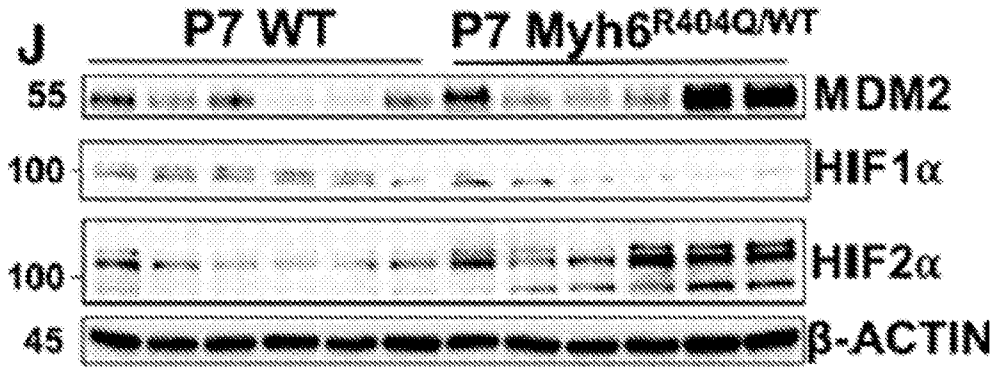

FIG. 6J

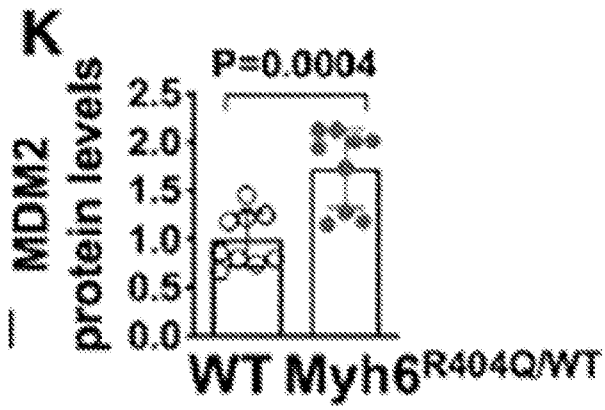

FIG. 6K

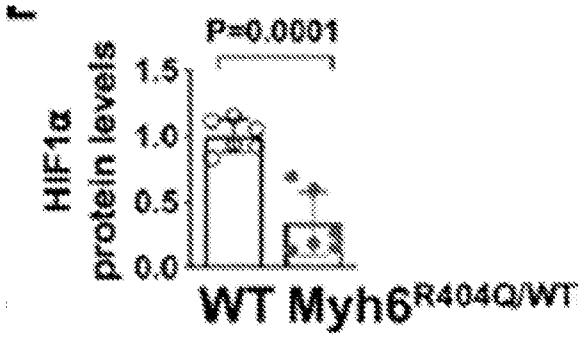

FIG. 6L

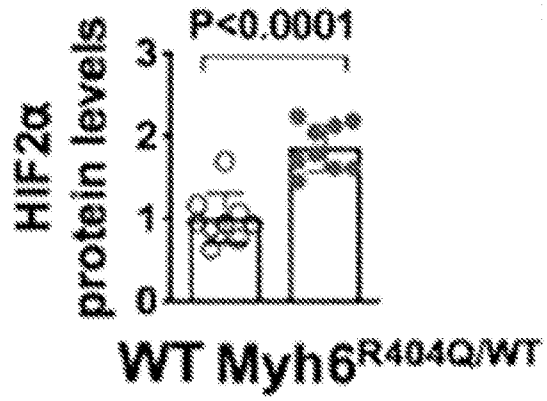
P<0.0001
HIF2α protein levels
3
2
1
0
WT
Myh6R404Q/WT

FIG. 6M

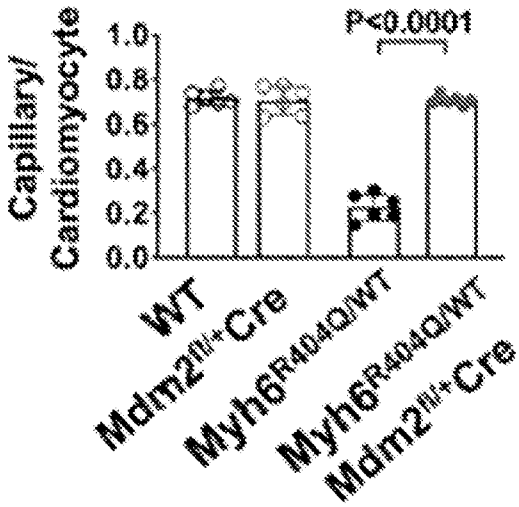
P<0.0001
Capillary/ Cardiomyocyte
1.0
0.8
0.6
0.4
0.2
0.0
WT
Mdm2fl/+Cre
Myh6R404Q/WT
Myh6R404Q/WT Mdm2fl/+Cre

FIG. 6N

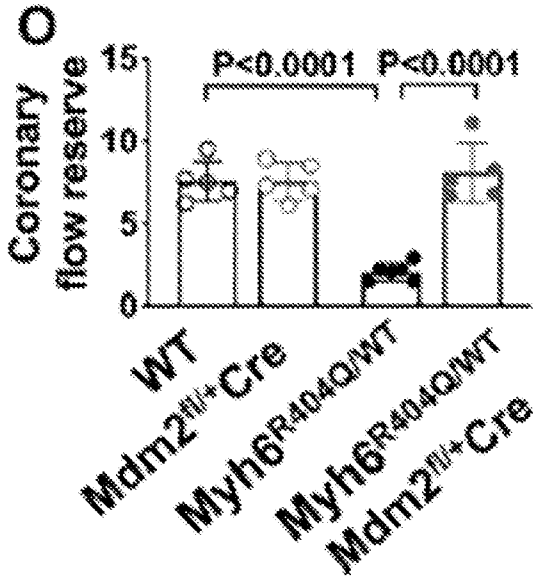
O
Coronary flow reserve
15
10
5
0
P<0.0001
P<0.0001
WT
Mdm2fl/+Cre
Myh6R404Q/WT
Myh6R404Q/WT
Mdm2fl/+Cre

FIG. 6O

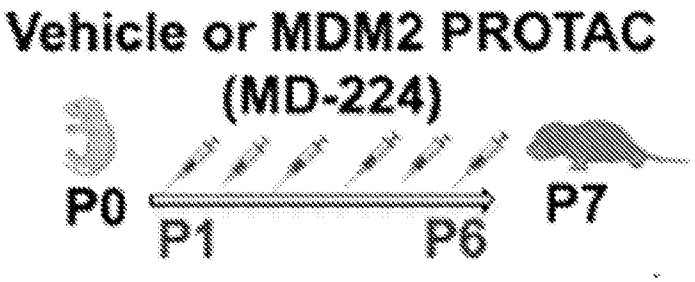
Vehicle or MDM2 PROTAC
(MD-224)
P0
P1
P6
P7

FIG. 7A

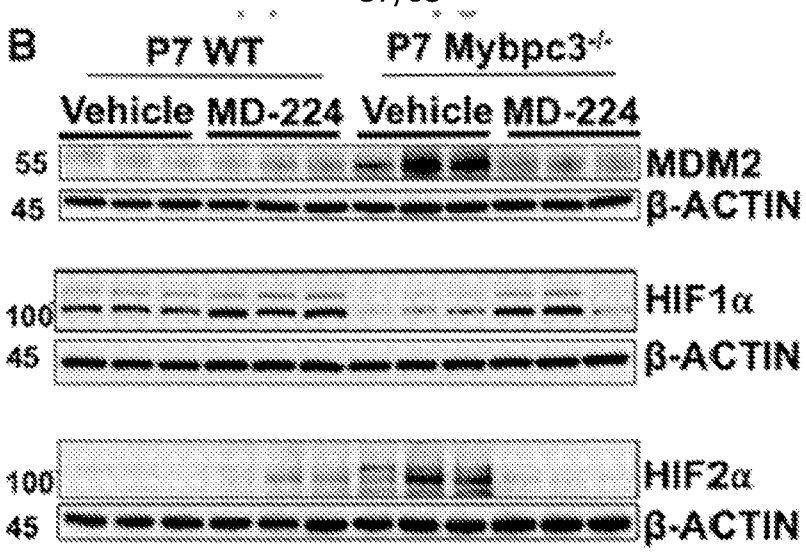
B
P7 WT
P7 Mybpc3-/-
Vehicle
MD-224
Vehicle
MD-224
55
MDM2
45
β-ACTIN
100
HIF1α
45
β-ACTIN
100
HIF2α
45
β-ACTIN

FIG. 7B

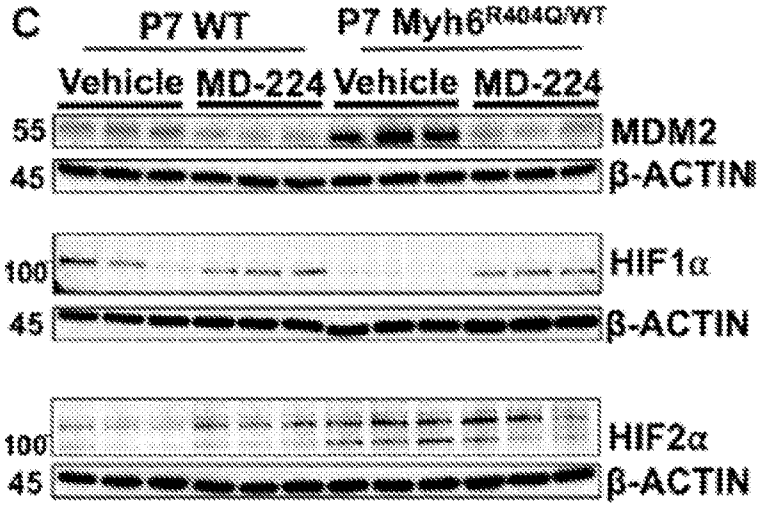
C
P7 WT
P7 Myh6R404Q/WT
Vehicle
MD-224
Vehicle
MD-224
55
MDM2
45
β-ACTIN
100
HIF1α
45
β-ACTIN
100
HIF2α
45
β-ACTIN

FIG. 7C

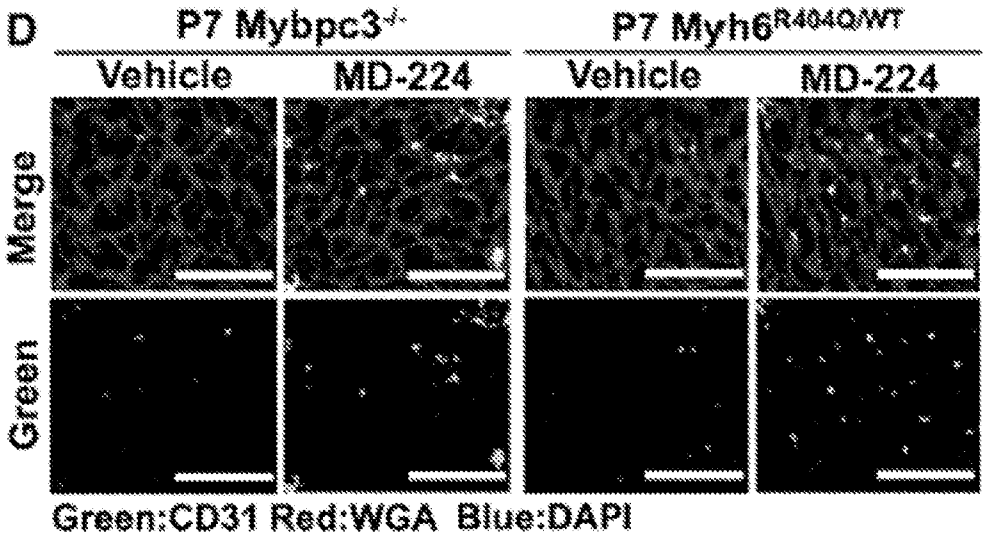
D
P7 Mybpc3-/-
P7 Myh6R404Q/WT
Vehicle
MD-224
Vehicle
MD-224
Merge
Green
Green:CD31 Red:WGA Blue:DAPI

FIG. 7D

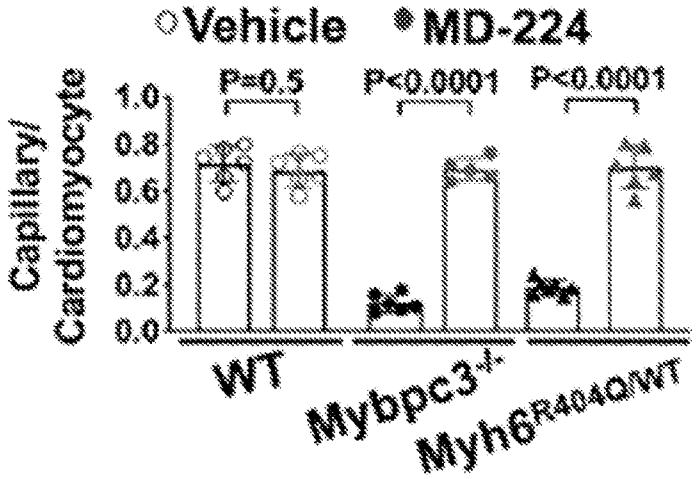
Vehicle
MD-224
Capillary/ Cardiomyocyte
1.0
0.8
0.6
0.4
0.2
0.0
P=0.5
P<0.0001
P<0.0001
WT
Mybpc3-/-
Myh6R404Q/WT

FIG. 7E

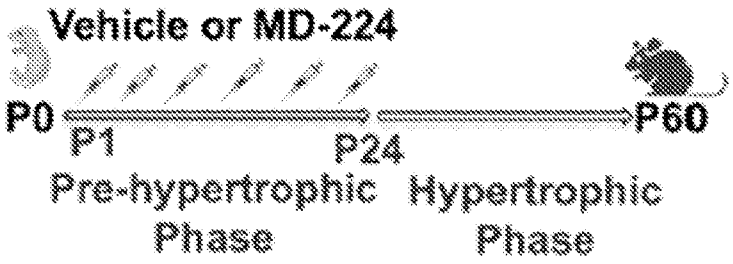
Vehicle or MD-224
P0
P1
P24
P60
Pre-hypertrophic Phase
Hypertrophic Phase

FIG. 7F

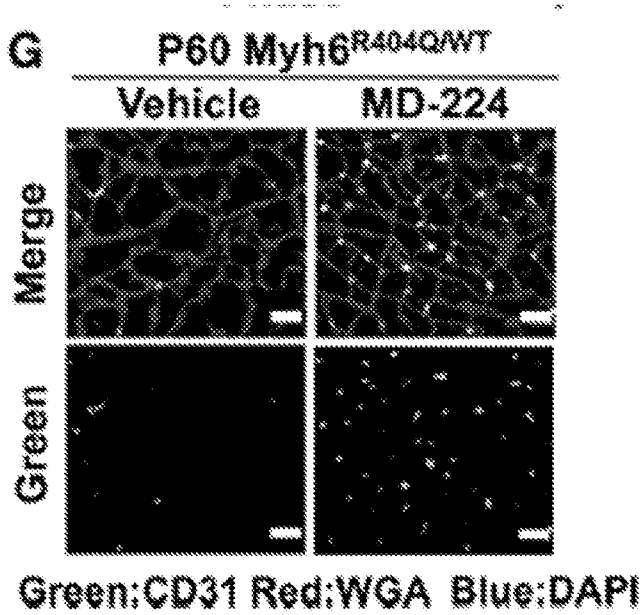
G
P60 Myh6R404Q/WT
Vehicle
MD-224
Merge
Green
Green:CD31 Red:WGA Blue:DAPI

FIG. 7G

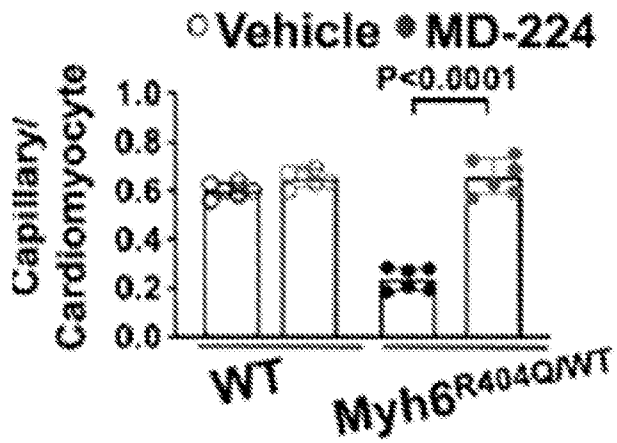
Vehicle
MD-224
P<0.0001
Capillary/ Cardiomyocyte
1.0
0.8
0.6
0.4
0.2
0.0
WT
Myh6R404Q/WT

FIG. 7H

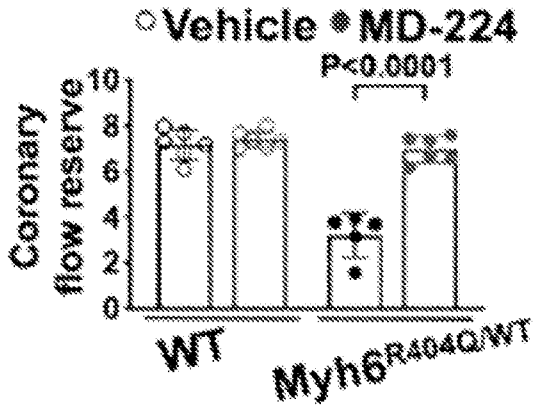
Vehicle
MD-224
P<0.0001
Coronary flow reserve
10
8
6
4
2
0
WT
Myh6R404Q/WT

FIG. 7I

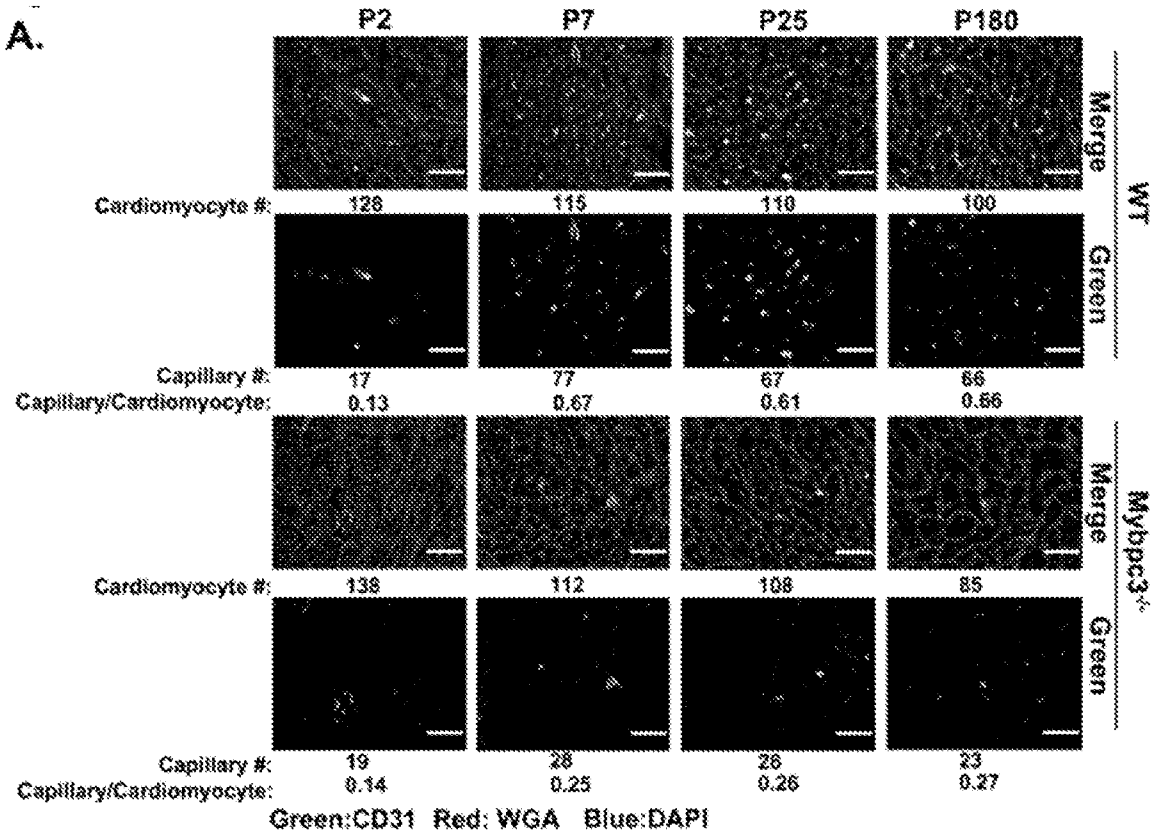
A.
P2
P7
P25
P180
WT
Merge
Green
Cardiomyocyte #:
128
115
110
100
Capillary #:
17
77
67
66
Capillary/Cardiomyocyte:
0.13
0.67
0.61
0.66
Mybpc3-/-
Merge
Green
Cardiomyocyte #:
138
112
108
85
Capillary #:
19
28
26
23
Capillary/Cardiomyocyte:
0.14
0.25
0.26
0.27
Green:CD31 Red: WGA Blue:DAPI

FIG. 8A

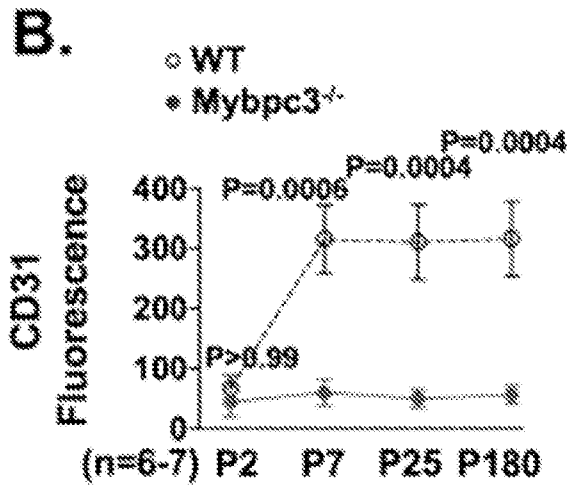
B.
WT
Mybpc3-/-
P=0.0004
P=0.0004
P=0.0006
P>0.99
CD31 Fluorescence
400
300
200
100
0
(n=6-7) P2 P7 P25 P180

FIG. 8B

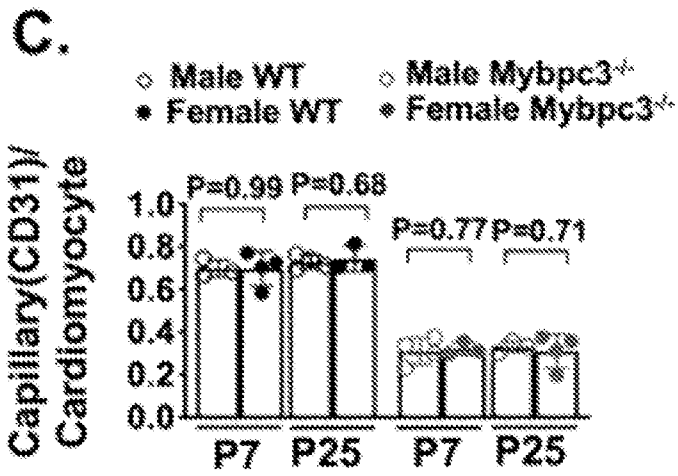
C.
Male WT
Female WT
Male Mybpc3-/-
Female Mybpc3-/-
Capillary(CD31)/ Cardiomyocyte
1.0
0.8
0.6
0.4
0.2
0.0
P=0.99
P=0.68
P=0.77
P=0.71
P7
P25
P7
P25

FIG. 8C

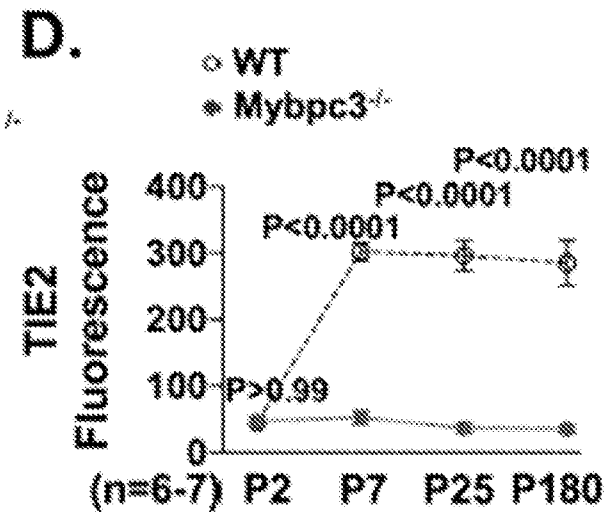
D.
WT
Mybpc3-/-
TIE2 Fluorescence
400
300
200
100
0
P<0.0001
P<0.0001
P<0.0001
P>0.99
(n=6-7)
P2
P7
P25
P180

FIG. 8D

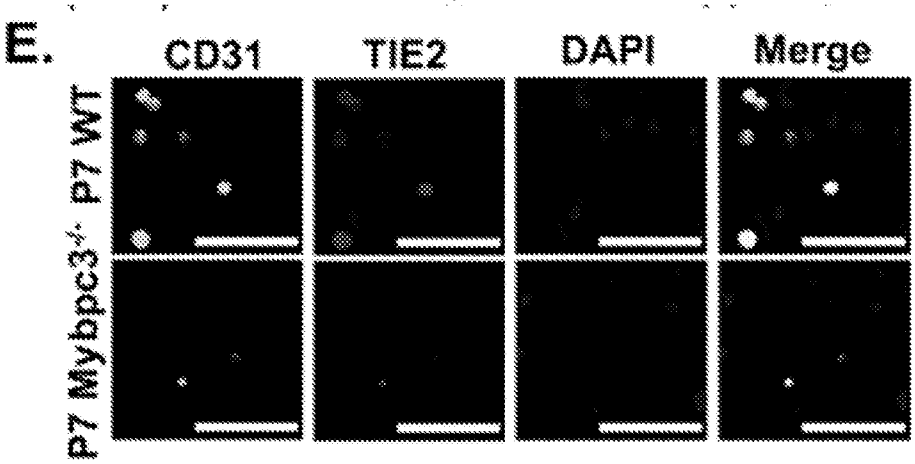

FIG. 8E

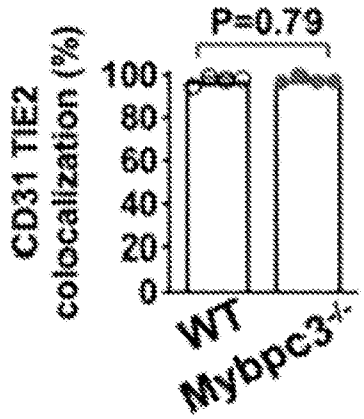

FIG. 8F

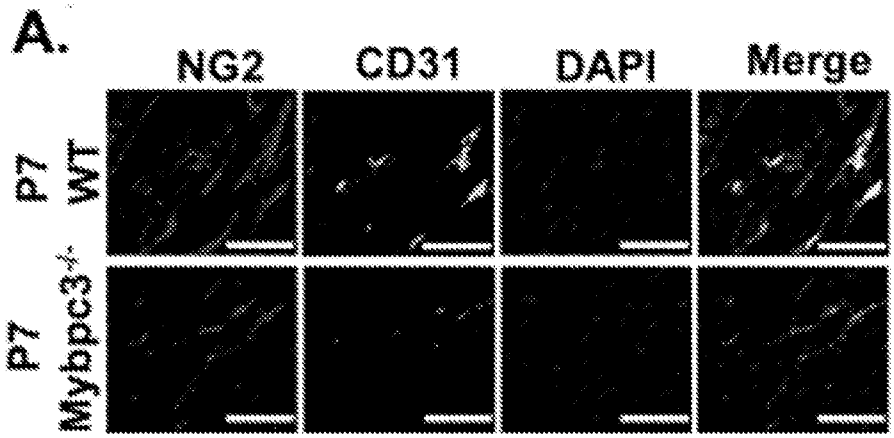

FIG. 9A

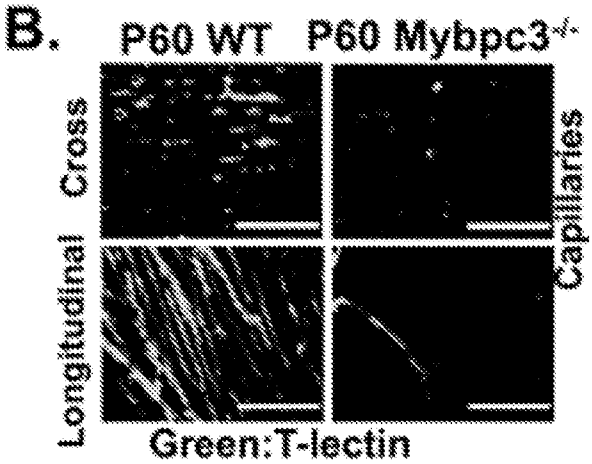
B.
P60 WT
P60 Mybpc3-/-
Cross
Longitudinal
Capillaries
Green:T-lectin

FIG. 9B

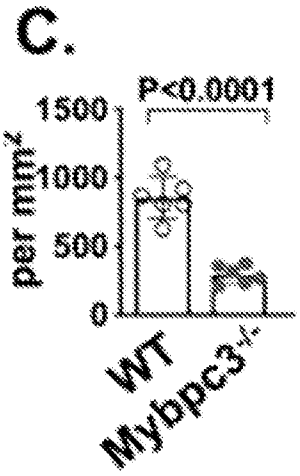
C.
P<0.0001
1500
1000
500
0
per mm2
WT
Mybpc3-/-

FIG. 9C

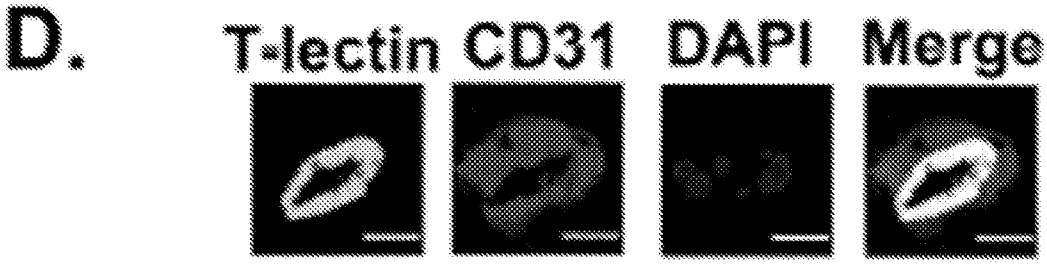

FIG. 9D

FIG. 9E

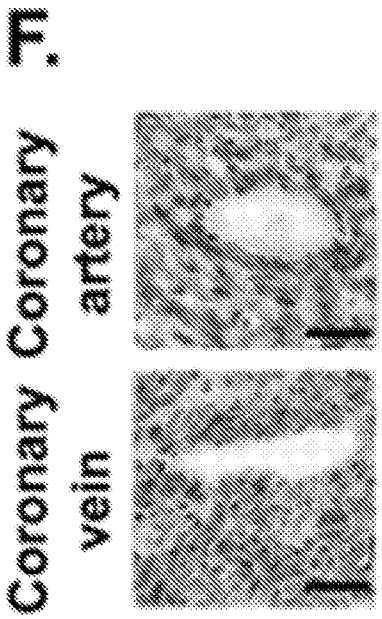

FIG. 9F

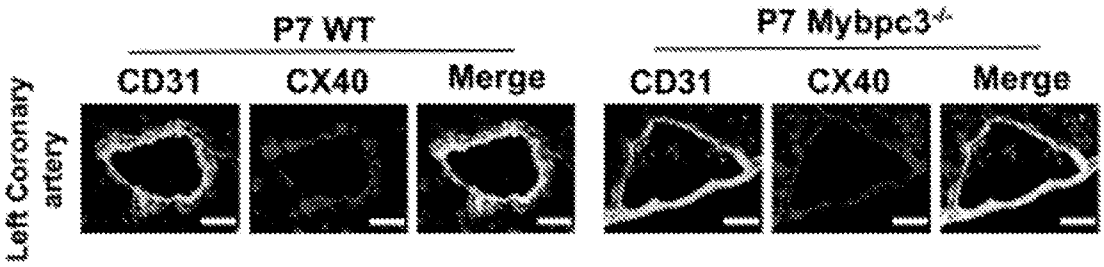

FIG. 9G

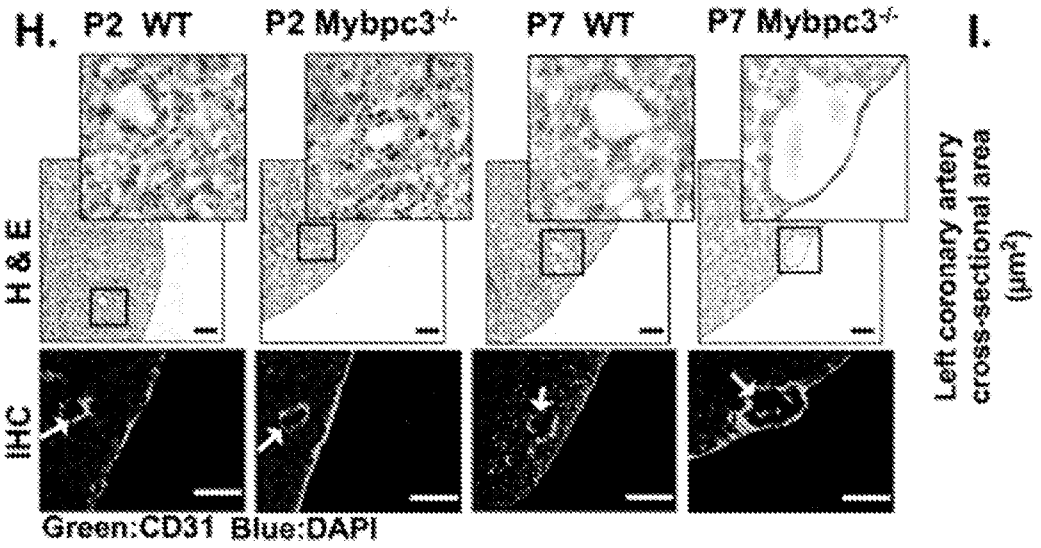

FIG. 9H

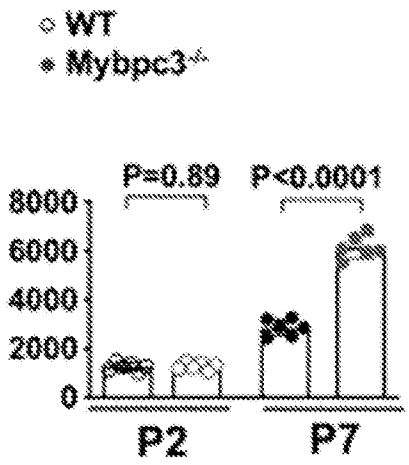

FIG. 9I

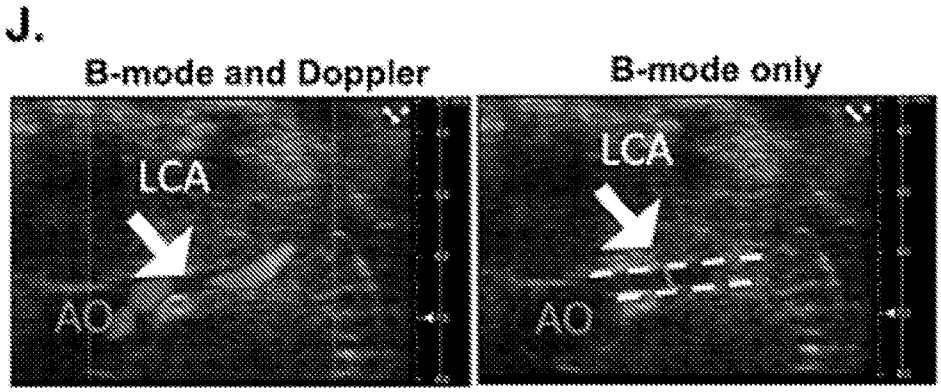

FIG. 9J

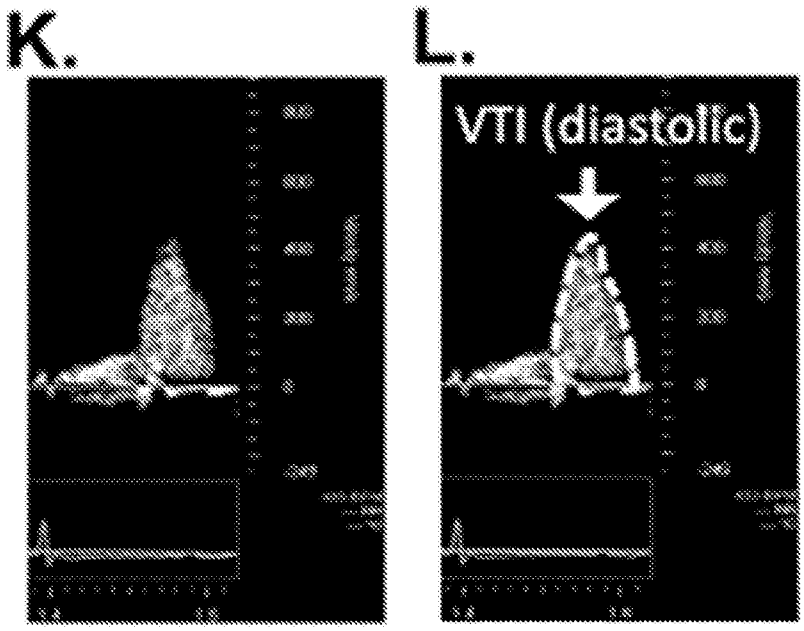

FIG. 9K, 9L

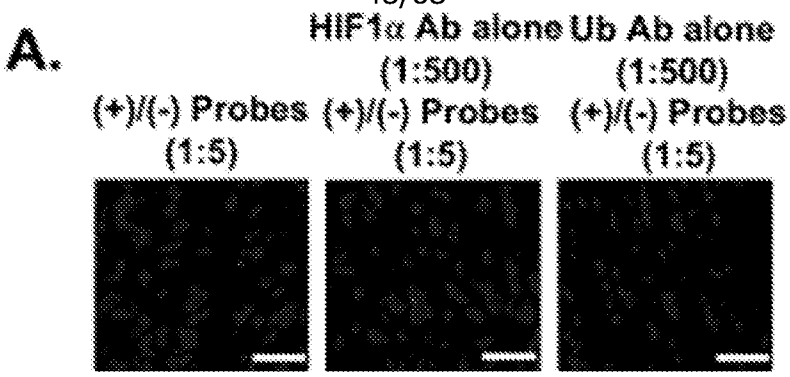

FIG. 10A

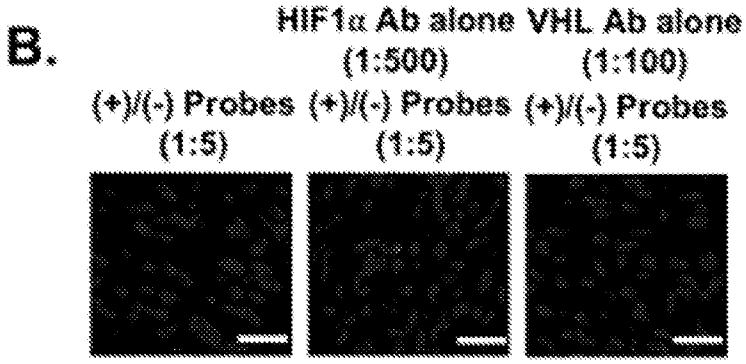

FIG. 10B

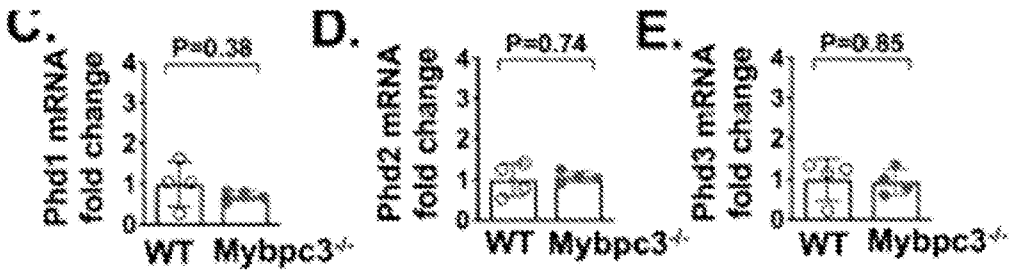

FIG. 10C, 10D, 10E

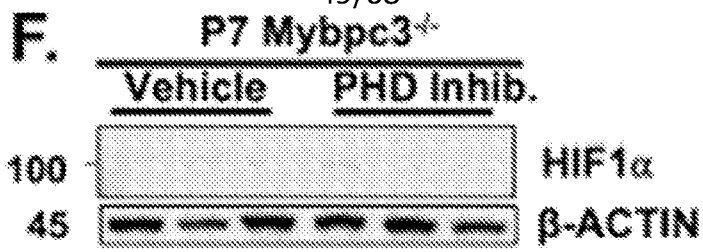

FIG. 10F

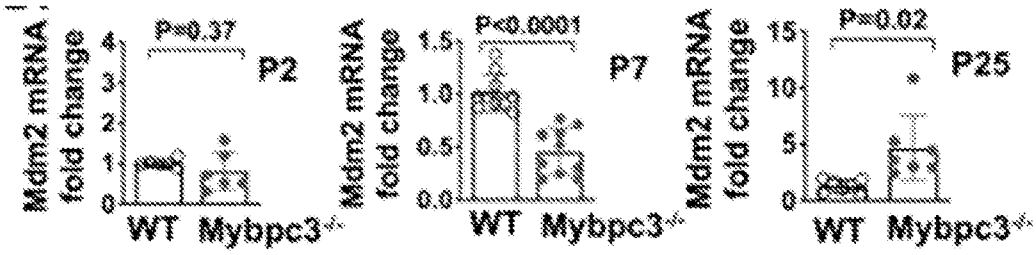

FIG. 10G

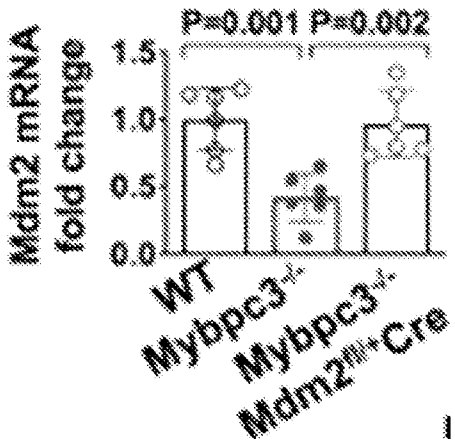

FIG. 10H

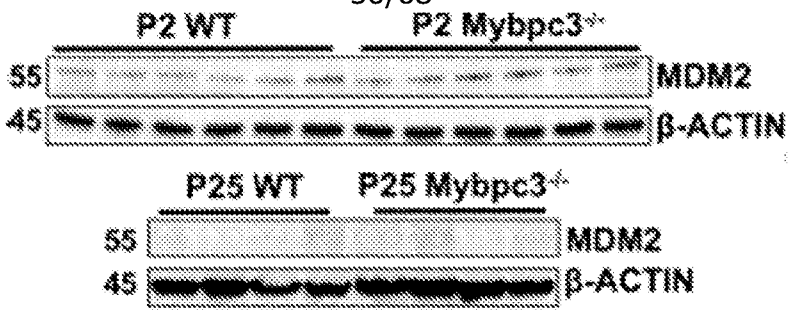

FIG. 10I

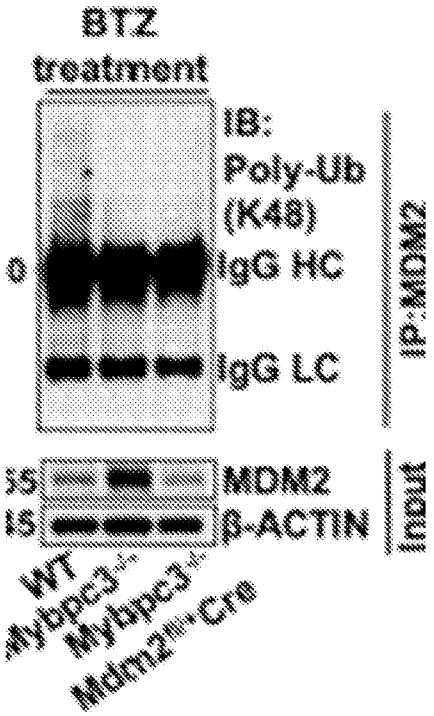

FIG. 10J

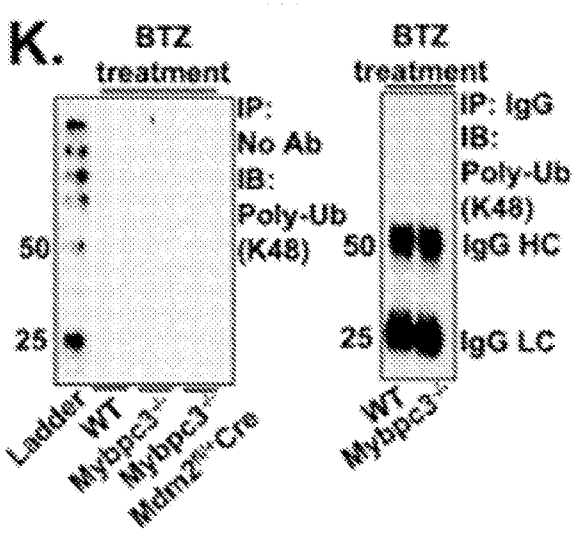

FIG. 10K

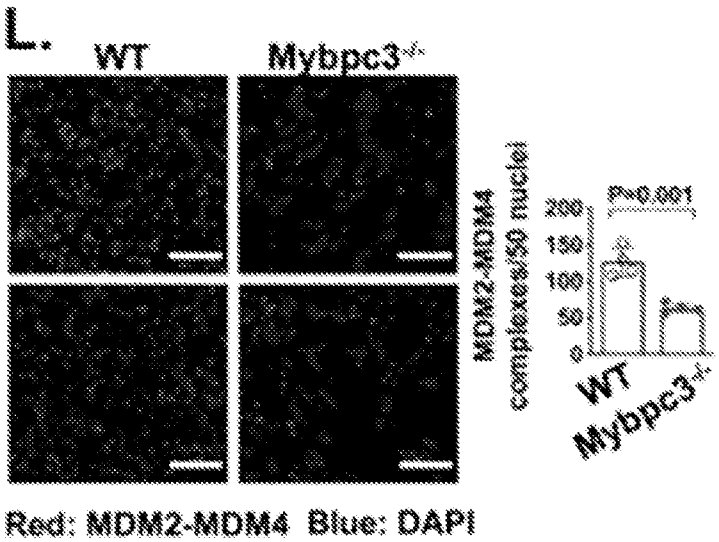

FIG. 10L

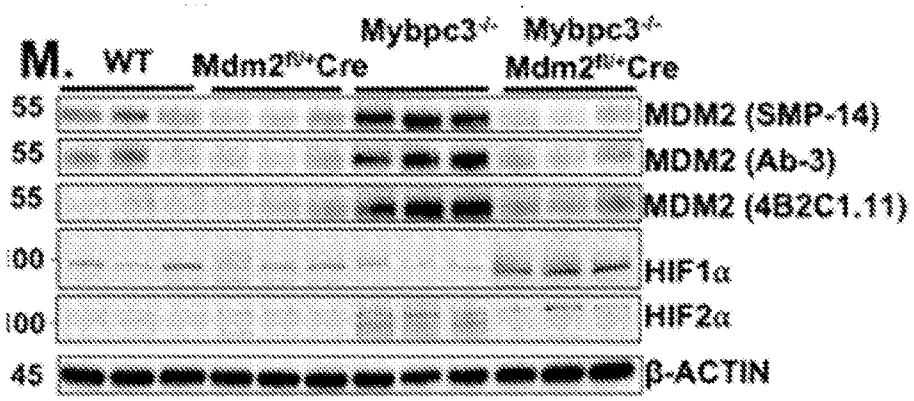

FIG. 10M

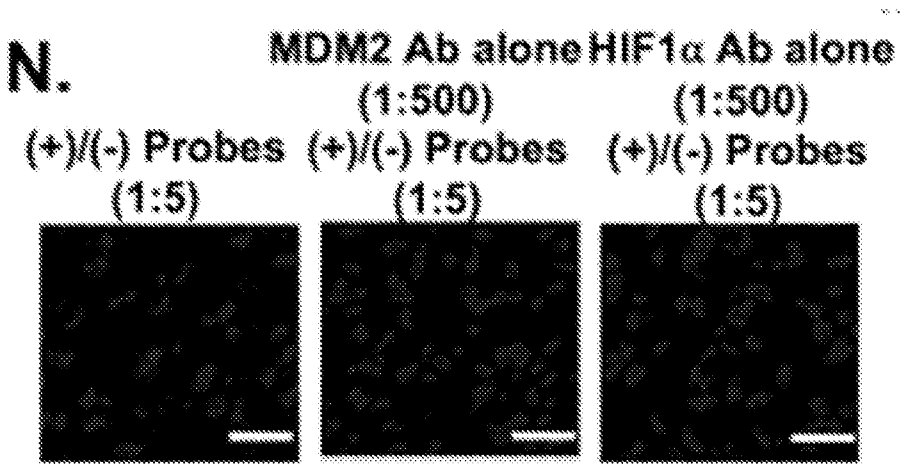

FIG. 10N

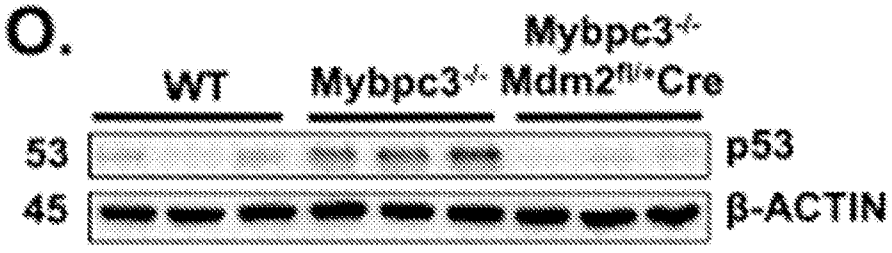

FIG. 10O

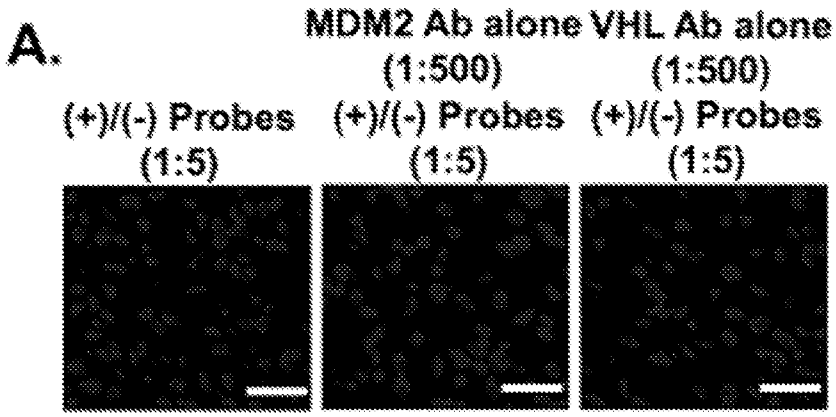

FIG. 11A

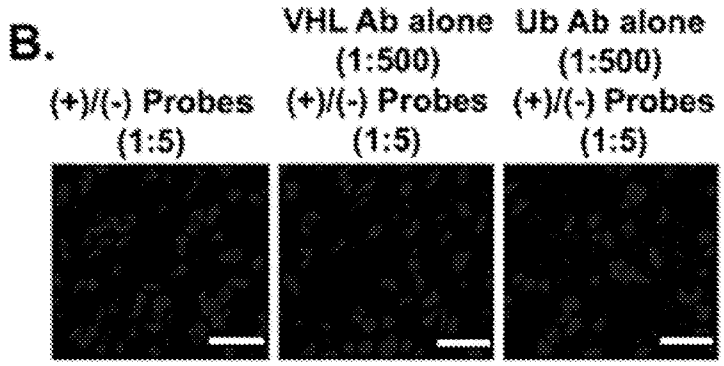

FIG. 11B

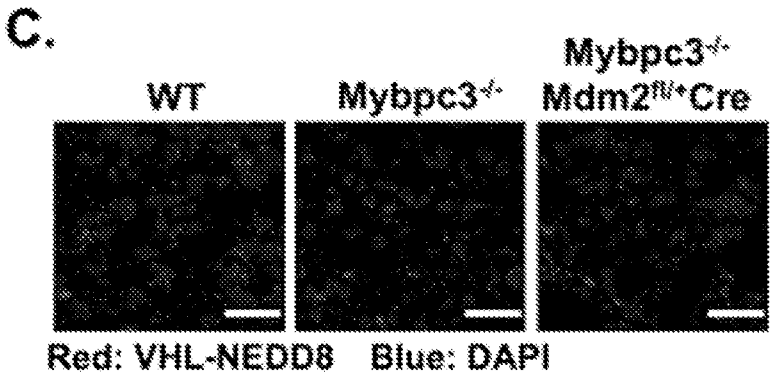

FIG. 11C

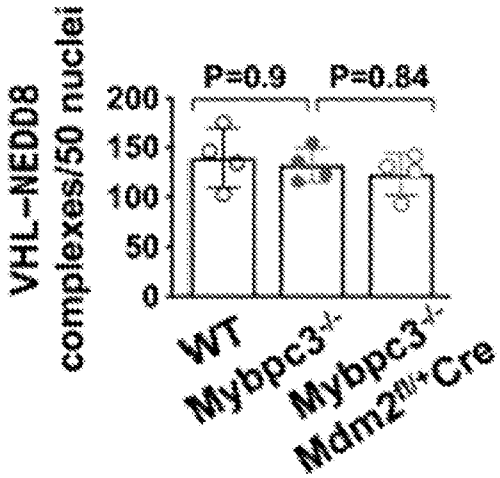

FIG. 11D

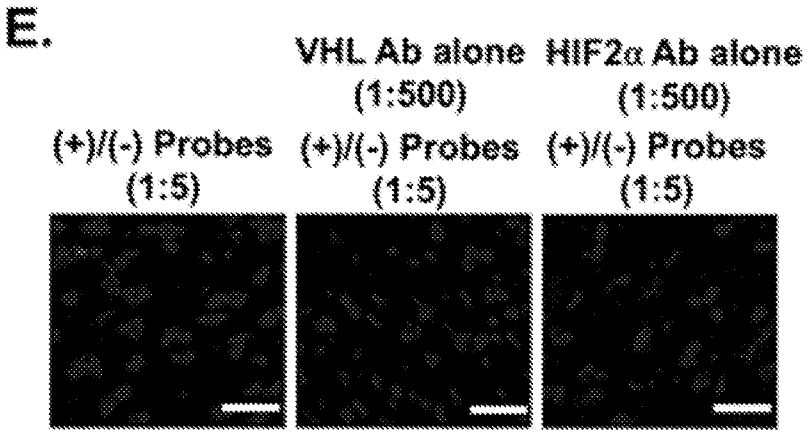

FIG. 11E

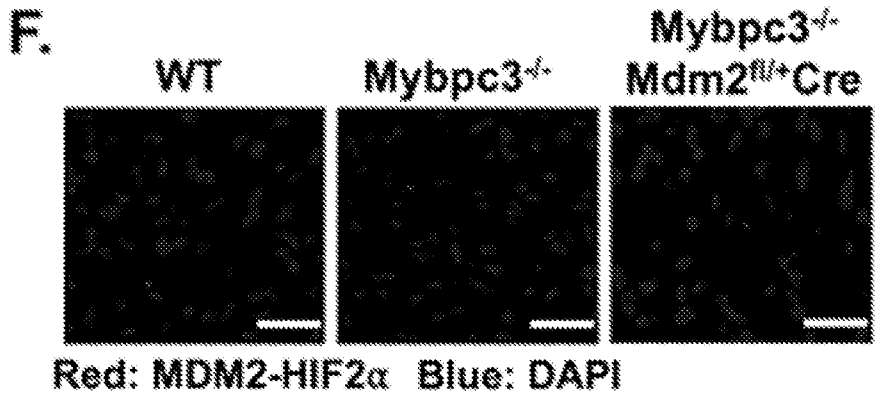

FIG. 11F

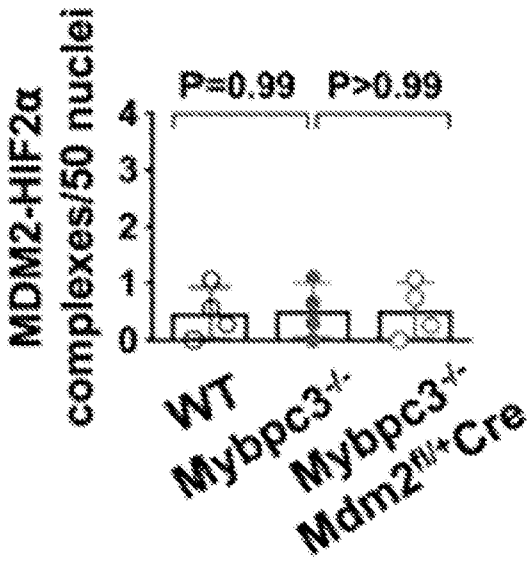

FIG. 11G

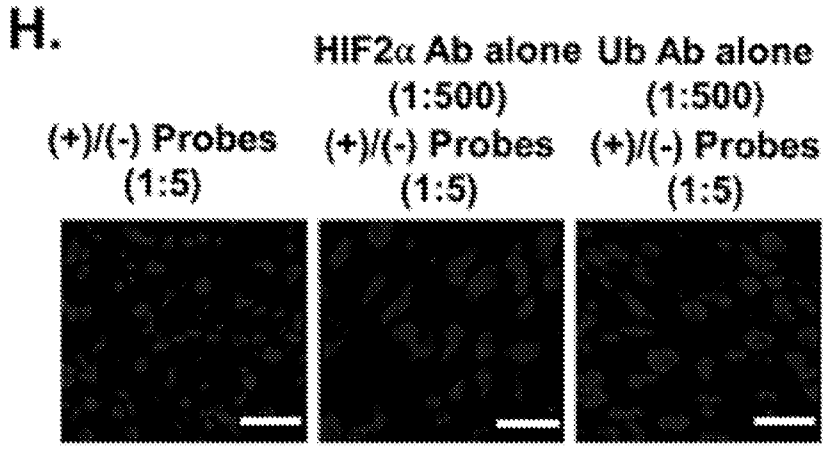

FIG. 11H

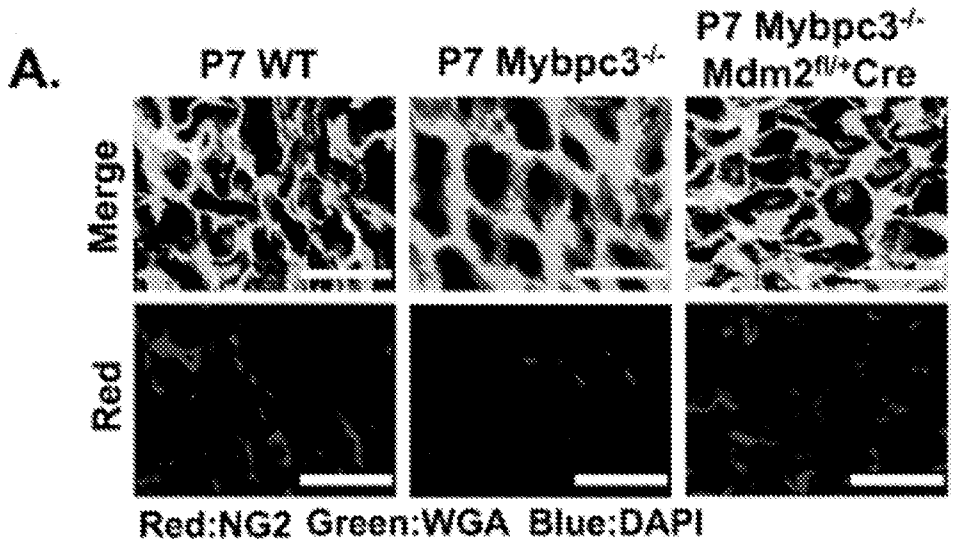

FIG. 12A

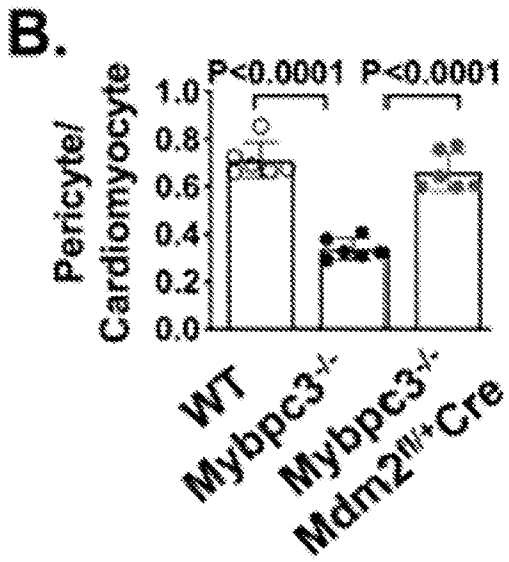

FIG. 12B

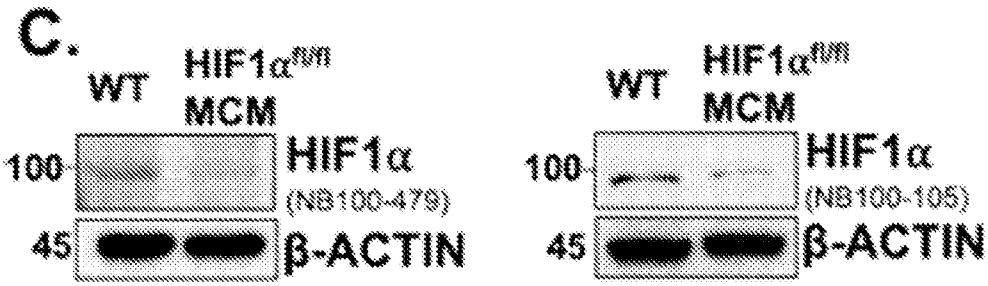

FIG. 12C

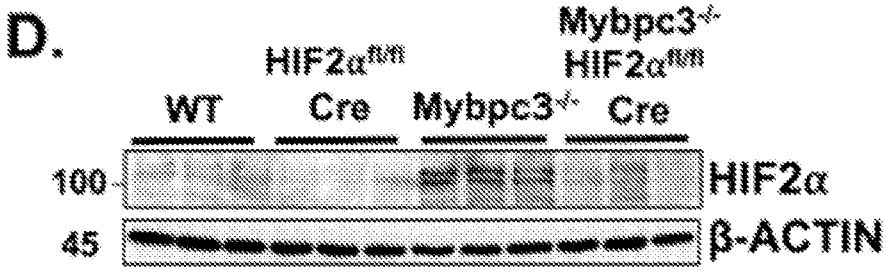

FIG. 12D

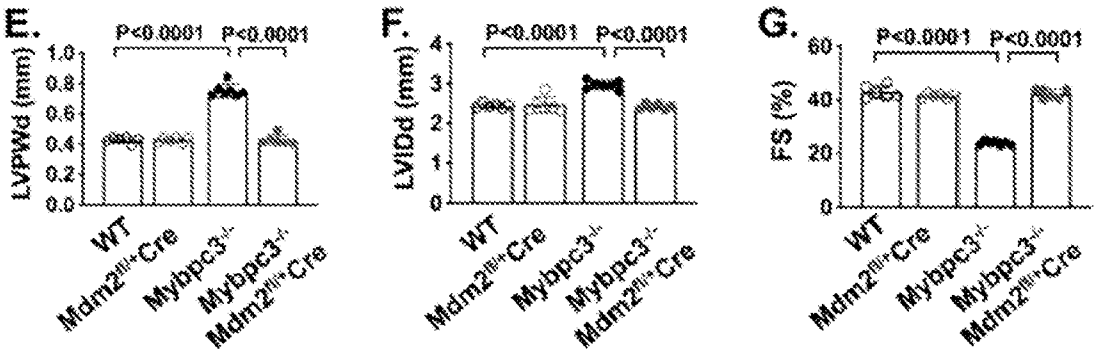

FIG. 12E, 12F, 12G

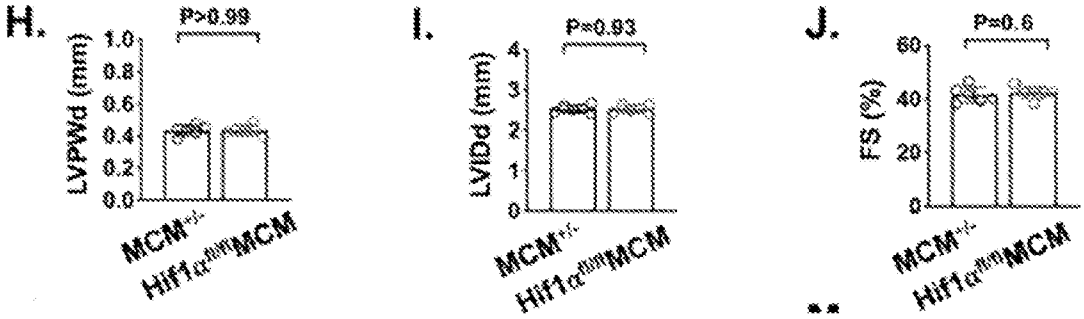

FIG. 12H, 12I, 12J

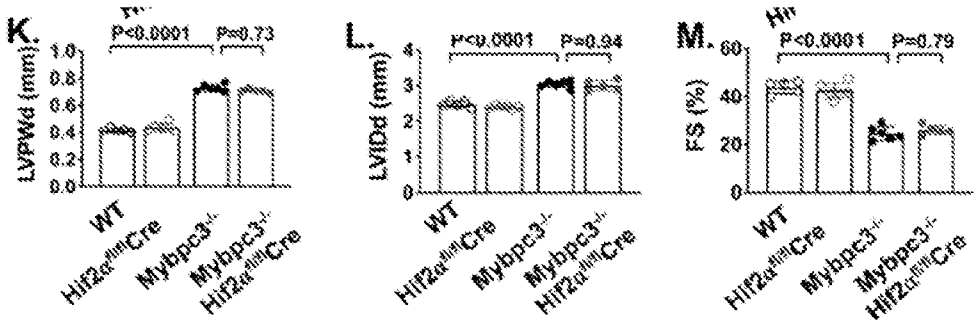

FIG. 12K, 12L, 12M

Human MYH7 WT	390	LNSADLLKGLCHPRVKVGNEYVTKGQNVQQ	419
Human MYH7 R403Q	390	LNSADLLKGLCHPQVKVGNEYVTKGQNVQQ	419
Mouse MYH6 WT	391	LNSADLLKGLCHPRVKVGNEYVTKGQSVQQ	420
Mouse MYH6 R404Q	391	LNSADLLKGLCHPQVKVGNEYVTKGQSVQQ	420

FIG. 13A

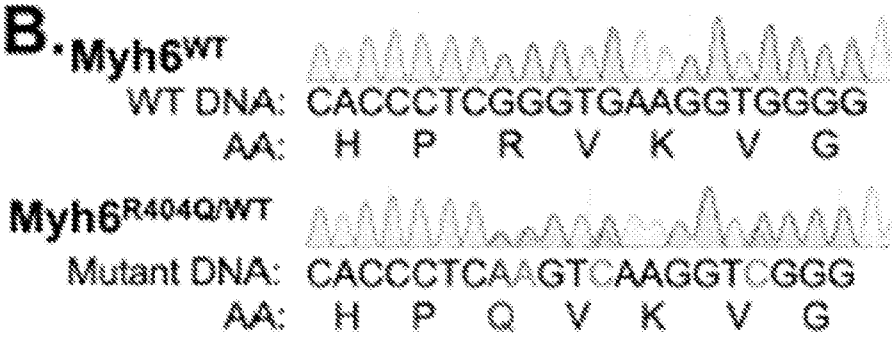

FIG. 13B

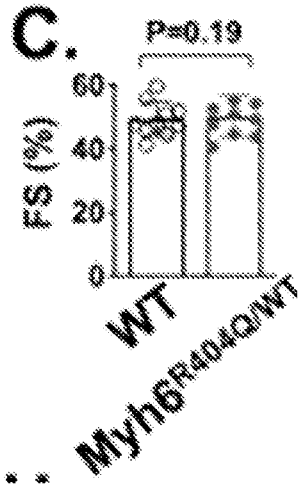

FIG. 13C

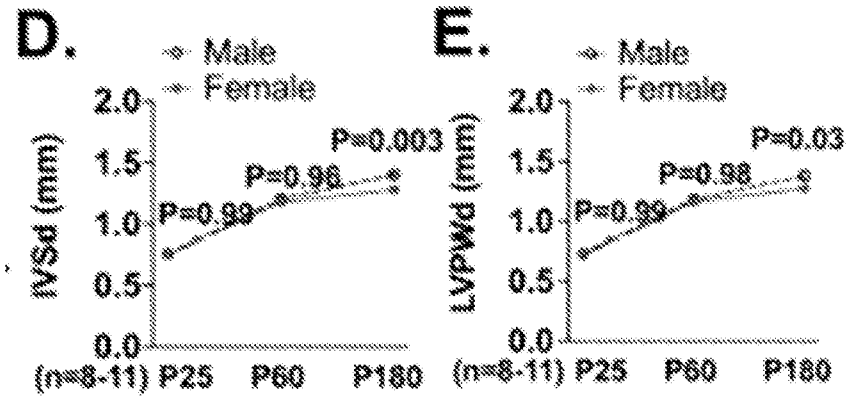

FIG. 13D, 13E

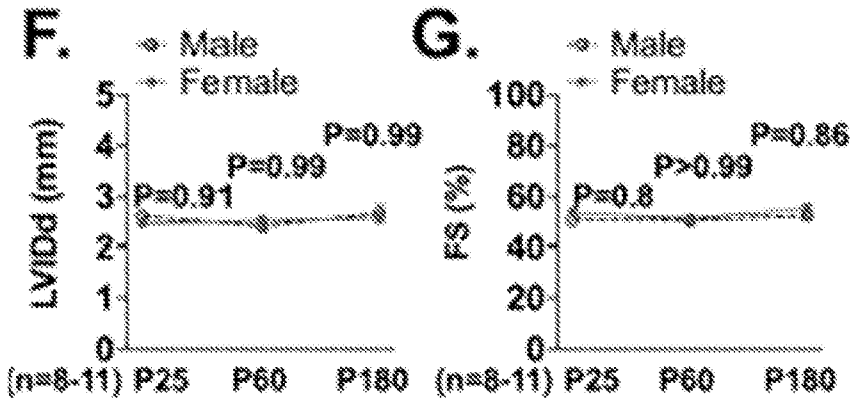

FIG. 13F, 13G

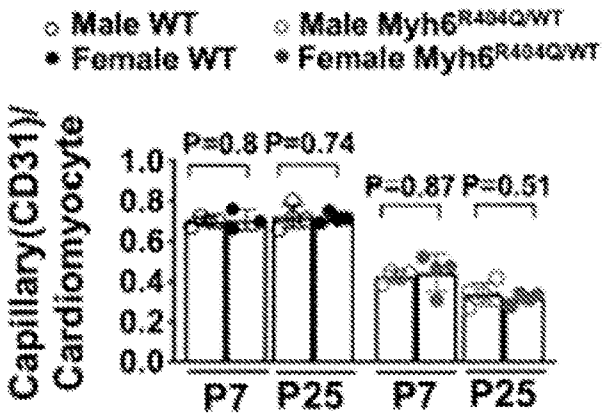

FIG. 13H

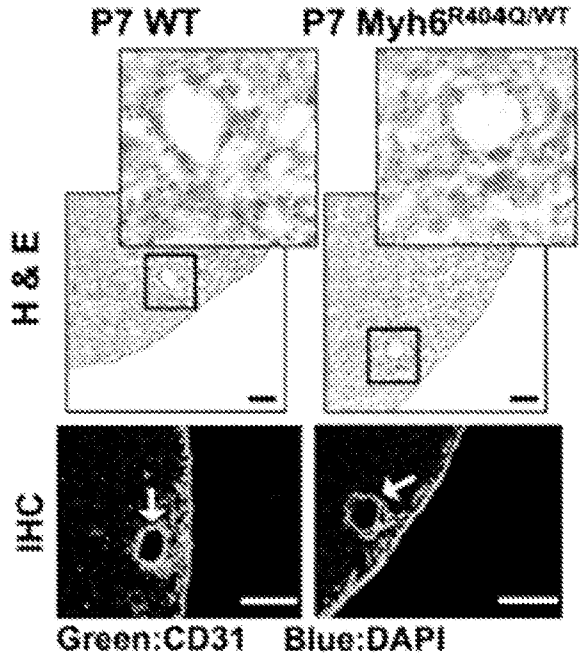

FIG. 13I

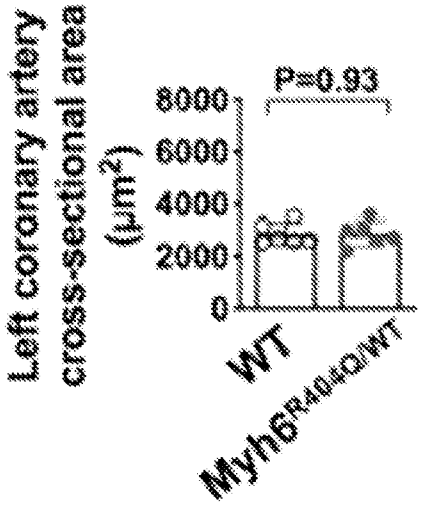

FIG. 13J

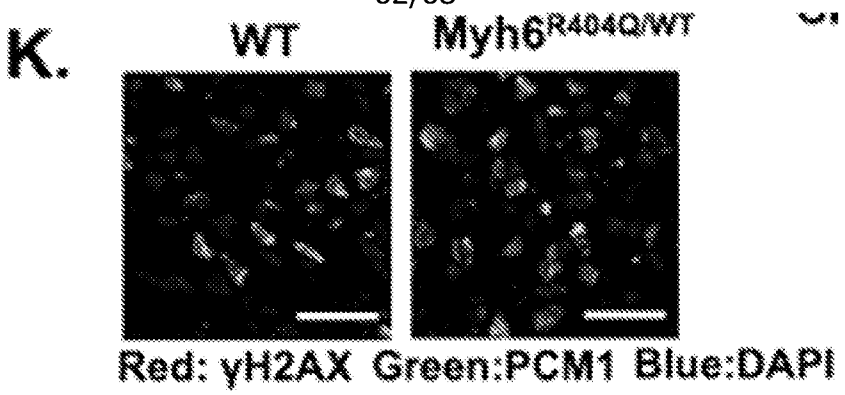

FIG. 13K

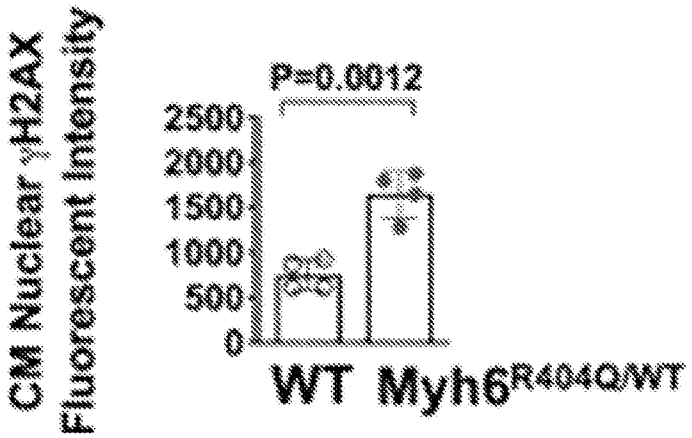

FIG. 13L

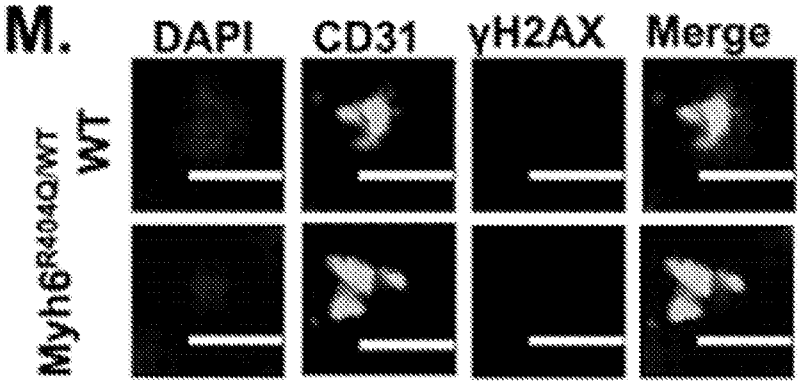

FIG. 13M

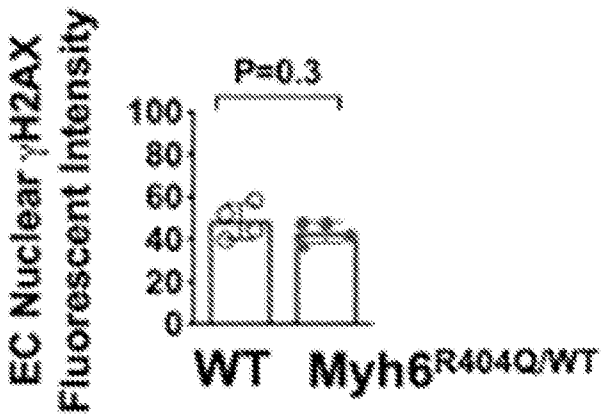

FIG. 13N

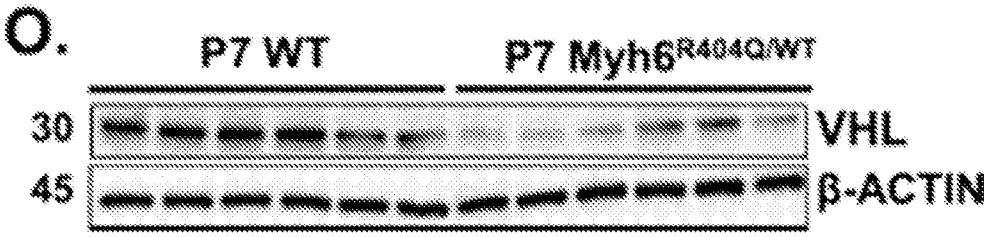

FIG. 13O

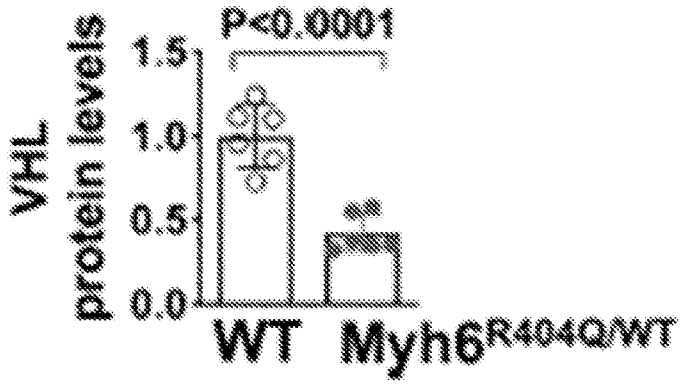

FIG. 13P

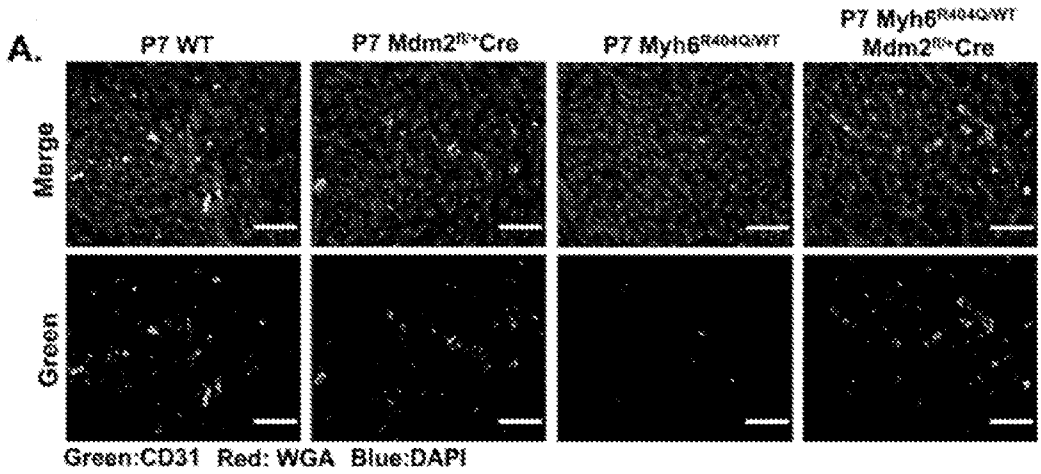

FIG. 14A

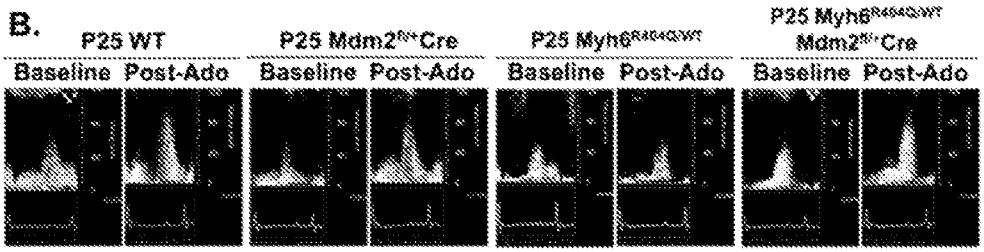

FIG. 14B

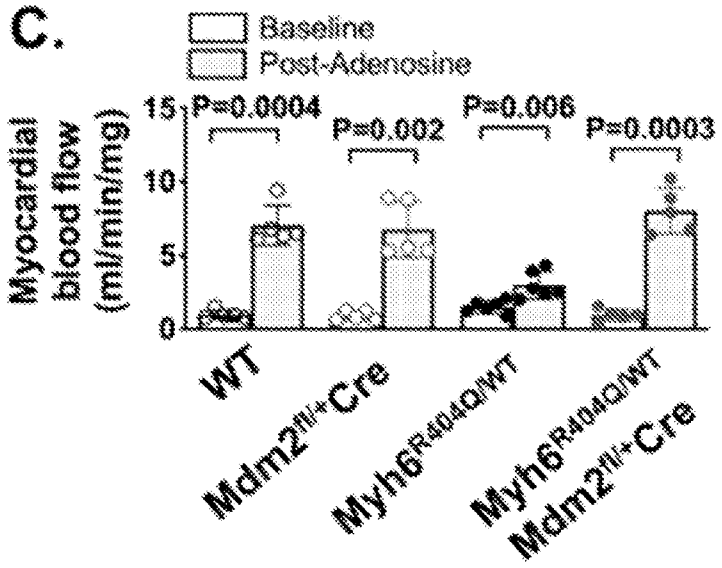

FIG. 14C

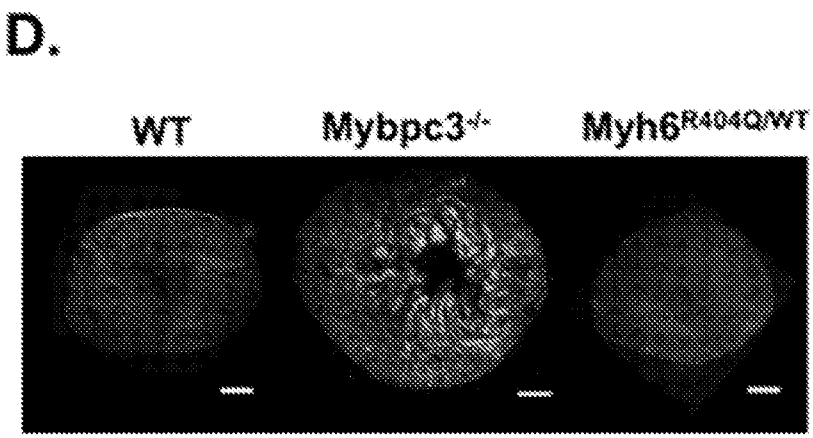

FIG. 14D

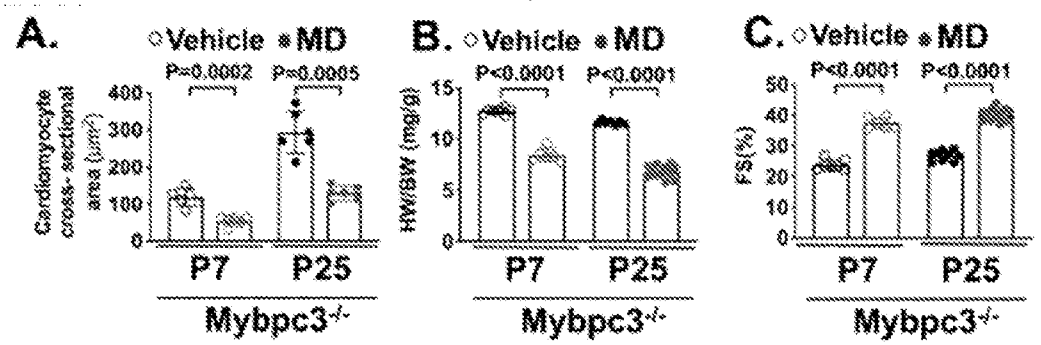

FIG. 15A, 15B, 15C

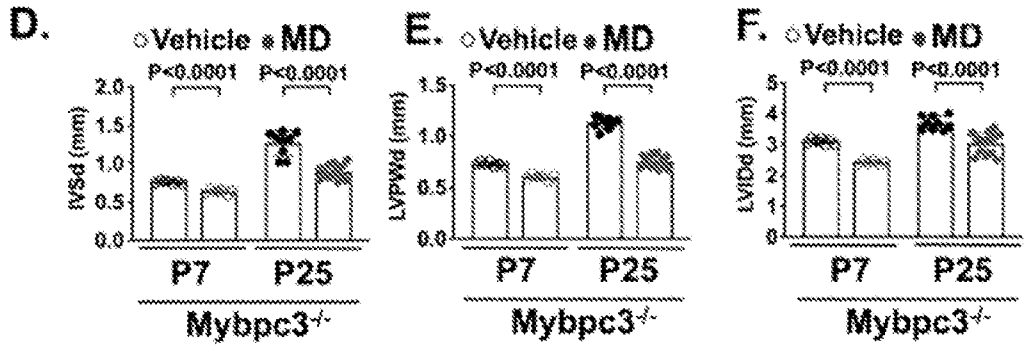

FIG. 15D, 15E, 15F

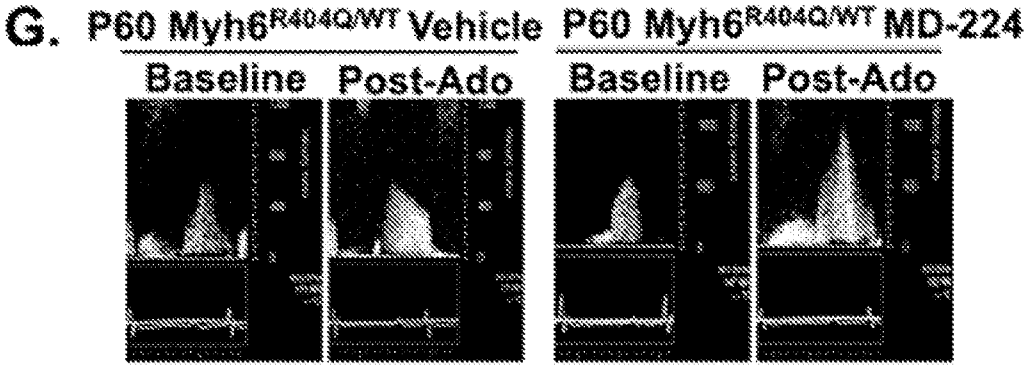

FIG. 15G

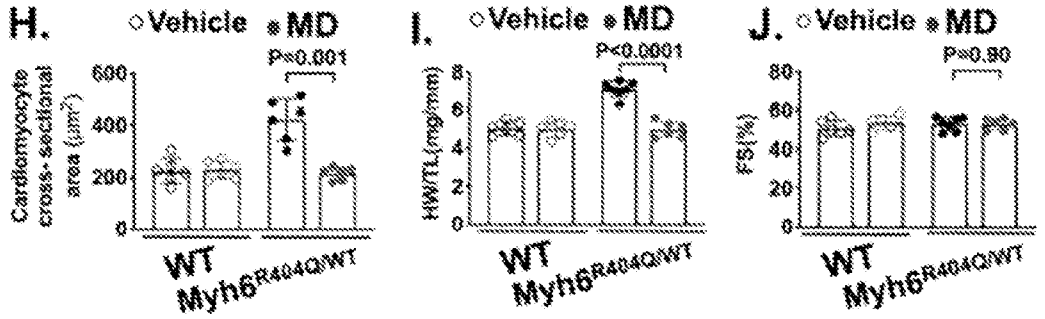

FIG. 15H, 15I, 15J

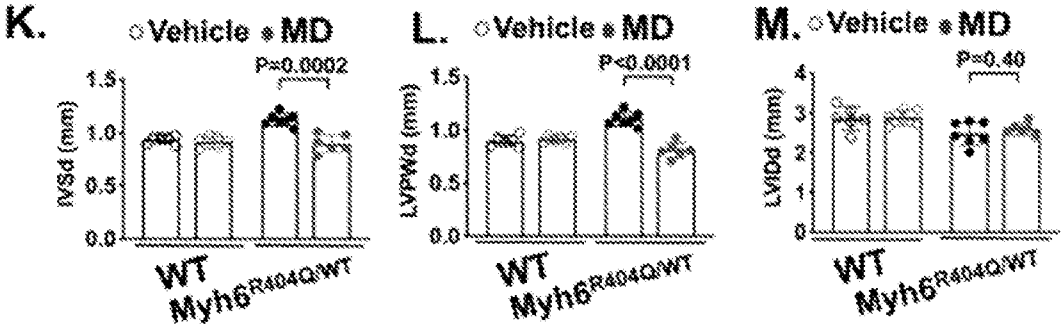

FIG. 15K, 15L, 15M

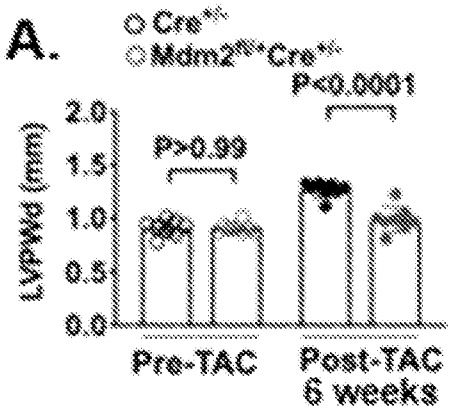

FIG. 16A

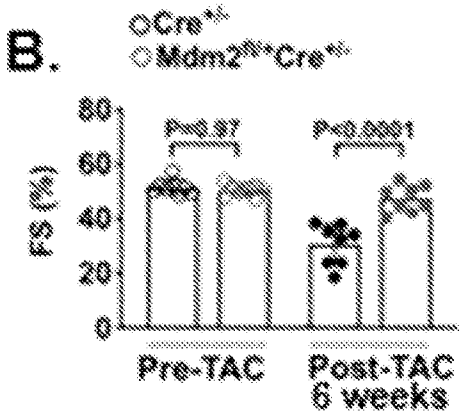

FIG. 16B

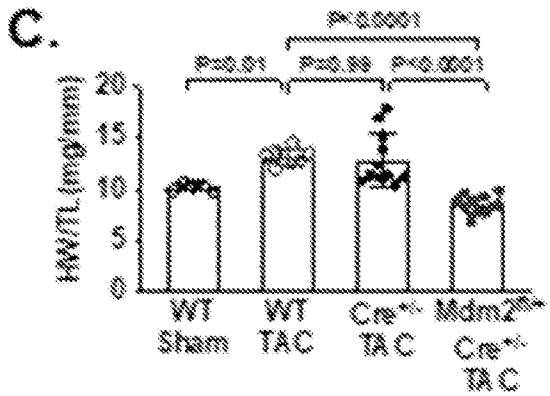

FIG. 16C

Table I

sgRNA
5’-TGTCACCCTCGGGTGAAGGT-3’ (SEQ ID NO: 10)
Myh6 R404Q mutant DNA template (mutation underlined and silent substitutions bolded)
AATCTGCCTACCTTATGGGGCTGAACTCAGCTGACCTGCTCAAGGGCCTGTGTC ACCCTC**A**AGT**C**AAGGT**C**GGGAACGAGTATGTCACCAAGGGGCAGAGTGTACAG CAAGTGTACTATTCCATCGGGGCACTGG (SEQ ID NO: 11)
Myh6 WT DNA template with CRISPR/Cas9 blocking mutations (silent substitutions bolded)
AATCTGCCTACCTTATGGGGCTGAACTCAGCTGACCTGCTCAAGGGCCTGTGTC ACCCTCG**A**GT**C**AA**A**GTGGGGAACGAGTATGTCACCAAGGGGCAGAGTGTACAG CAAGTGTACTATTCCATCGGGGCACTGG (SEQ ID NO: 12)

FIG. 17

INTERNATIONAL SEARCH REPORT

International application No.
PCT/US2024/045782

A. CLASSIFICATION OF SUBJECT MATTER

IPC: ***C12N 15/113*** (2024.01); ***C12Q 1/68*** (2024.01); ***G01N 33/53*** (2024.01); ***A61P 9/04*** (2024.01); ***A61P 9/10*** (2024.01)

CPC: ***C12N 15/113; A61P 9/10; A61P 9/04; C12Q 1/68; G01N 33/53***

According to International Patent Classification (IPC) or to both national classification and IPC

B. FIELDS SEARCHED

Minimum documentation searched (classification system followed by classification symbols)

See Search History Document

Documentation searched other than minimum documentation to the extent that such documents are included in the fields searched

See Search History Document

Electronic data base consulted during the international search (name of data base and, where practicable, search terms used)

See Search History Document

C. DOCUMENTS CONSIDERED TO BE RELEVANT

Category*	Citation of document, with indication, where appropriate, of the relevant passages	Relevant to claim No.
Y	US 2016/0339019 A1 (BUCK INSTITUTE FOR RESEARCH ON AGING et al.) 24 November 2016 (24.11.2016) entire document	1-3, 7, 19-21
Y	WO 2022/221051 A1 (PRESIDENT AND FELLOWS OF HARVARD COLLEGE et al.) 20 October 2022 (20.10.2022) entire document	1-3, 7, 19-21
Y	WO 2022/117049 A1 (WEST CHINA HOSPITAL SICHUAN UNIVERSITY) 09 June 2022 (09.06.2022) entire document	2, 3
Y	WO 2023/076665 A1 (IMBRIA PHARMACEUTICALS INC.) 04 May 2023 (04.05.2023) entire document	2, 7, 19, 21

☐ Further documents are listed in the continuation of Box C. ☐ See patent family annex.

* Special categories of cited documents:
"A" document defining the general state of the art which is not considered to be of particular relevance
"D" document cited by the applicant in the international application
"E" earlier application or patent but published on or after the international filing date
"L" document which may throw doubts on priority claim(s) or which is cited to establish the publication date of another citation or other special reason (as specified)
"O" document referring to an oral disclosure, use, exhibition or other means
"P" document published prior to the international filing date but later than the priority date claimed
"T" later document published after the international filing date or priority date and not in conflict with the application but cited to understand the principle or theory underlying the invention
"X" document of particular relevance; the claimed invention cannot be considered novel or cannot be considered to involve an inventive step when the document is taken alone
"Y" document of particular relevance; the claimed invention cannot be considered to involve an inventive step when the document is combined with one or more other such documents, such combination being obvious to a person skilled in the art
"&" document member of the same patent family

Date of the actual completion of the international search	Date of mailing of the international search report
14 October 2024 (14.10.2024)	**28 October 2024 (28.10.2024)**

Name and mailing address of the ISA/US	Authorized officer
COMMISSIONER FOR PATENTS **MAIL STOP PCT, ATTN: ISA/US** **P.O. Box 1450** **Alexandria, VA 22313-1450 UNITED STATES OF AMERICA**	**TAINA MATOS**
Facsimile No. **571-273-8300**	Telephone No. **571-272-4300**

INTERNATIONAL SEARCH REPORT

International application No.
PCT/US2024/045782

Box No. I Nucleotide and/or amino acid sequence(s) (Continuation of item 1.c of the first sheet)

1. With regard to any nucleotide and/or amino acid sequence disclosed in the international application, the international search was carried out on the basis of a sequence listing:
   a. ☑ forming part of the international application as filed.
   b. ☐ furnished subsequent to the international filing date for the purposes of international search (Rule 13*ter*.1(a)),
      ☐ accompanied by a statement to the effect that the sequence listing does not go beyond the disclosure in the international application as filed.

2. ☐ With regard to any nucleotide and/or amino acid sequence disclosed in the international application, this report has been established to the extent that a meaningful search could be carried out without a WIPO Standard ST.26 compliant sequence listing.

3. Additional comments:

INTERNATIONAL SEARCH REPORT

International application No.
PCT/US2024/045782

Box No. II Observations where certain claims were found unsearchable (Continuation of item 2 of first sheet)

This international search report has not been established in respect of certain claims under Article 17(2)(a) for the following reasons:

1. ☐ Claims Nos.:
because they relate to subject matter not required to be searched by this Authority, namely:

2. ☐ Claims Nos.:
because they relate to parts of the international application that do not comply with the prescribed requirements to such an extent that no meaningful international search can be carried out, specifically:

3. ☑ Claims Nos.: **4-6, 8-18, 22-30**
because they are dependent claims and are not drafted in accordance with the second and third sentences of Rule 6.4(a).